

Theory of Adsorption on Metal Substrates

M. Scheffler and C. Stampfl

Fritz-Haber-Institut der Max-Planck-Gesellschaft
Faradayweg 4-6
D-14195 Berlin, Germany

Handbook of Surface Science
Volume 2, edited by K. Horn and M. Scheffler

Contents

5.1 Introduction

5.1.1 The nature of the surface chemical bond: indeterminate concepts, yet useful ...

5.1.2 What will be discussed and why, and what is missing

5.2 Concepts and definitions

5.2.1 Density of states

5.2.2 Energies

5.2.3 Binding energy at kink sites

5.2.4 The surface energy barrier

5.3 The tight-binding picture of bonding

5.3.1 Adsorbate-substrate interaction

5.3.2 Adsorbate band structure

5.4 Adsorption of isolated adatoms

5.4.1 Geometry

5.4.2 Density of states $\Delta N(\epsilon)$

5.4.3 Electron density: $n(\mathbf{r})$, $\Delta n(\mathbf{r})$, and $n^{\Delta}(\mathbf{r})$

5.4.4 Surface dipole moments

5.5 Alkali-metal adsorption: the traditional picture of *on-surface* adsorption

5.5.1 The Langmuir-Gurney picture

5.5.2 Coverage dependence of the work function

5.5.3 Ionization of the adsorbate and screening by the substrate electrons

5.5.4 Surface band structure

5.6 Substitutional adsorption and formation of surface alloys

5.6.1 Na on Al(001)

5.6.2 Na on Al(111)

5.6.3 Co on Cu(001)

5.7 Adsorption of CO on transition-metal surfaces – a model system for a simple molecular adsorbate

5.8 Co-adsorption [the example CO plus O on Ru(0001)]

5.9 Chemical reactions at metal surfaces

5.9.1 The problems with “the” transition state

5.9.2 Dissociative adsorption and associative desorption of H_2 at transition metals

5.9.2.1 The potential-energy surface of H_2 at transition-metal surfaces

5.9.2.2 The dynamics of H_2 dissociation at transition-metal surfaces

5.10 The catalytic oxidation of CO

5.11 Summary outline of main points

References

5.1 Introduction

The theory of adsorption has reached a level where it is possible to calculate free energies, as well as the electronic and atomic structure, of medium-sized systems with predictive accuracy. Such *ab initio* calculations (i.e., starting from the electronic structure) typically employ complicated methods and significant computational resources. Clearly, the methodological developments of recent years have been impressive, although further developments, enhancements, and speed-ups of such methods are still necessary. Acknowledging the predictive power of density-functional theory calculations, however, we also note that the need remains for finding explanations and developing simple concepts. Today's concepts are largely based on experience from gas-phase chemistry, as for example the concepts of electronegativity, HOMO (highest occupied molecular orbitals), LUMOs (lowest unoccupied molecular orbitals), and the reactivity of open-shell systems. However, it is also clear that some concepts, which are powerful in the gas-phase chemistry of molecules, can be quite misleading when it comes to surfaces. One example is that of "the" transition state of a chemical reaction: For molecular chemistry this concept is typically useful, but for molecules at surfaces it turns out that the dimension of phase space is so high that not just one, but many transition states exist, and all of them may play a role (see Section 5.9).

What is needed now, and in the years to come, is to perform more predictive simulations of surface chemical reactions; but also the next step can and should be done, which is the development of *explanations* and *understanding*. For example, at this point we are not able to rationalize the factors that determine at which transition-metal surface a rotationally excited molecule will dissociate more easily than a molecule that is not rotationally excited (see Section 5.9.2). Also we are just starting to develop an understanding of why some adsorbates occupy a substitutional site, and not just simply adsorb *on* the surface, and why this geometry may change with coverage. Note that ten years ago substitutional adsorption of single adatoms was unheard of, but now, it is a well known and common phenomenon (see Section 5.6).

The discussion presented in this chapter is based on results from density-functional theory calculations. Rather than discussing details of these calculations, we simply use the results to show where we are on the way to attaining a rationalization of the factors which actuate the surface chemistry for different systems. This goal does not (and cannot) aim at a quantitative description, and it is clear that concepts, e.g., that of electronegativity, often do not withstand a quantitative analysis. However, describing the results in words and in a chemical language, is the basis on which "understanding" is built. Clearly, the quality (i.e., the nature or character) of an effect is linked to the quantitative numbers, and sometimes a small change in the quantity changes the quality. In this sense our goal is insecure. But we strongly believe that capturing the nature of a situation and understanding trends is the essence of "understanding". As we said above, theoretical surface science is now able to do this, and some examples along this route already exist, some of which will be discussed in this chapter.

5.1.1 The nature of the surface chemical bond: indeterminate concepts, yet useful ...

A crude classification of adsorption distinguishes two classes, namely that of a very weak (van der Waals type) interaction between adsorbate and substrate (physisorption), where

the adsorption energy is typically less than 0.3 eV per adsorbed particle (6.9 kcal mol⁻¹), and that of chemisorption, where the adsorption energy is larger.

For chemisorption systems there is a further classification of the nature of bonding which is frequently applied, although it is neither unique nor general. Nevertheless, it has some natural advantages and will also be applied in this chapter. It is based on a survey of electronic, electrical, vibrational, and thermal properties. Thus, altogether we will distinguish four different types of bonding:

1. van der Waals,
2. covalent,
3. metallic,
4. ionic.

As little the nature of bonds of types 2, 3, and 4 is well defined, that of van der Waals bonding is equally so. The concept of the van der Waals interaction is valid for large distances where orbitals do not overlap. It is due to electron-density fluctuations at the different atoms and the polarization that the fluctuations induce at the other atoms. However, at the equilibrium geometry of an adsorbate on a surface, the direct interaction of adsorbate and substrate orbitals is significant. This is indeed plausible as equilibrium geometries are determined by the interplay of attractive interactions and Pauli repulsion. As a consequence, at the bonding geometry of adsorbed noble-gas atoms which are regarded as exhibiting a van der Waals like bonding, and even more so at the turning point of noble-gas atom scattering at surfaces, the physics is largely determined by the interaction of orbitals and *static* polarization. Thus, *physisorption*, although implying a weak interaction strength, can induce a static dipole moment at the adsorbate (in particular for larger atoms, e.g., Xe), and the electrostatic interaction of this adsorbate dipole with the substrate contributes noticeably to the bond strength. Indeed, density-functional theory (DFT) calculations performed using either the local-density approximation (LDA) or the generalized gradient approximation (GGA) for the exchange-correlation interaction, which both lack a description of the nature of the van der Waals interaction, as this is intrinsically non-local, seem to give a reasonable description of adsorption of noble-gas atoms at surfaces (see, e.g., Brivio and Trioni, 1999). Nevertheless, it is not clear if the acting “overlap-modified dispersion forces” are described by the present exchange-correlation functionals with sufficient accuracy. In any case, what we like to emphasize is that even weak bonding can give rise to noticeable changes in the electrostatic field at the surface and therefore to changes in surface properties. We elaborate here on this discussion more than usual because the use of the above noted four bonding types has often caused confusion when they were interpreted literally. Knowing about the danger of over-interpreting the relevance of these concepts we still feel that the advantage of categorizing systems is important for identifying trends, noting unusual effects, and for *scientific understanding* in general. In Sections 5.3, 5.4, and 5.5 we will continue this discussion with respect to ionic and covalent bonding.

Metallic bonding, also noted in the above list, is a special case of covalent interaction where the electron density is more delocalized and not (strongly) peaked between the atoms. In principle, the attractive interaction is due to the fact that the electrons act like a structureless “glue” between the nuclei. This attraction is stabilized by a repulsive term due to the

kinetic energy of the electrons, because electrons do not like to become localized, but instead, as a consequence of the Heisenberg uncertainty principle, they like to spread out. For *isolated* adatoms, the concept of metallic bonding is not very useful because metallic bonding, and the concept of delocalized electrons, requires a high coordination. Therefore we will not allude to this concept in Section 5.4 where isolated atoms are discussed, but we will in Sections 5.5.4 and 5.6 when we compare adlayers of different density and discuss the formation of a surface electronic band structure.

5.1.2 What will be discussed and why, and what is missing

This chapter deals with various adsorbates on metal surfaces, where we focus on the electronic properties and the nature of the chemical bond. To some extent this also necessitates a discussion of the atomic geometries because the distances and directions between the atoms and their neighbors, determine which, and how, orbitals will hybridize. Just as one example we mention aluminum which is a nearly-free-electron metal. However, when an Al atom is placed in a certain local coordination, its *s*- and *p*-electrons can hybridize and form directional bonds. This is in fact well known even for bulk systems, as for example AlAs. This property of Al, namely being close to a covalent material, contributes to the low formation energy of surface vacancies at Al(111) (see Neugebauer and Scheffler, 1992) and is instrumental in the theoretical result that self diffusion at Al(001) proceeds via the exchange mechanism (see Feibelman, 1990; Yu and Scheffler, 1997).

We will keep the discussion in this chapter simple and accentuate the *qualitative* nature of the various mechanisms. Nevertheless, we emphasize that all results discussed below are based on quantitative calculations performed using density-functional theory (DFT) (Dreizler and Gross, 1990). Indeed, the dialectic relation of quantity and quality will become obvious through several examples discussed below: Often a small quantitative difference in certain values will cause a significantly changed electronic and/or geometric structure and as a consequence a different bonding quality or nature.

The exchange-correlation functional employed in many of the studies discussed below is the local-density approximation (LDA), which gives a reliable description of geometries and the nature of the bond. In the more recent studies, which are presented in Sections 5.7 – 5.10, the generalized gradient approximation (GGA) is employed. For equilibrium geometries the GGA gives results similar to the LDA. For the description of chemical reactions, in particular of transition states, where the breaking of old bonds and making of new bonds occurs, the GGA is in fact mandatory, i.e., the LDA often gives even qualitatively incorrect results (see for example Hammer et al., 1994, and references therein).

For simplicity's sake, we restrict ourselves to close-packed substrate surfaces [mainly fcc (111) and fcc (001)]. The more open surfaces are typically close to a structural instability and therefore sometimes already reconstruct when clean, or when adsorbates are added. We also limit the number of substrate materials with the view that this will ease the readability of the chapter. However, essentially all important mechanisms that we would like to discuss are represented by the systems presented.

Because of their large dipole moments and special role in various industrial applications, the discussion of alkali-metal adsorbates is addressed in particular detail. This presentation also focuses on the general properties; for more complete discussions we refer to some recent

review papers, e.g., Stampfl and Scheffler (1995) and Adams (1996). Noble-gas adatoms¹ and *f*-electron systems are not discussed, and also for metallic substrates not all “classes” are covered: We concentrate on elemental substrates (only a few words are said about alloys) and consider low coverages, i.e., from a single adatom up to a full monolayer.²

As the properties of adsorbates on metals are manifold, we are unable to address all features which may be relevant in one or another situation. For example, core-levels and surface core-level shifts (with their interesting initial state and final state effects) are not mentioned (see for example Andersen et al., 1994; Methfessel et al., 1995; Hennig et al., 1996; Ganduglia-Pirovano et al., 1997, and references therein). The same is true for surface electric resistance, magnetism, and more.

Otherwise, we trust that the selection of systems is representative. It covers a small fraction of work done by us over the last several years on adsorption, co-adsorption, and chemical reactions. We note that similar work has also been published by other groups (see, e.g., Hammer and Nørskov, 1997, and references therein).

5.2 Concepts and definitions

This section starts with some general remarks and then collects definitions of important quantities which are typically calculated in theoretical work on adsorption and will be used later in this chapter.

Accurate knowledge of the geometry of the adsorbate and substrate atoms is a prerequisite for any additional analysis of the adsorbate properties, as for example the surface electronic structure, adsorbate-induced work function changes, and the chemical reactivity. The apparent hierarchy expressed in this sentence reflects the fact that the atomic structure is somewhat more directly accessible for experimental studies. Nevertheless, we emphasize that electronic and atomic structure are closely interconnected and do not consider it very useful to analyze “the chicken and the egg problem”, i.e., to discuss whether the geometry creates the electronic structure or vice versa. In fact, we will stress in this chapter (particularly in Sections 5.5 and 5.6) that the same adsorbate can exhibit a different bonding character, depending on the adsorbate coverage and the local adsorbate geometry. We will discuss these aspects for special examples but note that these are *examples* which represent many systems; they are selected because they demonstrate the effects most clearly.

5.2.1 Density of states

An important quantity accessible in calculations, though not in experiments, is the local density of states

$$n(\mathbf{r}, \epsilon) = \sum_{i=1}^{\infty} |\varphi_i(\mathbf{r})|^2 \delta(\epsilon - \epsilon_i), \quad (5.1)$$

¹For a discussion of recent work on noble-gas atom adsorption see Bruch et al., 1997; Brivio and Trioni, 1999; Seyller et al., 1998; Petersen et al., 1996, 2000.

²The coverage is defined in this chapter such that for $\Theta = 1$, the number of adatoms is the same as the number of atoms in the clean, unreconstructed surface.

where $\varphi_i(\mathbf{r})$ are the single-particle eigenfunctions of the Kohn-Sham Hamiltonian. For those who like Green functions this is written as

$$n(\mathbf{r}, \epsilon) = -\frac{2}{\pi} \text{Im} \mathcal{G}(\mathbf{r}, \mathbf{r}, \epsilon), \quad (5.2)$$

where $\mathcal{G}(\epsilon)$ is the retarded Green-function operator of the adsorbate system. The electron density is

$$n(\mathbf{r}) = \int_{-\infty}^{\infty} f(\epsilon, T) n(\mathbf{r}, \epsilon) d\epsilon = \sum_{i=1}^{\infty} f(\epsilon_i, T) |\varphi_i(\mathbf{r})|^2, \quad (5.3)$$

with the Fermi distribution $f(\epsilon, T)$ at temperature T . Often, when the nature of a chemical bond is analyzed, electron density plots are shown, sometimes complemented with a discussion of charge transfer from atom A to atom B. We do not consider this approach so useful and emphasize that a small difference in the electron density sometimes implies a significantly different physical-chemical interaction. This is demonstrated in Fig. 5.1 which shows the electron density of bulk NaCl, that is a system, which is well accepted to have ionic bond character. However, even in this example the self-consistently calculated electron density (right) and that constructed by a superposition of electron densities of the *neutral* Na and *neutral* Cl atoms (left) differ only slightly, and just on the basis of inspecting $n(\mathbf{r})$ charge transfer can hardly be identified. The small changes brought about by the self-consistent rearrangement of electron density are that around the Na nucleus the charge density is very slightly decreased; but also at the Cl atom we see that the maximum of the electron density, which is rather close to the nucleus, becomes slightly lower. Thus, when one only inspects the electron density, even NaCl does not present a clear case for a system with ionic bonding. We emphasize that for low-symmetry situations, as for example a surface, this problem is even more pronounced. However, an analysis of the density of states (see, e.g., also Section 5.4.2) shows that it is indeed appropriate to describe the upper valence band in terms of Cl $3p$ and the lower conduction band in terms of Na $3s$ orbitals.

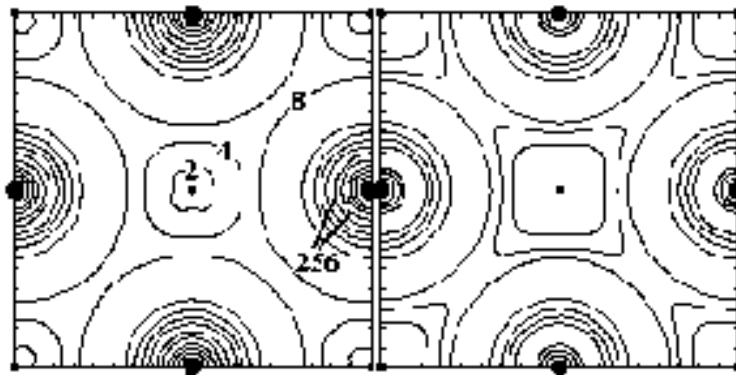


Figure 5.1: Lines of constant electron density (valence only) for a NaCl crystal, the prototype of ionic bonding. Left: Result obtained by a superposition of the electron densities of *neutral* Na and Cl atoms. Right: Result from a self-consistent DFT-LDA calculation. The units are $10^{-3} \text{ bohr}^{-3}$. Large dots mark the positions of the Cl atoms, and small dots mark the Na atoms. Adjacent contour lines differ by a factor of 2. The maximum density for the non-self-consistent calculation (left) is $265 \times 10^{-3} \text{ bohr}^{-3}$ and for the self-consistent calculation (right) the highest density is $253 \times 10^{-3} \text{ bohr}^{-3}$ (from Bormet et al., 1994a).

The example of Fig. 5.1 shows that despite the fact that the electron density can be considered the ruling quantity in density-functional theory, its inspection can be misleading. Sometimes, though not always, plots of density *differences*

$$\Delta n(\mathbf{r}) = n(\mathbf{r}) - n^0(\mathbf{r}) \quad (5.4)$$

give a better impression (see Sections 5.4 and 5.5.3). Here $n^0(\mathbf{r})$ is the electron density of the clean substrate where the geometry is (typically) chosen to be that of the adsorbate system. Also the *difference density*

$$n^\Delta(\mathbf{r}) = n(\mathbf{r}) - n^0(\mathbf{r}) - n^{\text{Na},f_{3s}}(\mathbf{r}) \quad (5.5)$$

is often a helpful quantity. Here $n^{\text{Na},f_{3s}}(\mathbf{r})$ is the (spherical) electron density of the partially ionized atom to be adsorbed, where the occupation of the valence level is given by the parameter f_{3s} . Just as an example, our indices here refer to a Na atom, where the valence level is 3s.

A typically more sensitive quantity is the density of states (DOS),

$$N(\epsilon) = \int n(\mathbf{r}, \epsilon) d\mathbf{r} = \sum_{i=1}^{\infty} \delta(\epsilon - \epsilon_i), \quad (5.6)$$

where the sum goes over all eigenstates of the Kohn-Sham Hamiltonian. The DOS gives a noticeable contribution to the electrons' kinetic energy

$$T_s[n(\mathbf{r})] = \int_{-\infty}^{\infty} f(T, \epsilon) N(\epsilon) \epsilon d\epsilon - \int V^{\text{eff}}(\mathbf{r}) n(\mathbf{r}) d\mathbf{r}, \quad (5.7)$$

where V^{eff} is the effective potential of the Kohn-Sham Hamiltonian (see Chapter 1 of this book). We also note that a one-to-one correspondence exists between $N(\epsilon)$ and the electron density,³ which (in addition to the argument of practicability and clarity) gives a premise to its use.

Throughout this chapter we will follow the thinking that the nature of bonding is determined by the interaction of the orbitals at the different atoms involved, and thus, it is more clearly identified by an inspection of the DOS and/or by the adsorbate-induced change (Δ DOS)

$$\Delta N(\epsilon) = N(\epsilon) - N^0(\epsilon), \quad (5.8)$$

where $N^0(\epsilon)$ is the DOS of the clean substrate where the geometry is typically chosen to be that of the adsorbate system. Furthermore, we note the state-resolved DOS, also called the projected DOS, as a very useful quantity:

$$N_\alpha(\epsilon) = \sum_{i=1}^{\infty} |\langle \phi_\alpha | \varphi_i \rangle|^2 \delta(\epsilon - \epsilon_i), \quad (5.9)$$

where ϕ_α is a properly chosen localized function. The spatial distribution of the electron density is viewed as a consequence (not the origin) of the hybridization of different orbitals.

³Obviously, as $N(\epsilon)$ defines the Kohn-Sham Hamiltonian, it also defines all ground-state and all excited-state properties.

The critic may argue that this is just (another) chicken-egg problem, and we agree with this assessment, i.e., our approach is simply taken because it is useful. We also note that information about $N_\alpha(\epsilon)$ can be obtained (though in a somewhat distorted way) from angle-resolved photoemission, inverse photoemission, and scanning tunneling spectroscopy.

Unlike the bond formation in molecular chemistry, the case of adsorption is one between very different partners: The adatom comes with discrete energy levels and few occupied states, but the substrate has a near-infinite number ($\sim 10^{23}$) of electrons. Thus, the valence level of the adparticle will interact with a semi-infinite continuum of levels $\epsilon \geq \epsilon_0$, where ϵ_0 is the bottom of the substrate valence band. The location of the highest occupied level, the Fermi energy, is determined by the substrate. On a surface, a description of the chemical bonding in terms of an elementary discrete level scheme has therefore to be extended: Levels lying in the band region of the substrate receive a finite width. These broad levels are called adsorbate-induced resonances and they get filled up to the substrate Fermi level. The wave functions of these resonances can be understood to arise from the adsorbate orbitals. In an alternative view, the states of the clean surface are described as standing waves, incident from the bulk and reflected at the potential-energy barrier of the clean surface, with a node at the surface. An adsorbed particle modifies the reflection properties, which can be described by introducing an energy-dependent phase shift, $\delta_\alpha(\epsilon)$, describing the scattering of bulk states of a certain representation α by the adparticle. This phase shift is defined by (Callaway, 1964, 1967)

$$\tan \delta_\alpha(\epsilon) = \frac{-\text{Im} D_\alpha(\epsilon)}{\text{Re} D_\alpha(\epsilon)}, \quad (5.10)$$

where D_α is the determinant

$$D_\alpha(\epsilon) = \det\{1 - \mathcal{G}^0(\epsilon)\Delta V\}_\alpha. \quad (5.11)$$

\mathcal{G}^0 is the Green's function of the bare substrate, and ΔV is the change in the potential due to the adsorbate

$$\Delta V = V^{\text{eff}}[n] - V^{\text{eff}}[n^0]. \quad (5.12)$$

The density of states, induced by the adparticle, is given by the derivative of the phase shift

$$\Delta N(\epsilon) = \frac{2d_\alpha}{\pi} \frac{d\delta_\alpha(\epsilon)}{d\epsilon}, \quad (5.13)$$

where d_α is the dimension of the representation α . A resonance in $\Delta N(\epsilon)$ will occur at an energy close to that at which the phase shift $\delta_\alpha(\epsilon)$ increases through $\pi/2$ with increasing energy, i.e., where the real part of the determinant D_α vanishes. Close to this energy, ϵ_α , the induced density of states takes a Lorentzian line shape

$$\Delta N(\epsilon) = \frac{d_\alpha \Delta_\alpha}{\pi} \frac{1}{(\epsilon - \epsilon_\alpha)^2 + (\Delta_\alpha/2)^2}. \quad (5.14)$$

The width of the resonance, Δ_α , is

$$\Delta_\alpha = \left[\frac{2\text{Im} D_\alpha(\epsilon)}{(d\text{Re} D_\alpha(\epsilon)/d\epsilon)} \right]_{\epsilon=\epsilon_\alpha}. \quad (5.15)$$

We note the close similarity between Eq. (5.14) and the Anderson-Grimley-Newns model of chemisorption (Grimley, 1975; Muscat and Newns, 1978, 1979). On the lower energy side of the resonance, the phase of the reflected wave is shifted such that electron density is accumulated in the region of the adparticle-substrate bond, indicating that these states are bonding in character. On the higher energy tail of the resonance, the electron density in the bond region is reduced, indicating that these states are antibonding in character (Lang and Williams, 1978; Liebsch, 1978). However, if the interaction with the substrate is very strong, bonding and antibonding states will split apart: A bound state (or resonance) is then formed below the substrate band, which is bonding in character, and a broad (antibonding) resonance will appear in the valence band (see also the discussion of Fig. 5.4 in Section 5.3.1).

5.2.2 Energies

We will assume that the dynamics of the electrons and the nuclei can be decoupled and that whatever the dynamics of the nuclei are, the electrons are in the electronic ground state of the instantaneous geometry. This is the Born-Oppenheimer approximation (Born and Oppenheimer, 1927; Born and Huang, 1954), which for adsorbates, and often also for chemical reactions, is well justified; for some reactions, and in particular for photo-chemistry, important violations of the Born-Oppenheimer approximation occur, but this is not the subject of this chapter. The *DFT total energy*, $E^{\text{total}}(T, V, N_A^{\text{nuc.}}, N_B^{\text{nuc.}}, \dots, \{\mathbf{R}_I\})$, at temperature T , volume V , and composition $N_A^{\text{nuc.}}, N_B^{\text{nuc.}}, \dots$, when studied as a function of the atomic coordinates, is often called the potential-energy surface (PES) because it defines the potential-energy landscape on which the nuclei A, B, \dots travel. It is related to an experimentally accessible quantity only in a restricted way: If, as is typically done, the self-consistent calculations are performed at constant volume, the *DFT total energy* corresponds to the Helmholtz free energy at zero temperature and neglecting zero-point vibrations. In general, the Helmholtz free energy is

$$\begin{aligned} F(T, V, N_A^{\text{nuc.}}, N_B^{\text{nuc.}}, \dots, \{\mathbf{R}_I\}) &= E^{\text{total}}(T, V, N_A^{\text{nuc.}}, N_B^{\text{nuc.}}, \dots, \{\mathbf{R}_I\}) \\ &+ E^{\text{vib.}}(T, V, N_A^{\text{nuc.}}, N_B^{\text{nuc.}}, \dots, \{\mathbf{R}_I\}) \\ &- T S(T, V, N_A^{\text{nuc.}}, N_B^{\text{nuc.}}, \dots, \{\mathbf{R}_I\}) \end{aligned} \quad (5.16)$$

with the vibrational contribution noted as $E^{\text{vib.}}$ and S is the entropy. At a given volume V , the atomic geometry of stable or metastable configurations is determined by

$$\left(\frac{\partial F(T, V, N_A^{\text{nuc.}}, N_B^{\text{nuc.}}, \dots, \{\mathbf{R}_I\})}{\partial \mathbf{R}_I} \right)_{T, V, N_A^{\text{nuc.}}, N_B^{\text{nuc.}}, \dots} = 0, \quad (5.17)$$

and for a given pressure p it is determined by

$$\left(\frac{\partial G(T, p, N_A^{\text{nuc.}}, N_B^{\text{nuc.}}, \dots, \{\mathbf{R}_I\})}{\partial \mathbf{R}_I} \right)_{T, p, N_A^{\text{nuc.}}, N_B^{\text{nuc.}}, \dots} = 0, \quad (5.18)$$

where

$$\begin{aligned} G(T, p, N_A^{\text{nuc.}}, N_B^{\text{nuc.}}, \dots, \{\mathbf{R}_I\}) &= F(T, V, N_A^{\text{nuc.}}, N_B^{\text{nuc.}}, \dots, \{\mathbf{R}_I\}) \\ &+ p V(T, p, N_A^{\text{nuc.}}, N_B^{\text{nuc.}}, \dots, \{\mathbf{R}_I\}) \end{aligned} \quad (5.19)$$

is the Gibbs free energy. If the system is in contact with a particle reservoir, for example, the sample is held in some gas phase, particles can be exchanged between the system and the reservoir. Then we have to add to Eq. (5.16) a term $-\sum_X \mu_X N_X^{\text{nuc.}}$, where μ_X is the atom chemical potential of atom-type X , which can be controlled by external reservoirs, i.e., by the environmental conditions (partial pressure and temperatur).

Later in this chapter we will study the *adsorption energy per adatom*. This is the difference of the total energy of the adsorbate system and the total energy of the clean substrate together with a corresponding number of free, neutral atoms. For *on-surface* adsorption this reads

$$E_{\text{ad}}^{\text{Na/Al(001)}} = - \left(E^{\text{Na/Al(001)}} - E^{\text{Al(001)}} - N_{\text{Na}}^{\text{nuc.}} E^{\text{Na-atom}} \right) / N_{\text{Na}}^{\text{nuc.}}, \quad (5.20)$$

where $E^{\text{Na/Al(001)}}$ is the total energy per adatom of the adsorbate system, $E^{\text{Al(001)}}$ is the total energy of the clean Al(001) substrate, and $N_{\text{Na}}^{\text{nuc.}} E^{\text{Na-atom}}$ is the total energy of $N_{\text{Na}}^{\text{nuc.}}$ free Na atoms that take part in the adsorption. We have used here as an example indices which refer to the adsorption of Na on Al(001), but translation to other systems is obvious.

Often adatoms are *not* adsorbed on the surface with only slight modification of the original surface structure, but instead adsorption may occur substitutionally. In this case the adatom kicks out an atom from the surface and takes its site. In thermal equilibrium the kicked out atom is then re-bound at a kink site at a step (the binding energy at a kink site equals the bulk cohesive energy, which is shown in the next section).

For substitutional adsorption, the adsorption energy is defined essentially the same way as above, only that the kicked off surface atoms that are re-bound at kink sites, have to be accounted for as well. Each rebound kicked out atom contributes an energy equal to that of a bulk atom (see Section 5.2.3). Thus, for the substitutional adsorption the adsorption energy is

$$E_{\text{ad}}^{\text{Na/Al(001)-sub}} = - \left(E^{\text{Na/Al(001)-sub}} + N_{\text{Na}}^{\text{nuc.}} E^{\text{Al-bulk}} - E^{\text{Al(001)}} - N_{\text{Na}}^{\text{nuc.}} E^{\text{Na-atom}} \right) / N_{\text{Na}}^{\text{nuc.}}. \quad (5.21)$$

$E^{\text{Al-bulk}}$ is the energy of an atom in a bulk crystal of aluminum and the quantity $E^{\text{Na/Al(001)-sub}}$ in Eq. (5.21) is the total energy of the slab with the adatoms adsorbed in substitutional sites.

We end this section with a warning that may be relevant for *Surface Science* studies more often than typically appreciated. The energy quantities defined in this section are relevant if thermal equilibrium conditions are attained, but often this is not the case. Instead, a surface is studied which may be in a metastable state and this state hopefully corresponds to an equilibrium situation of the sample's history (at best). This somewhat unclear situation will hopefully improve in the future, when not just UHV studies are performed but also experiments under well controlled atmospheres. We also note that structures in *local* thermodynamic equilibrium, or metastable geometries can have a very long life time – just consider diamond (a metastable structure of carbon) for which at room temperature the phase transition to its ground-state crystal structure (graphite) is known to be rather slow. In particular, for multi-component materials, the stoichiometry at the surface requires exchange of atoms or molecules with some reservoirs and this can be hampered by significant energy barriers. Metal oxides represent an example which comes to mind, as in UHV, oxygen can desorb into the chamber, but with respect to the metal content at the surface, attaining the thermal-equilibrium stoichiometry is hampered (see, e.g., Wang et al., 1998).

5.2.3 Binding energy at kink sites

As mentioned above, kicked out surface atoms may be re-bound at kink sites at steps. We will see that this is in particular relevant when we discuss below in this chapter the substitutional adsorption of alkali metals atoms and of cobalt. Therefore we now present a simple discussion of the energetics of substrate atoms at kink sites. Although we use a simplified model, we note that the conclusions are in fact valid in general.

The total energy of a many-atom system can be written as the sum over contributions assigned to the individual atoms,

$$E = \sum_{I=1}^{N^{\text{nuc.}}} E_I. \quad (5.22)$$

E_I is the energy contribution due to atom I . In an approximate way we can write $E_I = E_I(C_I)$, where C_I is the number of nearest-neighbor atoms of atom I . This is a simplified presentation of an approach which has many names (e.g., effective-medium theory, embedded-atom method, Finnis-Sinclair potentials, glue model) and which we all call *bond-cutting models*. The various implementations are similar but differ in the way the function $E(C)$ is represented. In the simplest, yet physically meaningful approach, the function $E(C)$ is roughly proportional to \sqrt{C} (see Spanjaard and Desjonquères, 1990; Robertson et al., 1994; Payne et al., 1996; Methfessel et al., 1992b; Christensen and Jacobsen, 1992).

If we consider a single-element system and place an atom at a kink site at a step of an fcc (001) surface, the changes of the local coordination are as noted in Fig. 5.2. Putting this information into Eq. (5.22) and calculating the *change* in the total energy by placing an atom ($I = 1$) at a kink site (i.e., $E_{\text{ad}}^{\text{kink}} = -E^{\text{after}} + E^{\text{before}}$) gives

$$\begin{aligned} E_{\text{ad}}^{\text{kink}} &= -(E_1(6) + E_2(7) + E_3(8) + E_4(10) + E_5(12) + E_6(11) + E_7(9)) \\ &\quad + E_1(0) + E_2(6) + E_3(7) + E_4(9) + E_5(11) + E_6(10) + E_7(8) \\ &= -E_5(12) + E_1(0). \end{aligned} \quad (5.23)$$

Thus, the adsorption energy at a kink site equals the cohesive energy. This result is in fact plausible if one considers that the adsorption at a kink site leaves the system essentially unchanged, because the kink site is simply moved by one atom and thus, the situation at the surface is physically not altered. Therefore the difference between the original and final situations is simply (and rigorously) the addition of one bulk atom, which has the energy $E(12)$.

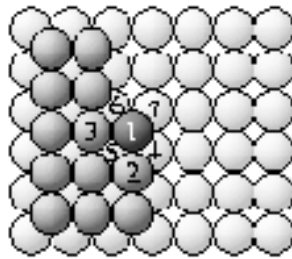


Figure 5.2: View of a kink site at a step on an fcc (001) surface. The local coordination of an atom (labeled 1) adsorbed at a kink site C_1 changed from 0 (that of the free atom) to 6. For its six neighbor atoms (labeled 2, 3, 4, 5, 6, 7) the coordination numbers are increased by one, thus attaining the values: $C_2 = 7$, $C_3 = 8$, $C_4 = 10$, $C_5 = 12$, $C_6 = 11$, $C_7 = 9$.

5.2.4 The surface energy barrier

We add some remarks on the behavior of the effective Kohn-Sham potential, V^{eff} (see Eq. (5.7) and Fig. 5.3). The increase in V^{eff} at the surface from its average bulk value up to the vacuum level is termed the surface barrier. Inside the solid, the potential V^{eff} seen by an electron becomes attractive, due to the electrostatic potential of the ion cores, due to the electrostatic field of the surface-dipole layer, and due to the lowering of the electron energy by the formation of an exchange-correlation hole. For an electron in the vacuum region, the potential is described by the classical image effect

$$V^{\text{eff}}(z) = -\frac{1}{4\pi\epsilon_0} \frac{(e^-)^2}{4(z-z_0)} \quad \text{for } (z-z_0) \gtrsim 2 \text{ \AA}, \quad (5.24)$$

where z is the position of the electron, z_0 is the position of the reference plane of the image effect, and ϵ_0 is the vacuum dielectric function. Figure 5.3 shows the electrostatic potential and the effective one-particle potential at an adsorbate-covered surface. Here, Φ is the work function, V^{es} is the electrostatic potential due to the electron density $n(\mathbf{r})$ and the nuclei, and V^{xc} is the exchange-correlation potential. The latter is attractive and varies roughly as $n(\mathbf{r})^{1/3}$. The only surface contribution to the total height of the surface barrier is due to the electrostatic potential; the contribution of the exchange-correlation term to the height is a property of the bulk and not of the surface.

Nevertheless, the behavior of the potential at the surface is largely determined by the distortion of the exchange-correlation hole which stays behind as an electron passes through the surface region into the vacuum. In the local-density approximation, the exchange-correlation hole is assumed to be spherically symmetric and centered on the electron. Although both assumptions are, in general, incorrect, this approximation affects the potential V^{eff} significantly

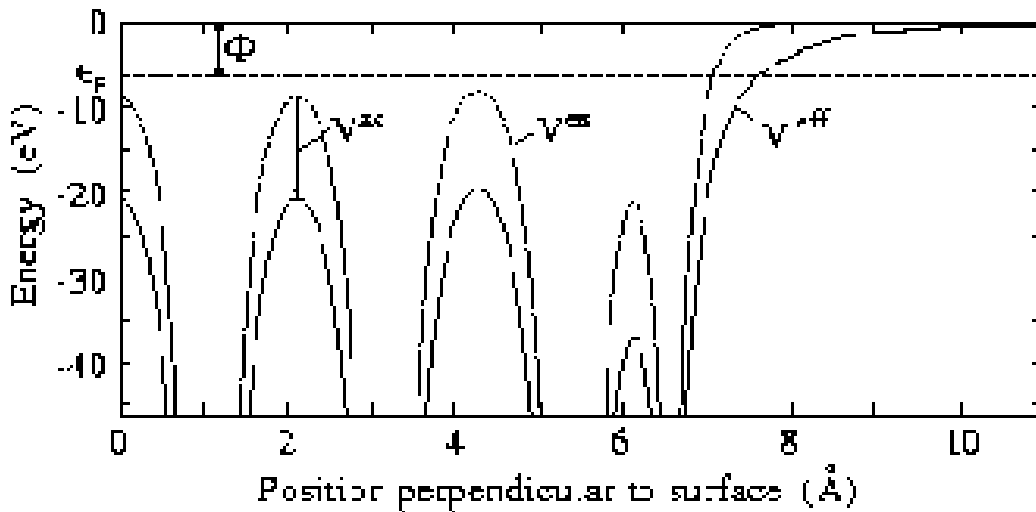


Figure 5.3: The Kohn-Sham effective potential V^{eff} (solid line) and the electrostatic potential V^{es} (broken line) at an adsorbate-covered surface. In the example, which shows results for O/Ru(0001), the electrostatic potential in the bulk is below the Fermi level, but for substrates with low electron density it will be above.

only in the surface region. The local-density approximation therefore yields an exponential decrease of the effective potential near the surface rather than the $1/z$ behavior of the image effect. This inaccuracy of the local-density approximation appears to become noticeable well outside the surface region in the vacuum. Properties such as the ground-state electron density, the work function, or the surface energy seem to be relatively little affected (see, e.g., Methfessel et al., 1992a, b). The detailed shape of the barrier thus appears to be of less importance than its position and height.

The barrier affects individual electron wave functions. For example, reflection of electrons from the inner side of the barrier can give rise to surface resonances when the electron is trapped between the barrier and the rest of the crystal. In particular, the barrier position influences the energies of adsorbate states. For excited states, there are additional effects. Virtual surface resonances will appear, which in LEED, for example, show up as narrow peaks in the intensity versus voltage curves (McRae, 1971; Jennings, 1979). Furthermore, the wavelength of an electron is longer outside the crystal than inside. This yields the well-known refraction effect which broadens the angular range of emitted electrons in the vacuum region such that, at high polar angles, the electron current vanishes (see, for example, Scheffler et al., 1978). Another effect is found in the interaction of light with the surface: Photoabsorption, and hence photoemission, require a gradient in the potential. The surface barrier thus yields a special contribution to this excitation, called the surface photoeffect. For photoemission from adsorbates on transition metals, this contribution appears to be very small compared to that due to the ion core potentials. However, it can be important in systems where the valence electrons are nearly free electron-like, i.e., where their interaction with the ion cores is small. For excited states, the inner potential will be modified (also becoming complex) due to inelastic electron-electron interactions such as the excitation of electron-hole pairs, plasmons or surface plasmons, and dynamical corrections (e.g., a delay in the response of the electrons).

5.3 The tight-binding picture of bonding

5.3.1 Adsorbate-substrate interaction

When an atom and a surface start to interact, the respective states mix and new states are created which have energy levels usually broadened and shifted with respect to the energy levels found in the uncoupled systems. Typically, the new states can still be related to the original ones, and Fig. 5.4 shows a schematic tight-binding description of the interaction of an atom with a transition metal surface. The free atom's electronic structure is noted in panel (b) of the figure, and the electronic structure of the substrate is sketched in panel (a). In principle we could choose any atom we like for this discussion, but for ease we take hydrogen. Therefore the two levels of relevance, which result from solving the Kohn-Sham equation are the hydrogen $1s$ and hydrogen $2s$ levels; for simplicity we neglect contributions from the H $2p$ and other higher-lying states. We note that the highest occupied DFT-LDA (and DFT-GGA) Kohn-Sham eigenvalue should not be confused with ionization energy (see the discussion of Fig. 5.5 and Eq. (5.25) below). Instead, for partially occupied valence states it is roughly at the mid value of the ionization and affinity energies.

Different transition-metal substrates mainly differ in the width of the d -band, which increases from $3d$ to $4d$ to $5d$; and they differ in the position of the Fermi level, which varies

from the left to the right of the periodic table as follows: For the 4*d* series it is at the lower edge of the *d*-band for strontium, just below the top of the *d*-band for palladium, and about 3 eV above the upper edge of the *d*-band for silver. Thus, in the example of Fig. 5.4 we use the Fermi level ϵ_F corresponding to palladium.

At first we consider the role of the substrate *s*-band. When the adsorbate and the substrate interact, the hybridization of the adsorbate wave functions and the states of the substrate *s*-band gives rise to a broadening of the adsorbate levels, and the atomic levels will shift because the substrate Fermi level and the electron chemical potential of the atom become aligned. The latter will result in a fractional electron transfer (see the discussion of Fig. 5.5 below). An analysis of the wave-function character in such a broadened peak shows that the low-energy part of the peak belongs to states which have an increased electron density between the adsorbate and the substrate (such states are called “bonding”), and the high-energy part of the peak belongs to states which have a node between the adsorbate and the substrate (such states are called “antibonding”). The substrate *s*-electrons spill out most into the vacuum, and that is why the broadening (and shifting) of electronic levels is the first change that happens when an atom is brought toward a surface. Broadening implies a coupling of the formerly localized electrons of the adatom to the substrate, thus a delocalization. In fact, still neglecting (for the moment) the interaction of the adatom with the *d*-band, there are three contributions which affect the adatom levels:

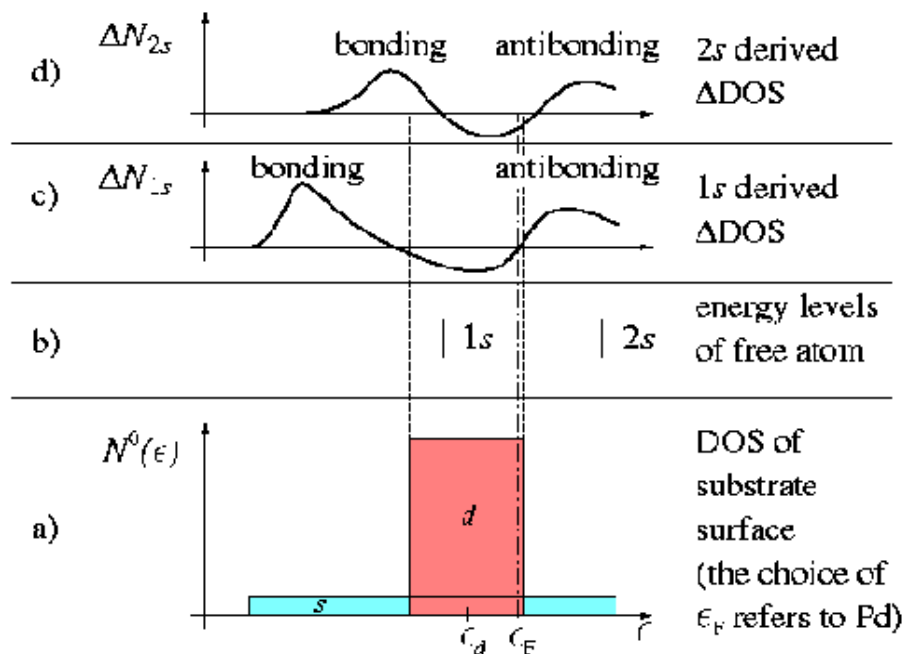


Figure 5.4: Formation of adsorbate-induced peaks in the DOS. The bottom panel (a) shows the density of states for a transition metal before adsorption (ϵ_d is the center of the *d*-band). Panel (b) shows the Kohn-Sham energy levels of a free atom (here as an example, H). The interaction between the H 1*s*-level and the substrate *s*- and *d*-bands gives rise to a broadening and the formation of an antibonding level (above the *d*-band) and a bonding level (below the *d*-band) – see panel (c). Panel (d) shows that the interaction between the H 2*s*-level with the substrate *s*- and *d*-bands gives rise to a broadening and the formation of a bonding level (at about the lower edge of the *d*-band) and an antibonding level (at about the empty free atom 2*s*-level).

- (i) A shift which can go in either direction and which is caused by charge transfer or charge redistribution (or polarization) at the adatom. For partially occupied valence states it largely reflects an alignment of the adsorbate DOS with respect to the substrate Fermi level.
- (ii) A shift toward lower⁴ energies because the potential at the surface is lower than that in vacuum (cf. Fig. 5.3 and/or Chapter 1 of this book).
- (iii) A contribution which implies a shift to lower⁴ energies because the self-interaction (an artifact in DFT-LDA and DFT-GGA calculations) is smaller for the more extended states of the adsorbate than for the states in the free atom.

These broadened and shifted energies are called “renormalized atomic levels”. The three contributions are indeed significant. As a consequence, a self-consistent treatment is crucial for calculating the adsorbate-substrate interaction.

We note that the self-interaction effect is indeed strong when DFT-LDA energy levels are studied. But in total-energy *differences* it nearly cancels out. This is demonstrated in Fig. 5.5, which shows the DFT-LDA eigenvalue for the atomic Na 3s-state as function of its occupation. For the neutral Na atom the occupation is 1 and the energy level is at -2.8 eV. The extent to which a Kohn-Sham energy eigenvalue ϵ_k reflects the ionization energy, which is the minimum energy to remove an electron from the k -th level, depends on how strongly the eigenvalue depends on the occupation number $f(\epsilon_k, T)$. If this dependence is negligible, then the negative of the energy eigenvalue equals the excitation energy. This is the density-functional theory analogue of Koopmans’ theorem in Hartree-Fock theory.

⁴Our wording is chosen as such that “higher energy” of a bound electronic state means closer to the vacuum level, i.e., with respect to Fig. 5.4 or 5.12 the energy is more to the right. Obviously, “lower energy” then refers to an energy more to the left in these figures.

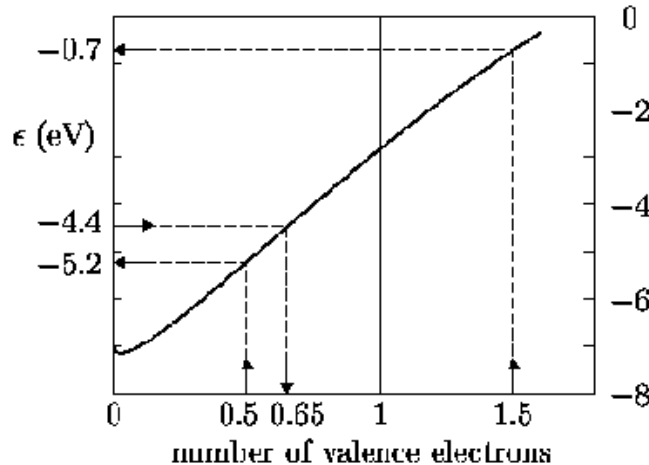


Figure 5.5: Kohn-Sham energy level (DFT-LDA) of the 3s-state of Na as function of the number of valence electron: $f_{3s} = 0$ is the Na^+ ion, $f_{3s} = 1$ is the neutral atom, and $f_{3s} = 2$ is the Na^- ion. For $f_{3s} = 0.5$ the eigenvalue gives the ionization energy (here 5.2 eV; the experimental result is 5.14 eV). For $f_{3s} = 1.5$ the eigenvalue gives the electron affinity (here 0.7 eV; the experimental result is 0.55 eV). If the eigenvalue were fixed by an electron reservoir to 4.4 eV, which is the Fermi level of Al(001), an occupation of 0.65 of the Na valence shell would result.

In general, the ionization energy (I_k) is defined by the total-energy difference of the neutral atom and the positively charged ion, and this can be read off from Fig. 5.5 as the energy at occupation 0.5. This approach only employs the mean-value theorem of integration

$$I_k = E^{N-1} - E^N = \int_N^{N-1} \frac{dE^{N'}}{dN'} dN' = - \int_0^1 \epsilon_k(f_k) df_k \approx -\epsilon_k(f_k = 0.5). \quad (5.25)$$

It is called the Slater-Janak transition-state approach of evaluating total-energy differences (Janak, 1978), which works very well in LDA and GGA calculations (for a discussion of the general proof see Perdew and Levy, 1997; Kleinman, 1997; and references therein). According to Fig. 5.5 the transition-state gives $I_k \approx 5.2$ eV, which agrees well with the experimental result for the ionization energy of 5.14 eV. Analogously we note that the highest occupied Kohn-Sham eigenvalue at occupation 1.0 agrees well with the mean value of the ionization and affinity energies.

The result shown in Fig. 5.5 is typical for all atoms. It demonstrates the importance of electron-electron correlation, though it is also largely due to self-interaction, an LDA artifact. Clearly, the measurable ionization energies (level at occupation 0.5) and the theoretical Kohn-Sham eigenvalue (level at occupation 1.0) are very different and should not be confused. Figure 5.5 also shows that typically only partial electron transfer is to be expected upon adsorption. If the substrate mainly plays the role of providing an electron reservoir, thus, the electron chemical potential is fixed by the substrate Fermi level, which for Al(001) is at 4.4 eV below the vacuum level, Fig. 5.5 then shows that the occupancy of the Na 3s-level will be adjusted to 0.65. Thus we obtain a partial ionization and a shift of the Na 3s-level, already from a study of the free-atom eigenvalue. This is fully in accord with what is suggested by the electronegativities of the atoms: $\kappa_{\text{Na}} = 0.93$ and $\kappa_{\text{Al}} = 1.61$.

We continue the discussion of Fig 5.4. At close distances of the adsorbate to the surface the *renormalized atomic levels* [i.e., the levels which result after the effects (i), (ii), and (iii)] will interact with the more localized *d*-states. Because the *d*-band is rather narrow and its width comparable to the interaction strength, the interaction will result in a splitting into the bonding states, $\psi_b \approx (\varphi_{\text{H}1s} + \varphi_{\text{Pd}4d})$ and the antibonding states, $\psi_a \approx (\varphi_{\text{H}1s} - \varphi_{\text{Pd}4d})$. The resulting adsorbate-induced density of states (DOS) for the H 1s-state is shown in panel (c) of Fig. 5.4. Panel (d) shows the corresponding result induced by the H 2s state. We note that the resulting peaks are close to the lower and upper edge of the *d*-band and inside the *d*-band the density is reduced, which simply reflects the fact that these states are shifted from inside the *d*-band to higher and lower energy upon hybridization with the adsorbate states.

Obviously, the bonding is strongest when bonding states are occupied and antibonding states remain empty. According to Fig. 5.4 this will happen when the Fermi level is in the middle of the *d*-band, as for example for Mo and Ru substrates.

Figure 5.6 describes the same physics as Fig. 5.4, but with an additional simplification: Now the broadening due to the substrate *s*-band is ignored and the *d*-band is replaced by just a single level, the *d*-band center. The energy levels of the “free” adatom are in fact the “renormalized levels”, and therefore we tagged them in Fig. 5.6 with a tilde: $1\tilde{s}, 2\tilde{s}$.

Deepening this discussion we show in Fig. 5.7 results of actual calculations where the distance dependence of the broadening and shift of the energy level is displayed for two qualitatively different systems: Na on Al(001) and O on Ru(0001). For both adatoms, Na and O, the ionization energy of the free atoms is below the Fermi level. In fact, the relevant

“energy level” to be considered is not the ionization energy and also not the electron affinity, but the mean value of those two (or alternatively, the Kohn-Sham eigenvalue of the highest occupied state; cf. the discussion above). This mean value is plotted in Fig. 5.7: For the Na atom it is at $(5.1+0.5)/2 \text{ eV} = 2.8 \text{ eV}$ and for the O atom it is at $(13.6+1.4)/2 \text{ eV} = 7.5 \text{ eV}$ below vacuum. When the adatoms approach the surface, the substrate Fermi level acts as an electron reservoir. For Na this implies a partial charge transfer from the adsorbate to the substrate (see the discussion of Fig. 5.5 above). But for oxygen, with its initially rather deep level, this implies a partial charge transfer from the substrate to the adatom. Upon close approach these partially ionized atoms interact with the substrate orbitals. For Na/Al(001) the DFT-LDA calculations predict a double peak structure, which has its main weight above the Fermi level, but with a tail reaching into the occupied states regime. For O/Ru(0001) the interaction is stronger because the adatom’s equilibrium position is very close to the surface and the substrate d -states impart a strong covalent bond and a splitting into bonding and antibonding states. The left panel of Fig. 5.7 nicely reflects the Gurney description of alkali-metal adsorption, and the right panel of Fig. 5.7 displays the corresponding result for an “opposite” adsorbate, namely one with high electronegativity and a strong covalent adsorbate-substrate interaction.

The adsorbate-induced DOS (as shown in Fig. 5.4c, d) enables us to decide on the nature of the bond. Assuming that the antibonding states are at least partially empty we have chemical bonding of either covalent or ionic character. When the states of the occupied peak are predominantly derived either from adsorbate or substrate orbitals the bonding character is called “ionic”. When the wave-function character of the occupied states is derived by about the same amount from the substrate and the adsorbate the bond is called “covalent”. The problem with this classification is in the assumption that a substrate and an adsorbate region can be defined and separated. However, for strong chemisorption situations it is typically not obvious how to assign electron density to the different atoms. Still the concepts are valuable and we will come back to them in Section 5.4. We note in passing that an intriguing way to

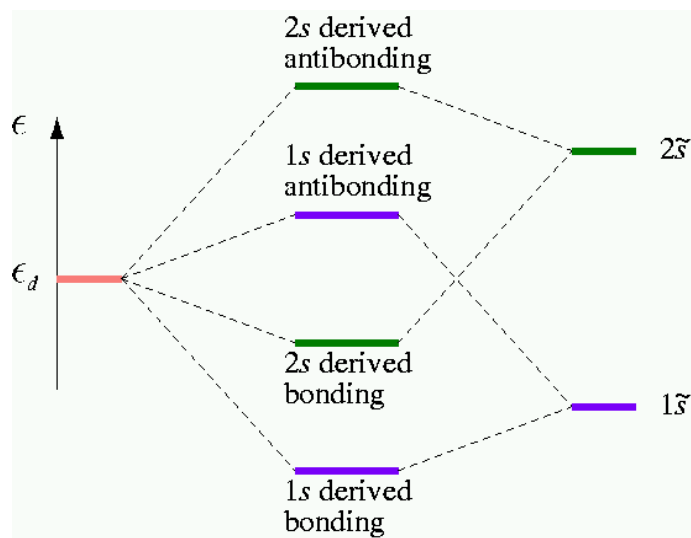


Figure 5.6: Schematic summary of the content of Fig. 5.4. Left: the d -band-center energy of the clean substrate. Right: the *renormalized energy levels* of the free atom (i.e., after interaction with the s -band, but before interaction with the d -band). Middle: the resulting bonding and antibonding H $1s$ - and H $2s$ -derived levels on adsorption.

assign electron density to individual atoms in a many-atom system was developed by Bader (1990, 1994, and references therein), but it is only now that these concepts are being used in solid-state calculations.

The concept behind the qualitative discussion presented in this section is essentially that of the Anderson-Grimley-Newns model for chemisorption (see, for example, Nørskov, 1990; Spanjaard and Desjonquères, 1990). The main difference is that free-atom levels are replaced by *renormalized* levels, that we have not introduced a restrictive assumption about electron correlation and the localization of the adsorbate-substrate interactions, and that we kept the discussion at a qualitative level. We believe that the approach sketched in Figs. 5.4, 5.6 is useful but should not be overinterpreted. It was used, for example, for a qualitative discussion of H_2 dissociation at transition metal surfaces (see Hammer and Scheffler, 1995; and Section 5.9). Nørskov et al. (see Hammer and Nørskov, 1997, and references therein) refined the approach and used it for a (semi-) quantitative discussion of adsorption at various transition metal surfaces. The results confirm the simple chemical picture that adsorption energies decrease with the d -band filling of the substrate (for $N_d \geq 5$). And when the d -band is full, the d -electrons only play little role; thus the adsorption energy is small, chemical activity is low, and the substrate is called noble. In fact, Hammer and Nørskov recently performed extensive DFT calculations of atomic and molecular adsorption at several metal surfaces and then used the above described approach to explain the main trends of bonding to metal surfaces in terms of the d -band filling. The crucial term in their approach is the adsorbate-substrate coupling matrix element. The latter depends on the adsorbate geometry (site and interatomic distances); unfortunately, but also quite obviously, this cannot be obtained from a simple Anderson-Gimley-Newns type of description.

As a warning remark we add that energy levels and the density of states, $N(\epsilon)$, are important ingredients of the total energy, but from the total-energy contribution

$$E^{\text{bands}} = \int_{-\infty}^{+\infty} f(\epsilon) N(\epsilon) \epsilon d\epsilon, \quad (5.26)$$

it is typically not possible to decide on the strength of chemical bonding. The situation

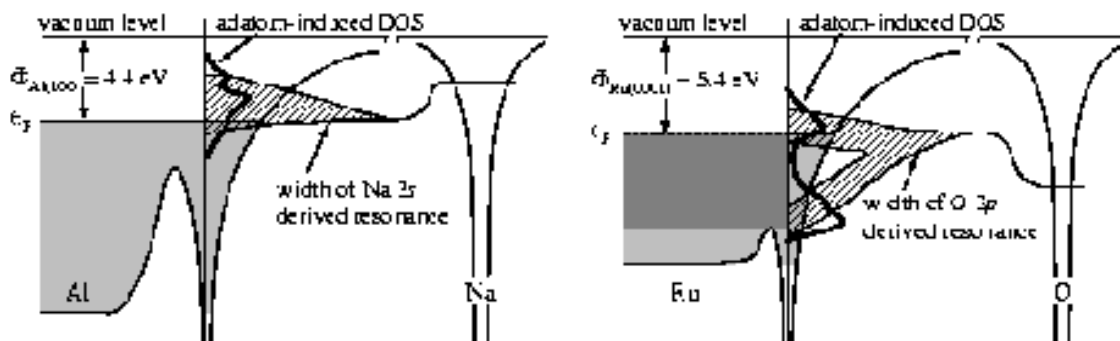


Figure 5.7: Side view of the surface, and the adsorbate-induced change in the density of states as a function of distance. Two chemically distinct systems are displayed. Left: Na on Al(001). Right: O on Ru(0001). The dark gray region in right figure marks the occupied part of d band of the Ru substrate. The energy levels noted for the atoms are the mean values of the ionization energy and electron affinity (Na: 2.8 eV, O: 7.5 eV), see text for details.

is different, when different geometries are compared and a frozen-potential approximation applied (the Andersen-Pettifor force theorem), as then (and only then) the other terms in the DFT total-energy expression cancel and *energy differences* based on Eq. (5.26) may give an approximate description (see Skriver, 1985, and references therein). In this context we note that many-atom systems tend to assume a geometry with an electron density as hard as possible, which means that either a band gap is opened or the density of states at the Fermi level is reduced. This may be viewed as a generalization of the Jahn-Teller theorem. In this sense $N(\epsilon)$, in particular its behavior at the Fermi level, is instructive.

5.3.2 Adsorbate band structure

To discuss covalent interactions between adparticles on a surface, we consider an ordered adlayer which is in registry with a crystalline substrate. Such a system has two-dimensional translational symmetry and the eigenfunctions are two-dimensional Bloch states which are defined by their reduced \mathbf{k}_{\parallel} -vector (in the surface Brillouin zone) as well as by their energy. Figure 5.8 shows the surface Brillouin zones for the clean surface and for a $c(2 \times 2)$ adsorbate overlayer on the (001) face of an fcc metal. To obtain the bulk band structure projected onto the surface of a clean semi-infinite system, it is necessary to integrate over k_z inside the bulk Brillouin zone and to shift regions outside the first two-dimensional Brillouin zone into its interior by a reciprocal lattice vector of the (two-dimensional) surface structure. This folding back of the \mathbf{k}_{\parallel} -resolved density of states of a clean, unreconstructed surface is indicated in Fig. 5.9a. The broken lines show the projection of the bulk Brillouin zone. Even for the clean surface, it is found that the surface Brillouin zone is usually smaller than the projection of the three-dimensional bulk Brillouin zone on the surface. For a periodic adlayer at fractional coverage, the surface Brillouin zone is further reduced compared with the clean surface, which again requires a shift of the \mathbf{k}_{\parallel} -resolved density of states of regions outside the new surface Brillouin zone into its interior, as shown in Fig. 5.9b. Because the back-folded density of states adds to the original one, the change in the \mathbf{k}_{\parallel} -resolved density of states is obviously quite large. We note, however, that this folding back is a purely mathematical effect. It takes into account the increase of the periodicity parallel to the surface but it is independent of the strength and the type of the physical mechanism causing this change in periodicity. The

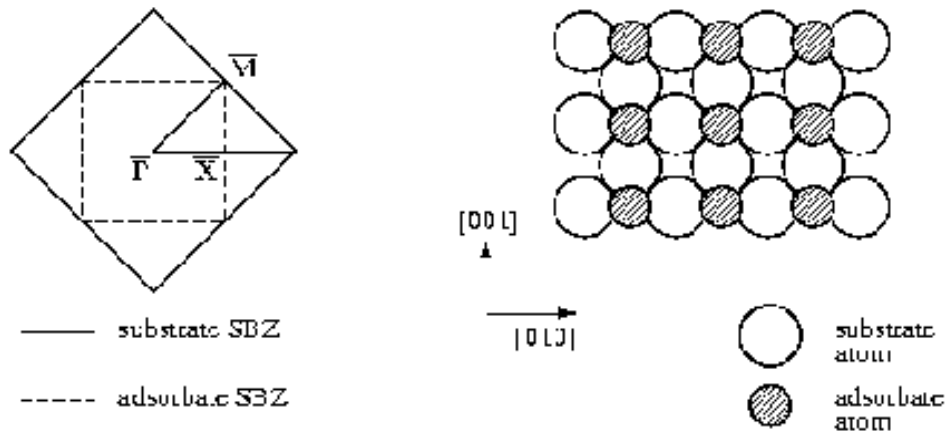


Figure 5.8: The surface Brillouin zones (SBZs) and real-space lattice of a $c(2 \times 2)$ adlayer on an fcc (001) surface. The lettering of the symmetry points refers to the adsorbate SBZ.

physical importance of this effect, i.e., the degree of the mixing of the wave functions involved in the surface region and in turn the question how strongly this effect will affect, for example, photoemission spectra, depends on the strength of the adsorbate-substrate interaction. We return to this back-folding effect in the discussion of Figs. 5.19 and 5.20 of Section 5.5.4 below.

The dispersion $\epsilon(\mathbf{k}_{\parallel})$ of the chemisorption-induced bands can be described in a simple tight-binding picture. It is appropriate to use a LCMO (linear combination of molecular orbitals) description where the MOs contain the interaction with the substrate as well as the intra-adsorbate mixing of wave functions. Because this method is very simple and gives a reasonable qualitative description, we consider it in more detail. Two-dimensional Bloch states are used as a basis

$$\chi_{\alpha}(\mathbf{r}, \mathbf{k}_{\parallel}) = \frac{1}{\sqrt{N^{\text{nuc.}}}} \sum_{\mathbf{R}_I}^{N^{\text{nuc.}}} e^{i\mathbf{k}_{\parallel} \mathbf{R}_I} \phi_{\alpha}(\mathbf{r} - \mathbf{R}_I), \quad (5.27)$$

where α labels the different (molecular) orbitals ϕ in the unit cell. The \mathbf{R}_I are two-dimensional lattice vectors. The wave functions of the system are thus given by

$$\varphi(\epsilon, \mathbf{k}_{\parallel}, \mathbf{r}) = \sum_{\alpha} C_{\alpha}(\epsilon, \mathbf{k}_{\parallel}) \chi_{\alpha}(\mathbf{r}, \mathbf{k}_{\parallel}). \quad (5.28)$$

For the Hamilton matrix we find

$$H_{\alpha, \alpha'}(\mathbf{k}_{\parallel}) = \langle \chi_{\alpha}(\mathbf{k}_{\parallel}) | H | \chi_{\alpha'}(\mathbf{k}_{\parallel}) \rangle = \sum_{\mathbf{R}_I}^{N^{\text{nuc.}}} e^{i\mathbf{k}_{\parallel} \mathbf{R}_I} H_{\alpha, \alpha'}(\mathbf{R}_I) \quad (5.29)$$

with

$$H_{\alpha, \alpha'}(\mathbf{R}_I) = \langle \phi_{\alpha}(\mathbf{r}) | H | \phi_{\alpha'}(\mathbf{r} - \mathbf{R}_I) \rangle. \quad (5.30)$$

Because the basis 5.27 is usually not orthogonal, we get an overlap matrix

$$S_{\alpha, \alpha'}(\mathbf{k}_{\parallel}) = \langle \chi_{\alpha}(\mathbf{k}_{\parallel}) | \chi_{\alpha'}(\mathbf{k}_{\parallel}) \rangle = \sum_{\mathbf{R}_I}^{N^{\text{nuc.}}} e^{i\mathbf{k}_{\parallel} \mathbf{R}_I} S_{\alpha, \alpha'}(\mathbf{R}_I) \quad (5.31)$$

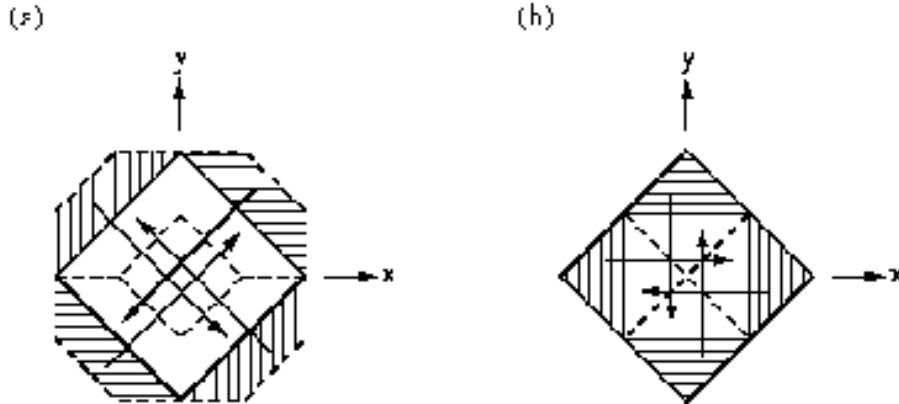


Figure 5.9: (a) The relation between the surface Brillouin zone (full line) and the projection of the bulk Brillouin zone of an fcc substrate onto the (001) surface (broken line). Hatched regions have to be shifted by a surface reciprocal lattice vector into the first surface Brillouin zone, as indicated by arrows. (b) Surface Brillouin zone for the c(2 × 2) adsorbate layer, showing shift of hatched regions by (adsorbate) reciprocal lattice vectors.

with

$$S_{\alpha,\alpha'}(\mathbf{R}_I) = \langle \phi_\alpha(\mathbf{r}) | \phi_{\alpha'}(\mathbf{r} - \mathbf{R}_I) \rangle. \quad (5.32)$$

The Schrödinger equation is then

$$\sum_{\alpha'} \left\{ \sum_{\mathbf{R}_I}^{N_{\text{nuc.}}} e^{i\mathbf{k}_{\parallel} \cdot \mathbf{R}_I} [H_{\alpha,\alpha'}(\mathbf{R}_I) - \epsilon(\mathbf{k}_{\parallel}) S_{\alpha,\alpha'}(\mathbf{R}_I)] \right\} C_{\alpha'}(\epsilon, \mathbf{k}_{\parallel}) = 0 \quad (5.33)$$

and must be solved at each \mathbf{k}_{\parallel} . The zeros of the determinant of the matrix in the curly brackets in Eq. (5.33) give the dispersion $\epsilon(\mathbf{k}_{\parallel})$. The required matrix elements $H_{\alpha,\alpha'}(\mathbf{R}_I)$ and $S_{\alpha,\alpha'}(\mathbf{R}_I)$ can be calculated numerically in some approximation (Bradshaw and Scheffler, 1979; Horn et al., 1978; Scheffler et al., 1979; Jacobi et al., 1980). Often, an empirical tight-binding calculation might be sufficient, which introduces the following three assumptions: (1) Orbitals ϕ_α at different centers are orthogonal, the overlap matrix $S_{\alpha,\alpha'}(\mathbf{R}_I)$ is thus equal to one for $\alpha = \alpha'$ and $\mathbf{R}_I = (0, 0)$ and zero otherwise. (2) Only nearest neighbors (sometimes also second nearest neighbors) are taken into account in the sum over \mathbf{R}_I in Eq. (5.33). (3) The matrix elements are fitted to experimental results; usually there are only very few remaining.

We will illustrate this for the example of an adsorbate with s -like states in a $c(2 \times 2)$ overlayer on an fcc (001) surface (p_z -like states would behave the same way). The corresponding adsorption-induced MOs ϕ_α belong to the a_1 representations of the C_{4v} point group (we assume that the adsorbate occupies a fourfold symmetric site). We then have two parameters in Eq. (5.33): $H_{a_1,a_1}(0)$ and $H_{a_1,a_1}(\mathbf{R}_I)$. Figure 5.10 shows schematically the Bloch states according to Eq. (5.27) for the three high symmetry points of the surface Brillouin zone (see Fig. 5.8)

$$\bar{\Gamma} : \mathbf{k}_{\parallel} = (0, 0), \quad \bar{X} : \mathbf{k}_{\parallel} = \frac{g}{2}(1, 0), \quad \bar{M} : \mathbf{k}_{\parallel} = \frac{g}{2}(1, 1), \quad (5.34)$$

where g is the length of the first two-dimensional reciprocal lattice vector of the adlayer. Figure 5.10 has been constructed by placing orbitals of s -like symmetry at all the atoms (or molecules) of the adlayer (only 9 of them are shown in the figure). The phase factors of

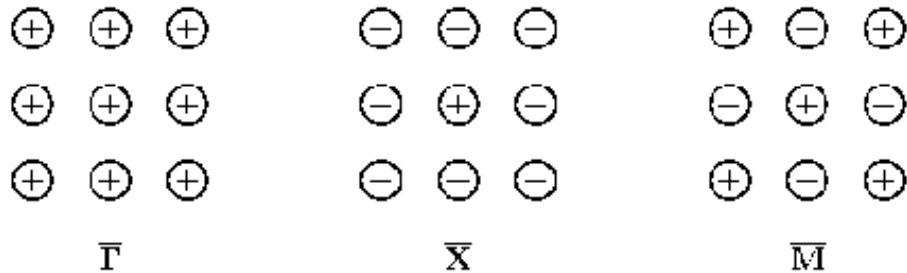


Figure 5.10: Top view of a schematic representation of the two-dimensional Bloch states formed from atomic or molecular orbitals belonging to the a_1 representation of the C_{4v} point group (s -like orbitals) at the high-symmetry points of the surface Brillouin zone (see Fig. 5.8 and Eq. (5.34)). We display a region of 9 adatoms. The sign of the orbital in the center \mathbf{R}_0 is chosen +, and the signs of other orbitals are then $e^{i\mathbf{k}_{\parallel} \cdot (\mathbf{R}_I - \mathbf{R}_0)}$ with \mathbf{k}_{\parallel} defined by Eq. (5.34).

orbitals at different sites is $e^{i\mathbf{k}_{\parallel}\mathbf{R}_I}$ corresponding to the appropriate \mathbf{k}_{\parallel} -point in the surface Brillouin zone. An analysis of this figure already yields the qualitative band structure. At $\bar{\Gamma}$ the a_1 -derived two-dimensional Bloch state is completely bonding in the adlayer, giving this state the lowest energy. At $\bar{\text{M}}$ it is completely antibonding (highest energy), and at $\bar{\text{X}}$, it is of mixed character. Thus, s -like adsorbate states give rise to an energy band which has the lowest energy at $\bar{\Gamma}$ and the highest energy at $\bar{\text{M}}$. The analogous discussion for p_x -, p_y -like states can be found in an earlier review article by Scheffler and Bradshaw (1983).

To discuss the interaction of an adsorbate with the s -band of the substrate, we consider in Fig. 5.11 as an example the adsorption of oxygen on jellium corresponding to a (1×1) overlayer on Al(111) (Hoffmann et al., 1979), which has been calculated using the two-dimensional KKR method (Kambe and Scheffler, 1979). The crystallographic point group is C_{6v} because the jellium model neglects the atomic structure of the substrate. Full lines show the center of the peaks; hatched regions indicate the width of the peaks. The strong dispersion of the levels is quite apparent. The width of the band structure (the dispersion of the full lines) indicates the extent of the splitting between states which are bonding with respect to neighboring adparticles and those which are antibonding, just as in the case of the tight-binding scheme discussed above. At $\bar{\Gamma}$ the p_x - and the p_y -derived Bloch states are degenerate because of the C_{6v} symmetry and the splitting between the p_z - and p_x, p_y -derived states is very small. The O $2p_z$ -induced level is broad but that derived from p_x, p_y is sharp. This different behavior of the two levels can be explained in the following way. For an ordered overlayer in registry with the substrate, two-dimensional Bloch states of the overlayer can only hybridize with those of the substrate which have the same \mathbf{k}_{\parallel} vector. The resulting wave functions inside the jellium can thus be given as a sum over plane waves propagating toward the surface and the reflected waves.

$$\varphi(\epsilon, \mathbf{k}_{\parallel}, \mathbf{r}) = \sum_{\mathbf{g}} U_{\mathbf{g}}^+ e^{i\mathbf{k}_{\mathbf{g}}^+ \cdot \mathbf{r}} + U_{\mathbf{g}}^- e^{i\mathbf{k}_{\mathbf{g}}^- \cdot \mathbf{r}}. \quad (5.35)$$

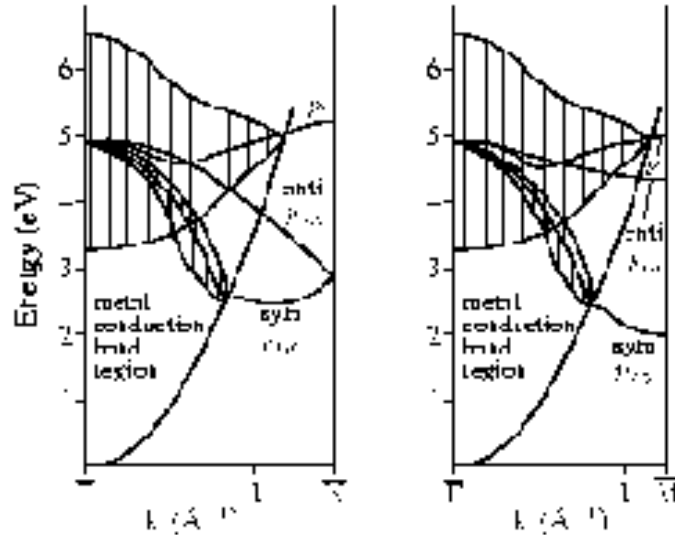


Figure 5.11: Calculated band structure for a hexagonal (1×1) oxygen layer on a jellium substrate, simulating the Al(111) surface. Reproduced after Hoffmann et al. (1979).

Because the potential is constant inside the jellium, the \mathbf{k}_g^\pm -vectors of these plane waves are given by

$$\mathbf{k}_g^\pm = \left(\mathbf{k}_\parallel + \mathbf{g}, \pm \sqrt{\frac{2m(\epsilon - V_0)}{\hbar^2} - (\mathbf{k}_\parallel + \mathbf{g})^2} \right), \quad (5.36)$$

where \mathbf{g} are reciprocal lattice vectors of the (two-dimensional) surface Brillouin zone. Obviously, for $\mathbf{k}_\parallel = (0, 0)$ and a wave function which is antisymmetric with respect to a mirror plane of the system, the coefficients $U_{(0,0)}^+$ and $U_{(0,0)}^-$ vanish. At energies close to the bottom of the conduction band of the substrate, all the remaining terms have an imaginary value for k_z , which implies that these states decay exponentially normal to the surface. These are true surface states and have a sharp energy. In other words, we could say that at the bottom of the band the substrate states are *s*-like and thus do not have the correct symmetry in order to hybridize with *p_x*, *p_y*-like adsorbate levels at $\mathbf{k}_\parallel = (0, 0)$. Only at higher energies could these states also couple to bulk bands and broaden. Figure 5.11 also shows that the levels change their width with \mathbf{k}_\parallel and become discrete when they lie outside the metal conduction band. We note the behavior of the symmetric *p_x*, *p_y*-derived band at the point at which it begins to hybridize with the substrate wave functions: just outside the metal conduction band region it bends slightly to lower⁴ energies. Here it is purely bonding in character. At the same \mathbf{k}_\parallel value, we note that the corresponding antibonding (broad) level occurs in the conduction band. When the band enters the conduction band, the bonding and the antibonding levels form one broad peak as mentioned above.

5.4 Adsorption of isolated adatoms

Calculations of isolated adatoms afford an analysis of the nature of the adsorbate-substrate bond without it being obscured by the influence of other adsorbates. In this section we will therefore summarize characteristic results of the adsorption of isolated atoms.

The calculations presented in the remaining part of this section were performed with the Green-function method, which provides the most accurate and efficient approach for calculating properties of truly isolated adatoms on extended substrates. For technical details of the method we refer the interested reader to the original papers (see in particular Bormet et al., 1994a; Lang and Williams, 1978; Bormet et al., 1994b; Wenzien et al., 1995; Scheffler et al., 1991; and references therein).

We consider group I, group IV, and group VII adsorbates, namely Na, Si, and Cl. By such a trend study of atoms from the left to the right side of the periodic table, a classification of the nature of the bond becomes rather clear, but we will also emphasize (again) the limitation and/or danger of “nature-of-bond” concepts. Three different substrates will be considered, namely,

- jellium with an electron density corresponding to aluminum,
- Al(111),
- Cu(111),

which enables us to identify the role of substrate *s*-, *p*-, and *d*-states. For the Al(111) and Cu(111) systems the adsorbates were placed in the fcc-hollow site. In this section we discuss

on-surface adsorption; substitutional adsorption, where the adatom replaces a surface atom, will be treated in Section 5.6, and subsurface adsorption will be briefly touched upon in Section 5.10.

5.4.1 Geometry

Table 5.1 gives the adsorbate heights Z and effective radii R of the adsorbates, as obtained from the distances between the adatom and its nearest-neighbor substrate atoms, using the substrate atomic radii from the bulk. Both the calculated heights and the effective radii (the bond length is given by the sum $R + R_{\text{Al}}$ or $R + R_{\text{Cu}}$) are found to be noticeably smaller for Al(111) than for the jellium substrate. This is due to the fact that jellium is devoid of any information concerning the atomic structure. Thus, the shell-like property of electrons, i.e., their s -, p -, d -like character is missing which hinders the formation of directional orbitals in the substrate; and aluminum, despite its reputation of being a jellium-like system, is in fact a material with noticeable ability for covalent bond formation. On comparison of the results for adsorption on the Cu and Al substrates, it is found that the trend from jellium to aluminum continues: The effective radius of the studied adsorbates on Cu(111) is smaller than on Al(111). The smaller values reflect that bonding of the adsorbates is stronger on Cu(111) than on Al(111), which was identified as being due to the Cu d -electrons (Yang et al., 1994); although the top of the Cu d -band is about 2 eV below the Fermi level, the d -states play a noticeable role.

The results demonstrate that stronger bonds go together with shorter bondlengths. As noted above in Table 5.1 we considered a threefold coordinated adsorption site. For other sites with lower coordination the strength per individual bond will typically increase, because the same number of adsorbate electrons have to be distributed (by tunneling or hopping) over fewer bonds. As a consequence, the bond length will typically decrease. This does not mean that the binding energy will increase as well, because this is determined by *all* bonds. This correlation between local coordination and bond strength, and the correlation between bond

Substrate	Na			Si			Cl		
	Z (Å)	R (Å)	$\Delta R/R_J$	Z (Å)	R (Å)	$\Delta R/R_J$	Z (Å)	R (Å)	$\Delta R/R_J$
Jellium	2.79	1.82	0	2.37	1.46	0	2.52	1.59	0
Al(111)	2.69	1.73	-5%	1.95	1.13	-22%	2.09	1.24	-22 %
Cu(111)	2.43	1.56	-14%	1.68	0.96	-34%	1.78	1.03	-35 %

Table 5.1: Calculated geometrical parameters for adsorbed atoms from the left to the right side of the periodic table, and for different substrates. The height Z is defined with respect to the center of the top substrate layer. The effective radii of the adatoms R are evaluated by subtracting from the calculated bond lengths the radius of a substrate atom (as given by the inter-atomic distances in the bulk). Thus, we use $R_J = R_{\text{Al}} = 1.41$ Å and $R_{\text{Cu}} = 1.27$ Å. For the jellium substrate we assume the geometry of Al(111). Also noted as a percentage is the difference of the adatom radii with respect to that of the jellium calculation: $(R_J - R)/R_J$. The jellium results are from Lang and Williams (1978), the Al(111) results are from Bormet et al. (1994a), and the Cu(111) results are from Yang et al. (1994).

strength and bond length is well known (see, e.g., Pauling, 1960; Methfessel et al., 1992a). But we also emphasize that when significant changes in hybridization occur for different geometries, and/or when the system cannot attain the geometry of optimum bond angles, this simple picture breaks down.

5.4.2 Density of states $\Delta N(\epsilon)$

As emphasized in Sections 5.1.1, 5.2.1, and 5.3, inspection of the adsorbate-induced change in the density of states $\Delta N(\epsilon)$ is particularly informative. Together with the knowledge of the position of the Fermi energy, it tells us whether the electronic states which are formed upon adsorption are occupied, unoccupied, or partially occupied, and this enables us to discern the nature of the chemical bond. Figures 5.12a and b show such results for adsorbates on Al(111) and on jellium. The adsorbates investigated in the work of Bormet et al. (1994a) (Fig. 5.12a) were Na, Si, and Cl, and in that of Lang and Williams (1978) (Fig. 5.12b) they were Li, Si, and Cl. The results of both of these calculations agree qualitatively and show the following: For both alkalis (Na and Li) the adsorbate resonance lies well above the Fermi level and is thus largely unoccupied. This indicates that the valence electron of the alkali metal

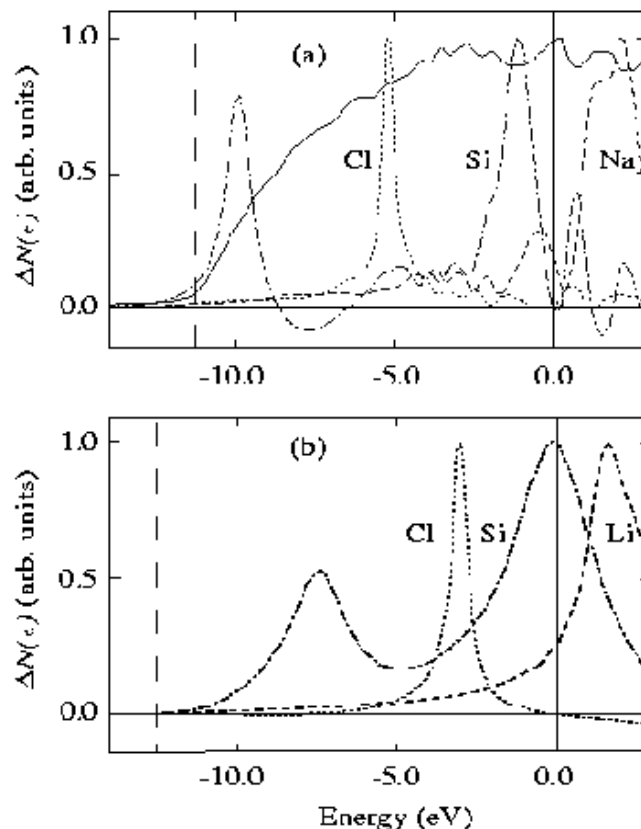


Figure 5.12: Adsorbate-induced change of the density of states (cf. Eq. (5.8)) for three different adatoms (group I, IV, and VII of the periodic table) on an Al(111) substrate (top: a) and on jellium with an electron density corresponding to Al (bottom: b). For the Al substrate also the bulk density of states is displayed (the full line in figure a). The results are from Bormet et al., 1994a (top), and from Lang and Williams, 1978 (bottom). The Fermi level ϵ_F is at the energy equal to zero. The vertical dashed line indicates the bottom of the band of the substrate.

atom (or part thereof) has been transferred to the substrate and the adatom is partially positively charged. In an opposite manner, on adsorption of chlorine, the resonance in the curve corresponding to the Cl $3p$ resonance lies 5 eV below the Fermi level, and the Cl $3s$ peak is positioned even below the substrate valence band at about -18 eV, i.e., outside the energy range displayed in Fig. 5.12. This result implies that a transfer of electron density from the substrate to the Cl adatom has taken place; the adsorbed Cl atom is partially negatively charged. Thus, Li and Na constitute examples of positive ionic chemisorption and Cl is an example of negative ionic chemisorption.

For the adsorption of an isolated Si atom it can be seen from the jellium calculations that the Si $3p$ resonance lies just at the Fermi level, which implies that it is about half occupied. As noted in Sections 5.2.1 and 5.3.1, the states of the energetically lower half of the resonance are bonding between the adatom and the substrate and the energetically higher states are antibonding. Because the Fermi level cuts the p -resonance approximately at its maximum, the bonding nature of Si is covalent, i.e., the bonding states are filled and the antibonding states are empty. The results for atomistic (Al and Cu) substrates also show that the bond is covalent. In this case, however, more structure occurs in the DOS than in the jellium calculations. This arises because the atomic structure of the substrate leads to band-structure effects, clearly reflected by the structure of the bulk DOS at ϵ_F in Fig. 5.12a. As a consequence, adsorption of a covalent atom, such as Si, results in a splitting of the bonding and antibonding states, and the adatom density of states exhibits a minimum at the Fermi level (Bormet et al., 1994a). Similarly to the jellium substrate, also for Si/Al(111) the Fermi level cuts the Si $3p$ -induced DOS roughly in the middle. We note in passing that for Si on Al(111) (cf. Fig. 5.12a) the structure of the p -like adsorbate density of states is largely determined by the clean-substrate density of states: With the Green function \mathcal{G}^0 of the clean substrate, we find at maxima of $\text{Im}\{\text{Tr}(\mathcal{G}^0(\epsilon))\}$ minima of $\Delta N(\epsilon)$, and at minima of $\text{Im}\{\text{Tr}(\mathcal{G}^0(\epsilon))\}$ we find maxima (see Bormet et al., 1994a, for more details).

Despite the differences, which clearly exist between jellium and Al(111), we find for both systems that the adsorbate-induced change in the DOS confirms the expected picture for a chemisorbed adsorbate on a metal surface:

- Atomic levels of the adsorbate are broadened due to the hybridization with the extended substrate states (in particular the substrate s -states).
- Compared to the free atom DFT-LDA level⁵ the adsorbate-induced peak is found at higher⁴ energy for adsorbed Na, at about the same energy for adsorbed Si, and at lower energy for adsorbed Cl. The calculated shifts are $\Delta\epsilon(\text{Na } 3s) \approx +0.6$ eV, $\Delta\epsilon(\text{Si } 3p) \approx +0$ eV, $\Delta\epsilon(\text{Cl } 3p) \approx -0.5$ eV.

This trend also conforms to the finding that the ionic character of the adatoms changes from plus to minus when going from Na to Si to Cl. It reflects that partially occupied levels have to align with respect to the substrate Fermi level (contribution (i) discussed in Section 5.2). But fully occupied levels (such as the $3p$ states of the Cl^- ion) are more affected by the surface potential (contribution (ii) discussed in Section 5.2).

⁵For open-shell systems, which are discussed here, the DFT-LDA Kohn-Sham eigenvalue of the highest occupied level is a good estimate of the mean value of the ionization energy and the electron affinity (cf. Figs. 5.5, 5.7 and their discussion).

For a core (or semi-core) state the shift of an adsorbate level upon adsorption mainly reflects the effects (i) (due to the changed electrostatic potential caused by transfer or redistribution of valence electron density) and (ii) (due to the substrate surface potential). With respect to the latter, we note that core levels are affected more by the electrostatic part of the potential than by the full effective potential, because the change in the exchange-correlation potential for core electrons due to the substrate electrons is negligible: At the high electron density in the core region, the exchange-correlation potential is only weakly affected by the relatively slight increase in electron density due to the substrate valence electrons. The shift of core levels due to effects (i) and (ii) of Section 5.3.1 is the initial-state contribution of X-ray spectroscopy of the adsorbate core-level shift. The results of Fig. 5.12 reveal that the Si 3s semi-core level is shifted by 3.4 eV and the Cl 3s-level by only 1.67 eV toward lower⁴ energy. For Si the shift largely reflects how the adatom core states feel the substrate potential. The shift of Cl is smaller because the Cl is positioned further away from the surface than Si, and because the electron transfer toward the Cl adatom implies a repulsive potential for the core and semi-core states implying a contribution shifting their energy levels to higher⁴ energies.

5.4.3 Electron density: $n(\mathbf{r})$, $\Delta n(\mathbf{r})$, and $n^\Delta(\mathbf{r})$

The trend seen in the results of Fig. 5.12 is in accordance with what is expected from electronegativity considerations: Na is electropositive with respect to the neighboring Al atoms, i.e., it gives up an electron more readily than Al. Cl, on the other hand, is strongly electronegative on Al and electron transfer from Al to Cl should occur. Silicon has nearly the same (or slightly higher) electronegativity as Al.

The formation of bonding and antibonding levels, together with the position of the Fermi level, will be reflected in the electron density $n(\mathbf{r})$. With this hierarchy in mind it is useful to inspect *in addition* to the DOS (Fig. 5.12) the electron density and, what is more instructive, the electron-density *change*, i.e., comparing the adsorbate system and the uncoupled systems. Figure 5.13 shows the electron density of the valence states.

In the case of sodium, the charge transfer from the adsorbate toward the substrate is clearly visible. From the vacuum side the sodium looks practically naked. Figure 5.13 may overemphasize this impression because it shows a wide range of electron density in order

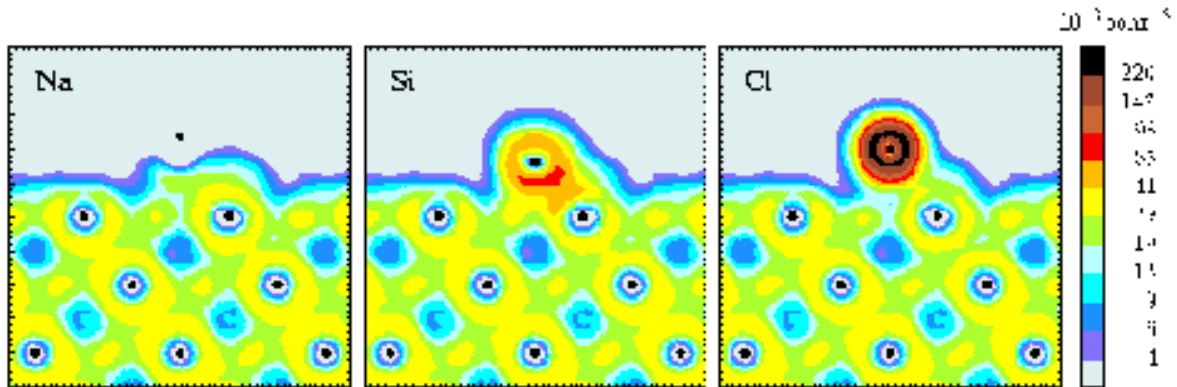


Figure 5.13: Electron density (valence only), cf. Eq. (5.3), for three different adatoms (groups I, IV, and VII of the periodic table) on an Al(111) substrate. We display a cut along the $(1\bar{1}0)$ plane, perpendicular to the surface. The results are from Bormet et al. (1994a).

to be able to compare atoms from the left to the right of the periodic table. The first displayed contour has a very low value which supports (again) the description of Na as being a (partially) ionized adatom and that particles which approach the adsorbed Na from the vacuum side will experience the “naked” side of the adsorbate. Figure 5.13 also shows that the electron density between the Na adatom and the Al substrate is increased. Thus, charge has been displaced from the vacuum side of the Na atom toward the substrate side. The details of this charge transfer are more clearly visible in the electron *difference density* $n^\Delta(\mathbf{r})$, which is the difference of the density of the adsorbate system, displayed in Fig. 5.13, of the density of the clean surface, and of the free atoms (cf. Eq. (5.5)). This *difference density* is shown in Fig. 5.14. The maximum of $n^\Delta(\mathbf{r})$ is located between the adsorbate and the substrate. In a more detailed discussion given in Section 5.5.3 we show that the shape of this induced charge density is the quantum-mechanical realization of the classical image effect which is actuated by the partially ionized adsorbate.

For Si, as expected from the adsorbate-induced DOS, a directional covalent bond is present between the Si adatom and the nearest-neighbor substrate atom (see Figs. 5.13 and 5.14). Furthermore, it can be seen that the maximum of the charge density of the chemisorption bond is closer to the more electronegative Si atom. We also see a typical increase of electron density on the opposite side of the bonding hybrid.

In the case of Cl on Al the charge density distribution around the adsorbate is almost spherical, again supporting the picture we had derived from the DOS in Fig. 5.12 of a

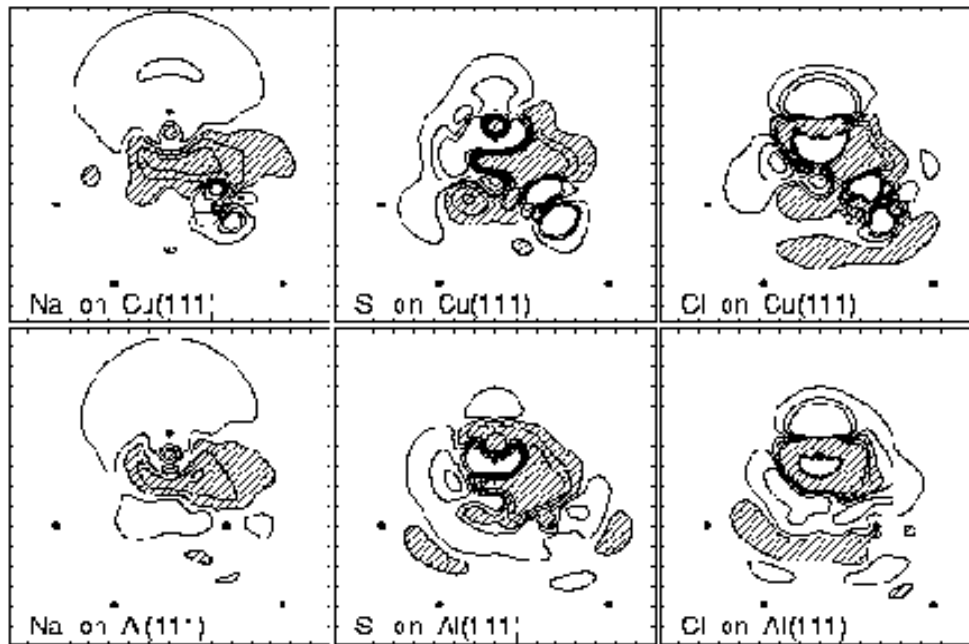


Figure 5.14: Electron *difference density* $n^\Delta(\mathbf{r})$ (see Eq. (5.5)), considering for the free adatom the neutral charge state, for three different adatoms (group I, IV, and VII of the periodic table) on a Cu(111) substrate (top) and on an Al(111) substrate (bottom). We display a cut along the $(1\bar{1}0)$ plane, perpendicular to the surface. Densely hatched areas indicate accumulation of electron density [positive $n^\Delta(\mathbf{r})$]. Non-hatched areas correspond to electron depletion [negative $n^\Delta(\mathbf{r})$]. The positions of nuclei are marked by dots. Results are from Yang et al., 1994, (top), and Bormet et al., 1994a, (bottom).

(partially) negatively charged adatom.

The results for the Al and Cu substrates show a number of similar features, and some interesting differences. Firstly, it can be noted that in each case the perturbation to the system caused by the adsorbates does not reach very far into the metal substrate. The interior is essentially identical to that of the clean surface for layers deeper than the second. We emphasize that this localization holds for the electron density *perturbation* but not for individual wave functions. For Na adsorption the results of Fig. 5.14 imply the building up of a surface dipole which locally decreases the work function. The opposite situation is found for Cl, which is negatively charged and sits on an adsorption site that is positively charged. In this case charge has moved from the substrate toward the Cl atom, and the local work function therefore will be increased relative to the value of the clean surface. For both substrates, Si appears covalently bound with a slight electron transfer toward the adatom. Comparing in more detail the results for Al and Cu, we see that there is more charge between the Na adatom and the top layer of the Cu substrate. Also, there is a greater depletion of charge at the vacuum side. These effects are consistent with the fact that the electronegativity difference between Na and Cu ($0.93 - 1.9 = -0.97$) is larger than that between Na and Al ($0.93 - 1.61 = -0.68$). The Si atom, which clearly forms a covalent bond with both substrates, is slightly more electronegative than Al (by 0.27). In this respect, it can be seen that more charge resides on the Si atom when adsorbed on Al than when on Cu for which the electronegativity difference is zero. In all cases for the adsorbates studied, the adsorption on Cu exhibits some structure in the valence-electron density change near the nucleus of the Cu atom closest to the adsorbate, which reflects the participation of the Cu *d*-electrons in the bonding.

5.4.4 Surface dipole moments

A further interesting quantity obtainable in adsorption calculations is the change in the adsorbate induced dipole moment as a function of adsorbate height. In a naive picture one would expect that for ionic bonding the dipole moment μ changes linearly with the adatom height Z_{ad} . For a covalent bond the dipole moment should be approximately constant (for small variations of the adsorbate height). Indeed we find that this picture applies. For Na we obtain a nearly linear increase of the dipole moment with increasing adsorbate height, and for Cl we obtain a decrease. The dynamical charge, which is the slope of $\mu(Z_{\text{ad}})$, is given in Table 5.2 and is in good agreement with the jellium calculations of Lang and Williams. These results support again the usefulness of the ionic pictures for Na and for Cl, and of the

Substrate	Adsorbate		
	Na	Si	Cl
Jellium	+0.4	+0.0	-0.5
Al(111)	+0.4	-0.1	-0.5

Table 5.2: Dynamic charge $d\mu/dZ_{\text{ad}}$, as obtained for isolated adatoms on jellium, and from supercell calculations for adsorbates on Al(111) at a low coverage of $\Theta = 1/16$. The units are electron charges. The results are from Bormet et al. (1994a).

mainly covalent description of Si adatoms on Al(111).

A homogeneously distributed layer of adatoms induces an electric field due to the adatom induced dipoles. The dipole strength is related to the adsorbate induced change in the work function, $\Delta\Phi_{\text{ad}}$, by the Helmholtz equation:

$$\Delta\Phi_{\text{ad}} = \Theta \mu(\Theta) / \varepsilon_0. \quad (5.37)$$

We have seen (cf. Figs. 5.13 and 5.14) that adsorption on a metal surface only significantly affects the electron density of the bare metal substrate in the outermost layers. The spatial distribution of the electronic charge with respect to the adsorbate nuclei gives rise to a dipole moment which changes the work function. Furthermore, charge transfer toward (or away from) the adparticle, as well as a permanent dipole moment give rise to a long range repulsive electrostatic interaction between different adparticles. If this is the dominant lateral interaction, which is true in some cases at low coverage, it will further result in a depolarization of the adsorption-induced dipole moment with increasing coverage (Antoniewicz, 1978; Topping, 1927; Kohn and Lau 1976).

It is convenient to illustrate this depolarization effect by considering the physisorption of rare gases. For these systems there is practically no charge transfer, and we only have to consider the static adsorbate dipole. For not too small adsorbate-substrate separation, we can calculate, using classical electrostatics, the dipole moment μ which enters Eq. (5.37). The dipole moment on each atom as a function of coverage is written as

$$\mu(\Theta) = \mu_{\text{st}} + \alpha \mathcal{E}_z(\Theta), \quad (5.38)$$

where μ_{st} is the static dipole moment of the adparticle alone, i.e., without considering the effect of screening by the metal conduction electrons and for $\Theta \rightarrow 0$. $\mathcal{E}_z(\Theta)$ is the component normal to the surface of the microscopic electric field at the adparticle under consideration and α is its polarisability. To calculate the field $\mathcal{E}_z(\Theta)$, it is necessary to take the image dipoles into account. Thus, as well as the direct dipole-dipole interaction, the dipole-image and image-image interactions must be considered. The actual dipole moment at coverage Θ then is

$$\mu(\Theta) = \frac{\mu_{\text{st}}}{1 + \alpha[T + V - 1/4D^3]}, \quad (5.39)$$

where D is the distance of the adparticle dipole to the effective image plane, and T and V are lattice sums of the direct and the indirect interactions (see Scheffler and Bradshaw, 1983, for details). The dipole moment of an adparticle at zero coverage is thus given by

$$\mu_0 = \frac{\mu_{\text{st}}}{(1 - \alpha/4D^3)}. \quad (5.40)$$

Due to the screening by the substrate, the adatom-induced dipole moment is thus enhanced from the value μ_{st} to μ_0 . Equation (5.39) shows that with increasing coverage, i.e., increasing value of $T + V$, the particle is depolarized. Expressions similar to Eq. (5.39), but without the image terms ($V - 1/4D^3$) were proposed by Topping (1927) and Miller (1946). Equation (5.39) has been applied to the physisorption system Xe/Pd(001) (Bradshaw and Scheffler, 1979). Figure 5.15 shows measured and calculated changes in work function. D has been taken to be 1.5 Å, and for the polarizability the gas phase value, $\alpha = 4 \text{ Å}^3$, was used. For the

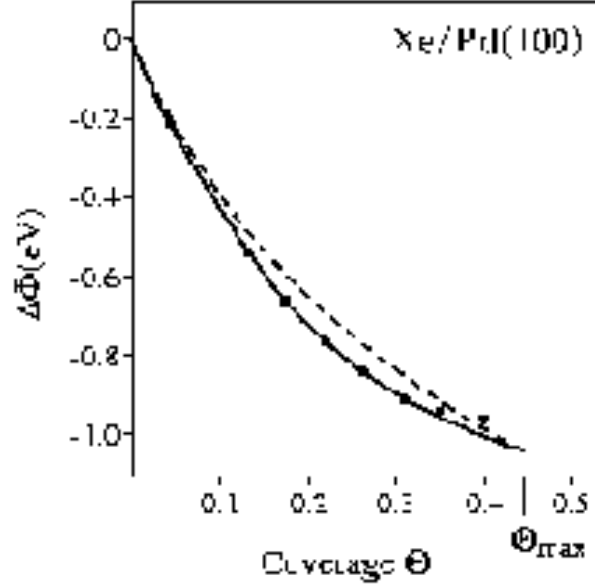


Figure 5.15: Calculated work function change for the adsorption system Xe/Pd(001) as a function of coverage.² Solid line: lattice sums proportional to $\Theta^{3/2}$. Broken line: lattice sums proportional to Θ . The points represent the experimental results of Palmberg (1971). After Bradshaw and Scheffler (1979).

monolayer obtained at $\Theta = 0.44$, the lattice sums are given by $T + V = 0.17 \text{ \AA}^{-3}$. The only remaining parameter is the dipole moment of the single adsorbed Xe atom, μ_0 . For the best fit to the experimental data, this is given by 0.93 Debye with the positive end away from the surface. At coverages between zero and Θ_{\max} , the lattice sums are either proportional to $\Theta^{3/2}$ (Topping, 1927), if an ordered array is present at every coverage, or proportional to Θ (Miller, 1946), if the adlayer is disordered. Both cases yield similar behavior and are shown in Fig. 5.15. We thus see that the work function does not change linearly with coverage but that depolarization causes a less rapid change at higher coverages.

5.5 Alkali-metal adsorption: the traditional picture of on-surface adsorption

In this section we discuss the traditional picture of alkali-metal adsorption. This implies that we consider situations where alkali-metal atoms adsorb *on the surface* without disrupting the substrate very much, which is in contrast to *substitutional* adsorption (see Section 5.6) where the adatom kicks out an atom from the substrate and takes its place. We recall that we discuss only the closed-packed substrate surfaces, namely fcc (111) and fcc (001). For more open surfaces, adsorbates, in particular alkali-metal atoms, can induce significant surface reconstructions. That substitutional adsorption at close-packed surfaces (and in more general terms, surface alloy formation) can happen even with adsorbates that do not mix in the substrate bulk, was first found by Schmalz et al. (1991) in a combined study of surface extended X-ray absorption fine structure (SEXAFS) experiments and DFT total-energy calculations. This subject will be discussed in Section 5.6 below. In this section we discuss *on-surface* adsorption and note only in passing that in the past, several experiments have been interpreted inappropriately by incorrectly assuming an on-surface adsorbate geometry. We

will take care that only those experiments are discussed below for which the adatom indeed sits on the surface. In fact, attaining the substitutional adsorbate geometry is hampered by an energy barrier, and therefore for low-temperature adsorption, adatoms are likely to stay on the surface. For the example discussed below, in which Na is at Al(001), the transition temperature is $T = 160$ K.

Substitutional adsorption has been observed for Na, K, and Rb on Al(111), where the tendency toward the substitutional adsorption seems to decrease with increasing adatom radius. Thus, for Cs substitutional adsorption has not been found.

5.5.1 The Langmuir-Gurney picture

In the seminal work of Taylor and Langmuir in (1933) for the Cs/W system, it was shown that the work function of the clean surface is reduced by several electronvolts on Cs adsorption and that for thermal desorption at low coverage, almost all the Cs adatoms leave the surface as positive ions. In the light of such results, the alkali metal bond to the substrate was viewed as a spectacular example of ionic bonding akin to that in alkali halides (see also Naumovets, 1994). As discussed above (see Fig. 5.1), even in NaCl the nature of bonding is debatable, and it is therefore not a surprise that the question whether or not alkali-metal adsorption should be described in terms of ionic bonding has sometimes been raised. With all the warnings mentioned in Section 5.1 in mind, we argue (and already did so in Section 5.4) that the ionic picture is appropriate. For a more detailed analysis of the controversy about the ionic nature of the bond we refer to the publications of Scheffler et al. (1991) and Bormet et al. (1994a).

A simple picture of the interaction between alkali-metal atoms and a metal surface, and of the resulting chemisorption bond was proposed by Langmuir (1932). He assumed that the alkali-metal atom transfers its valence s -electron completely to the substrate. In a more rigorous theoretical description of alkali-metal adsorption Gurney, in 1935, proposed a quantum-mechanical picture applicable at low coverages, where the discrete s -level of the free alkali metal atom broadens and shifts, becoming partially emptied as a result of the interaction with the substrate states as it approaches the surface. Figure 5.7 (left) summarizes this view. The partially positively charged adatom then induces a negative screening charge density in the substrate surface giving rise to an adsorbate-induced dipole moment which naturally explains the reduction in the work function of clean surfaces.

The building up of such adsorbate-induced dipole moments also leads to the understanding that the dominant interaction between the adsorbates is repulsive and that the adatoms should form a structure with the largest possible interatomic distances compatible with the coverage. In this description it is expected that with increasing coverage the adsorbate-adsorbate distance gradually decreases, and the electrostatic repulsion between the adatoms increases. To weaken this repulsion, i.e., to lower the total energy, some fraction of the valence electrons flows back from the Fermi level of the metal to the adsorbate. Thus, a reduction of the adsorbate-induced dipole moment, i.e., depolarization takes place. This picture of Langmuir and Gurney is fully supported by systematic studies of Lang and Williams, Bormet et al., and others, some of which were discussed in Section 5.4 above. If the coverage-dependent depolarization is strong and/or the nature of the adsorbate-substrate binding changes with the local coverage, it is also possible (and observed) that with increasing coverage a phase separation occurs into close-packed islands (also called “condensation”) (Neugebauer and

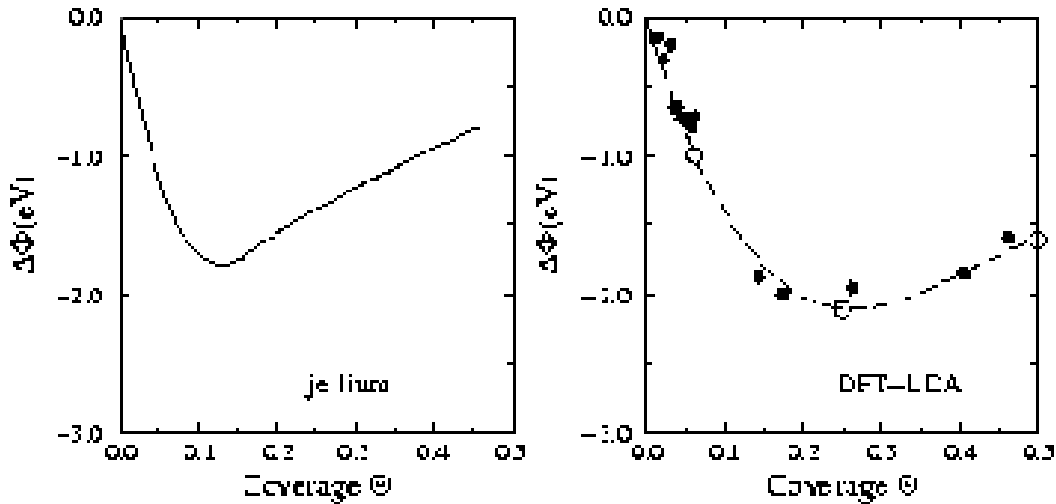


Figure 5.16: Change in work function with increasing coverage (cf. footnote 2). Left: Results of Lang (1971) using a jellium on jellium model with parameters corresponding to Na on Al(001). Right: DFT-LDA calculations (open circles) for periodic Na adlayers on Al (001). Closed circles are experimental results from Porteus (1974) and Paul (1987), obtained by adsorption at low temperature ($T = 100$ K).

Scheffler, 1993; Over et al., 1995).

5.5.2 Coverage dependence of the work function

In his earlier work, Lang (1971 and 1973) studied the alkali metal-induced work-function change using the jellium model for the substrate and for the adsorbate layer. Despite the extremely approximate nature of this approach, the results demonstrated that many ground-state properties of metal surfaces and metal-adatom systems can be described in a physically transparent manner. As an example, we show in Fig. 5.16 the change in work function with increasing coverage (cf. footnote 2) for parameters corresponding to Na on aluminum (in the jellium approach; left side). The right side of the figure shows a calculation for Na on Al(001), which takes the atomic structure into account. We note that for coverages $\Theta_{\text{Na}} \gtrsim 0.15$ the on-surface geometry is a metastable structure which only exists at temperatures below 160 K (Andersen et al. 1992; Aminpirooz et al., 1992).

The coverage dependence of the work function possesses a form similar to that often observed experimentally. It is explained as a consequence of the above-mentioned depolarization of the alkali metal-induced surface dipole-moment induced by continuous reduction of the adsorbate-adsorbate distance and corresponds to a rapidly decreasing work function at low coverage, reaching a minimum at about $\Theta = 0.1$ (Fig. 5.16, left) or $\Theta = 0.25$ (Fig. 5.16, right), and subsequently rising toward the value of the pure alkali metal.

5.5.3 Ionization of the adsorbate and screening by the substrate electrons

We will now, for the moment, assume that we can neglect any effect due to the chemical interaction (i.e., hybridization of orbitals) upon adsorption and that the substrate mainly plays the role of providing an electron reservoir, i.e., fixing the electron chemical potential to its Fermi level. Using the Fermi-level position of Al(001), Fig. 5.5 shows that then the

occupancy of the Na $3s$ -level will be 65%. Thus 35% of the Na $3s$ -electron is now in the substrate.

A partially ionized atom in front of a metal surface will not leave the metal electrons unaffected. To discuss this, we will at first sketch the quantum mechanical concept of screening at a metal surface which asymptotically, for large distances, includes the classical image effect. When a charged particle approaches a metal surface a screening charge will be created at the surface. The quantum-mechanical realization of the classical image effect is an induced electron density which has its center of gravity at the “effective metal surface”, i.e., the image plane (cf. Lang and Williams, 1978). Thus, whereas in the classical description the electrostatic screening of a *point charge* at a distance D in front of a metal surface is modeled by an image point charge inside the metal at a distance $-D$ away from the surface, the truth is that there is no image point charge inside the substrate but a charge density right at the surface (see Fig. 5.18b), which creates the same electrostatic field in the vacuum as the (fictitious) point charge of classical electrostatics.

Considering close-packed surfaces, the image-plane position (see Eq. (5.24)) is on the vacuum side of the center of the outermost atomic layer, because electrons spill out into the vacuum to lower their kinetic energy. At small distances (typically $d < 2 \text{ \AA}$) the justification of the image-plane concept gradually breaks down. However, it is still approximately valid, however, because metallic screening is still important. The concept can be approximately justified by assuming that for a charged system close to the surface, the image plane (z_0 in Eq. (5.24)) is displaced toward the substrate. This is what we have in mind when we use the term “image effect” in the following discussion. For a deeper discussion of this problem we refer to Scheffler and Bradshaw (1983), Finnis et al. (1995), and references therein.

Figure 5.17 shows that the description of partial ionization of the Na adatom and building up a screening charge in the substrate remains *qualitatively* valid when the alkali-metal atom is adsorbed. Figure 5.17 displays the *difference density* $n^\Delta(\mathbf{r})$ (cf. Eq. (5.5)) using a neutral atom ($f_{3s} = 1$). It can be seen that the upper half of the adsorbed Na atom has a negative

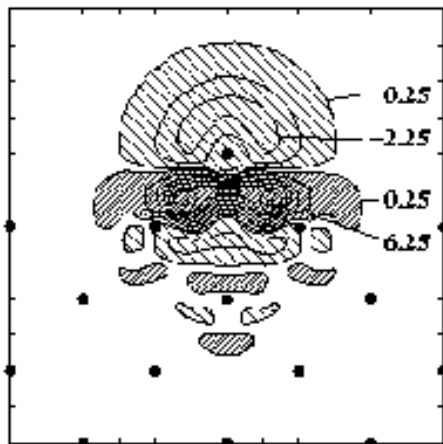


Figure 5.17: Electron *difference density* $n^\Delta(\mathbf{r})$ for Na adsorbed on Al(001). For the definition of n^Δ see Eq. (5.5); n^{Na} is taken from a free, neutral atom. Units are $10^{-3} \text{ bohr}^{-3}$. The contour line spacing is $10^{-3} \text{ bohr}^{-3}$. Densely hatched areas indicate accumulation of electron density [positive $n^\Delta(\mathbf{r})$]. Sparsely hatched areas correspond to electron depletion [negative $n^\Delta(\mathbf{r})$]. The positions of nuclei are marked by dots (from Scheffler et al., 1991).

n^Δ thus less electron density than the free, neutral alkali atom, and on the substrate side of the adatom there is an increase of electron density.

Figure 5.18 a shows a plot of $n^\Delta(f_{3s} = 0.1)$, where n^{Na} (cf. Eq. (5.5)) is now taken from a self-consistent calculation for the partially ionized free atom. This picture looks very similar to the pure screening charge density which we obtain for an external point charge (see Fig. 5.18b). The shape of this screening charge density is very similar for a negative point charge and for a positive point charge, as long as the latter is sufficiently weak so that it cannot bind an electron. The magnitude of the contour lines nearly scale linearly with the magnitude of the external point charge. The similarity between Figs. 5.18 a and 5.18 b is quite surprising, because a Na-ion is – of course – different from a point charge. Nevertheless, the response of the metal is similar for both cases. The slight differences between Figs. 5.18 a and b may be interpreted as an indication that some covalency and some s - p_z mixing are present in the Na-Al(001) interaction, but these contributions are not very large. From the similarity of Figs. 5.18 a and b we conclude that the “charge transfer picture” is indeed useful and appropriate to describe the physics of alkali adsorption at low coverage. However, charge transfer alone is not sufficient to understand the adsorbate-substrate interaction because the charge transfer actuates a significant change in the substrate surface electron density. We also note that the metal screening charge is largely located in front of the metal, i.e., between the adsorbate and the substrate (see Fig. 5.18b). As a consequence, the adsorbate-induced electron-density change cannot be divided *directly* into adsorbate and metal contributions.

5.5.4 Surface band structure

At low coverages the interaction between adsorbed alkali-metal atoms will originate from their strong dipole moments. As the coverage increases, wave functions will overlap and a surface electronic band structure will form. This band is of s -character and its dispersion

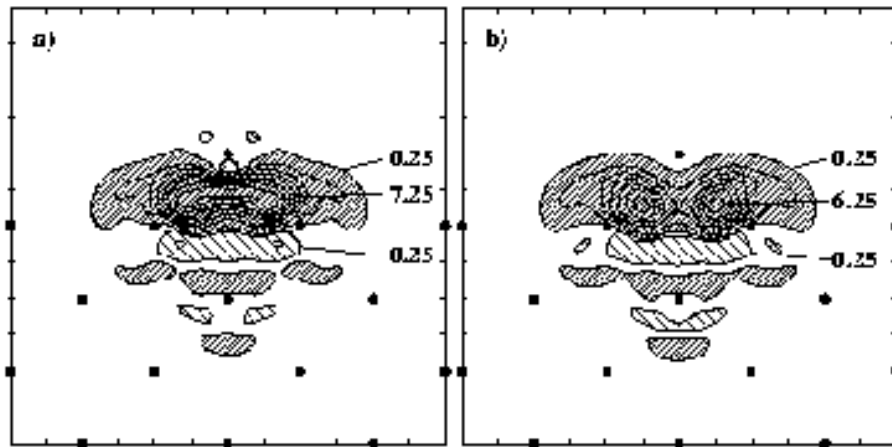


Figure 5.18: Panel (a): Electron *difference density* $n^\Delta(\mathbf{r})$ for Na adsorbed on Al(001). For the definition of n^Δ see Eq. (5.5); n^{Na} is taken from a partially ionized, free Na atom ($f_{3s} = 0.1$). Units are 10^{-3} bohr $^{-3}$. The contour line spacing is 10^{-3} bohr $^{-3}$. Panel (b) shows the screening charge density of an external, positive point charge of $-0.09e^-$. Here the units are 10^{-4} bohr $^{-3}$. Densely hatched areas indicate accumulation of electron density [positive $n^\Delta(\mathbf{r})$]. Sparsely hatched areas correspond to electron depletion [negative $n^\Delta(\mathbf{r})$]. The positions of nuclei are marked by dots (from Scheffler et al., 1991).

was discussed in Section 5.3.2 above. In Fig. 5.19 we show experimental (left panels) and calculated (right panels) surface states/resonances for (a) the clean Al(001) surface, (b) the on-surface $c(2 \times 2)$ -Na/Al(001) structure, and (c) the substitutional $c(2 \times 2)$ -Na/Al(001) adsorbate structure (discussed in more detail in Section 5.6.1 below). Firstly, we note that there is good overall agreement between theory and experiment. The main, lower-lying band in each case is Al-derived, as indicated by the circles in the theoretical plot. The bands represented by squares are Na-derived. Compared to the position of the surface-state band of the clean surface, it can be seen that the Al-derived band of the on-surface adsorbate phase lies around half an eV lower in energy. The mechanism giving rise to this downward shift is discussed below. Interestingly, the experimental results show clearly that this state does not have the $c(2 \times 2)$ periodicity of the adsorbates, but rather has kept the (1×1) periodicity of the clean surface (cf. Fig. 5.19a). Indeed, inspection of the electron density reveals that the on-surface adsorbate represents only a modest perturbation of the surface electronic structure, which cannot be resolved in the photoemission experiments (see the

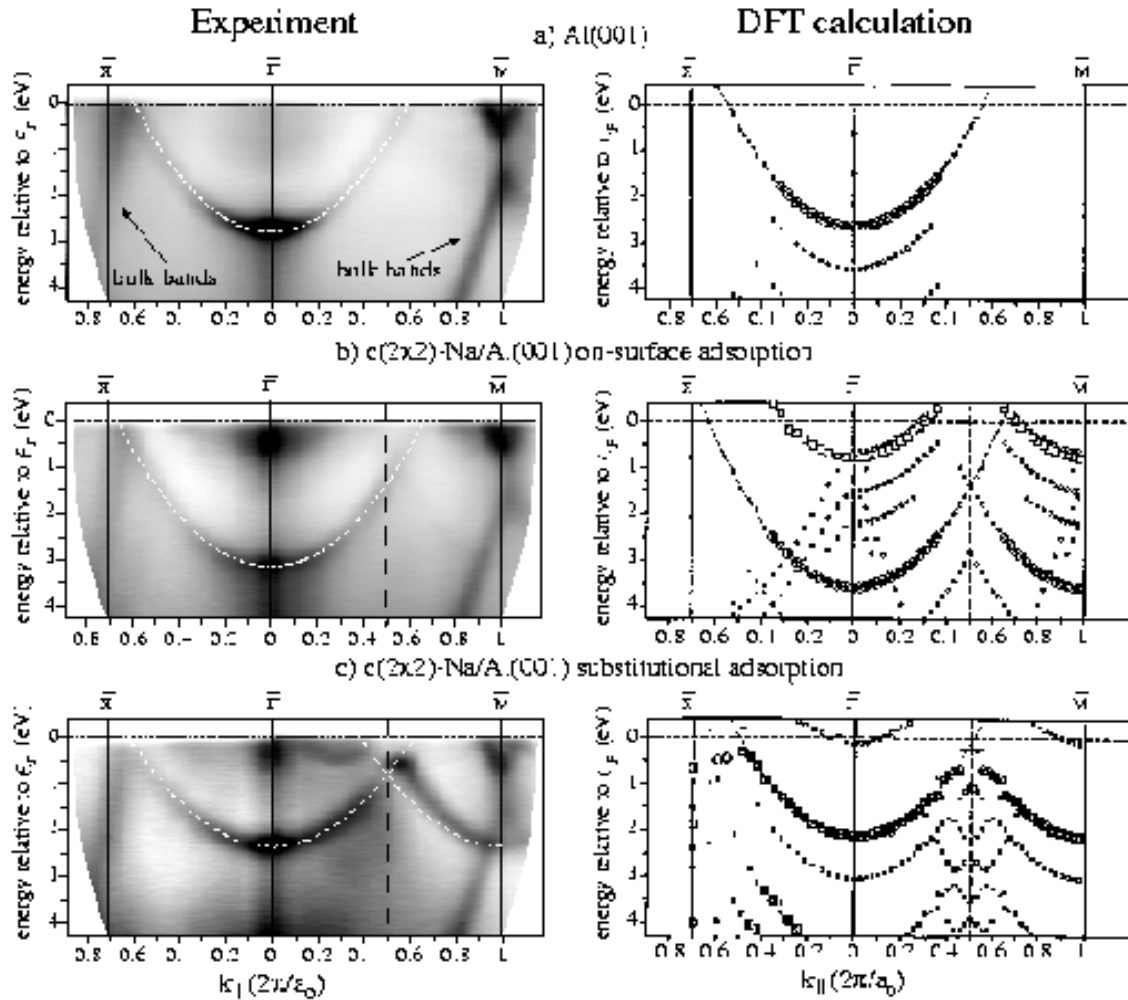


Figure 5.19: Comparison of experimental (left panels) and calculated (right panels) surface band structures. The symbols used are such that squares and circles represent Na- and Al-derived bands, respectively (for a precise definition see the paper by Stampfl et al., 1998). Panels (a) show results for the clean Al(001) surface, panels (b) the on-surface hollow site, and panels (c) display results for the substitutional adsorption. The results are taken from Stampfl et al. (1998).

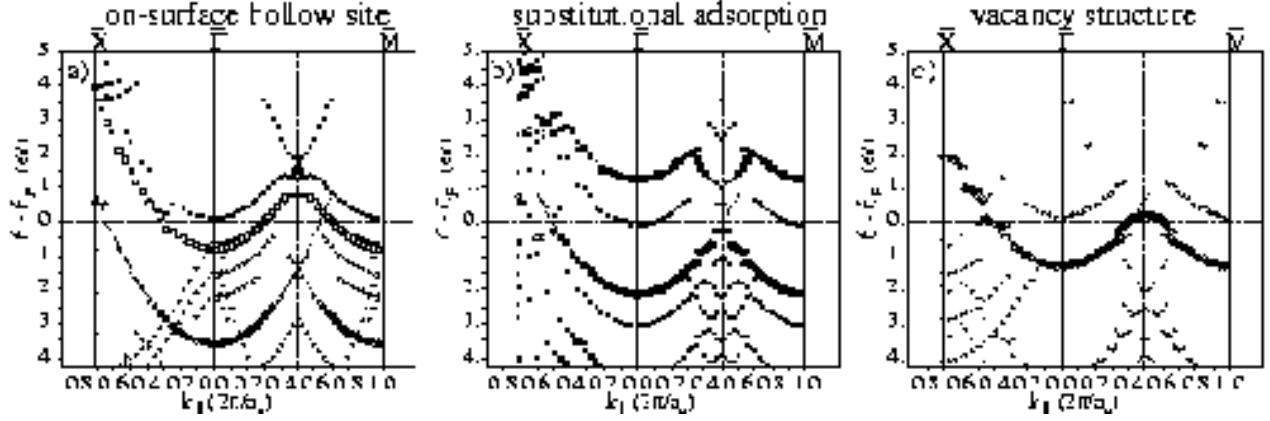


Figure 5.20: Surface band structures of $c(2 \times 2)$ Na on Al(001) for (a) on-surface adsorption, (b) substitutional adsorption, and (c) the vacancy structure, including the energy range above the Fermi level. The symbols used are such that squares and circles represent Na- and Al-derived bands, respectively (for a precise definition see the paper by Stampfl et al., 1998).

discussion of Fig. 5.9 above).

From the calculated bands of the on-surface adsorbate phase (right middle panel of Fig. 5.19), it can be seen that there is also a surface-state/resonance with an energy of about 0.7 eV below the Fermi level at $\bar{\Gamma}$. As indicated by the open squares, it is a Na-derived band (of Na 3s character). It crosses the Fermi level and is partly occupied. From Fig. 5.20, which shows the calculated band structure also in the region *above* the Fermi level, it can be seen that the part of the Na-derived band above ϵ_F exhibits a band structure with $c(2 \times 2)$ periodicity of the adsorbed Na layer. Thus the higher coverage of Na present in this phase, as compared to the situation of an isolated adatom, has given rise to the development of significant adsorbate-adsorbate bonding and band formation.

From construction of electron “difference density” plots (cf. Eq. (5.5)), that is, subtracting off from the total valence electron density of the system, the superposition of the electron densities of the clean Al substrate and the Na atoms (arranged in the same $c(2 \times 2)$ periodicity), it is found that due to Na adsorption there is an increase of electron density at the position of the surface-state band (the band of parabolic shape which has a lower energy at 2.8 eV in Fig. 5.19a, left and 3.2 eV in Fig. 5.19b, left), and from the region between the Na atoms electron density is depleted. These results, together with comparison of the band structure of a *free* $c(2 \times 2)$ -Na monolayer which has an electron occupancy *larger* than the Na-derived band seen in Fig. 5.19, suggests electron transfer occurs from the Na atoms directly into the pre-existing surface states of Al(001). Thus, the Na-induced structures seen in Fig. 5.19 b, left (see the dark regions at $\bar{\Gamma}$) originate from a coupling between the 3s-derived band of the free $c(2 \times 2)$ monolayer of Na and the surface-state band of the clean Al(001) surface. This may be understood as being due to the formation of bonding and antibonding states, leading to the downward shift of the Al-derived band with an increase in population and the upward shift of the Na-derived band with a decrease in population. Nevertheless, the electron density of the Al-derived band lies well below the smeared-out density of the Na-derived band, and also below the position of the Na atoms. Therefore the traditional picture of a thin metallic film covering a metallic substrate, as in the jellium model, remains qualitatively valid. We will see in the next section that this is *not* the case for the substitutional-adsorbate phase.

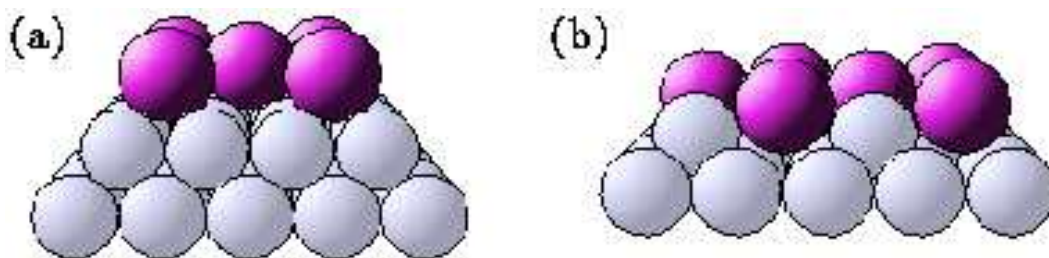


Figure 5.21: Perspective view of the atomic structure of $c(2 \times 2)$ -Na on Al(001). Dark and light gray circles represent, respectively, Na atoms and Al atoms. (a) On-surface hollow site geometry and (b) substitutional geometry, where every second Al atom in the top unreconstructed Al layer has been kicked out.

5.6 Substitutional adsorption and formation of surface alloys

Recent experimental and theoretical studies of the adsorption and co-adsorption of alkali metals on Al surfaces have shown that the traditional view of alkali-metal adsorption outlined in Section 5.5 above, is in fact, only part of the whole picture and that phenomena such as the following may occur:

1. The alkali-metal atoms may not necessarily assume highly coordinated sites on the surface.
2. The alkali-metal adatom may kick out surface substrate atoms and adsorb substitutionally. Substitutional adsorption has been shown in three cases to occur as the result of an irreversible phase transition from an “on-surface” site by warming to room temperature, without change in the periodicity of the surface unit cell or of the coverage, i.e., order-preserving phase transformations between metastable and stable structures occur.
3. The alkali-metal atom may switch site on variation of coverage.
4. Island formation may occur.
5. There may be a strong intermixing of the alkali-metal atom with the substrate surface, as for example the formation of a four-layer ordered binary surface alloy which was identified for Na on Al(111) at a coverage $\Theta_{\text{Na}} = 0.5$ (Stampfl and Scheffler, 1994c). Also ternary surface alloys form for the co-adsorption of Na ($\Theta_{\text{Na}}=0.25$) with either of K, Rb, or Cs on Al(111) (Christensen et al., 1996).

Only some of these aspects will be discussed below. A comprehensive description of the updated, modern view of alkali-metal adsorption can be found in a special issue of Surface Reviews and Letters (SRL, 1995) which collected review papers of the key groups which were working on this subject. There, and also in Adams (1996), it is shown in greater detail than possible here that the adsorption and co-adsorption of alkali metals on Al surfaces exhibit a wealth of previously unexpected phenomena.

Although it is well known that many, though not all, materials mix and form alloys, up until recently intermixing was not considered to be very relevant for adsorption on close-packed surfaces. Thus, adsorbates on such surfaces were assumed to occupy on-surface sites.



Figure 5.22: Possible mass-transport scenario for substitutional adsorption and the formation of a surface alloy for the system Na/Al(111). (a) Island formation occurs with a $(\sqrt{3} \times \sqrt{3})R30^\circ$ structure with Na atoms in substitutional sites, for coverages $0 < \Theta_{\text{Na}} \leq 1/3$: Every third Al atom is “missing”; Al atoms diffuse to steps. (b) Surface alloy formation with a (2×2) geometry implies diffusion of Al atoms back from steps.

Figure 5.21a gives an example for Na on Al(001). It was also assumed that this view is justified, in particular, for systems where the adatom is insoluble in the bulk substrate. This standard picture was questioned in 1991 by a combined study of surface-extended X-ray adsorption fine-structure (SEXAFS) experiments and DFT total-energy calculations for the system Na on Al(111) (Schmalz et al., 1991); by now it is well established that often adatoms do not adsorb on the surface, but instead, it can be energetically favorable that they kick out atoms from the substrate and take their sites. The kicked out atoms then diffuse to a step (see Fig. 5.22a). The process may be kinetically hindered, but this hindrance may be overcome even at rather low temperatures, e.g., for Na on Al(001) for $T \geq 160$ K (Andersen et al. 1992; Aminpirooz et al., 1992) and/or by the heat of adsorption. Whether the solubility in the substrate bulk is low or even zero is of no relevance at all for substitutional adsorption. Atoms, which are too big to fit into a bulk vacancy, can still prefer to take a substitutional site, because at the surface bigger atoms can simply sit somewhat above the center of the created surface vacancy. Since 1991 many examples of substitutional adsorption have been reported, as for example K on Al(111) (Neugebauer and Scheffler, 1992, 1993; Stampfl et al., 1992, 1994a), Na on Al(001) (Stampfl et al. 1994b), Au on Ni(110) (Pleth Nielsen, 1993), Sb on Ag(111) (Oppo et al., 1993), Co on Cu(111) (Pedersen et al., 1997), Mn on Cu(001) (Rader et al., 1997), Co on Cu(001) (Nouvertné et al., 1999), to name a few. Thus, the phenomenon is not at all exotic, but rather general.

In this section we will discuss in particular three systems, Na on Al(001), Na on Al(111), and Co on Cu(001), as these exhibit qualitatively different behavior.

Alkali metal-induced surface reconstructions are well known on the more open surfaces (Somorjai and Van Hove, 1989; Barnes, 1994; Behm, 1989) as these clean surfaces are close to a structural instability (Heine and Marks, 1986). But that significant reconstruction can occur on close-packed fcc (111) and (001) surfaces had not been expected previously.⁶ As a warning for future work we mention that for alkali-metal adsorbates, several studies, had found “good agreement” between LEED experiments and theory as well as band-structure calculations and photoemission experiments (this also was the case for the example discussed

⁶The late 5d transition metals (Ir, Pt, Au) are exceptions to this rule. In these systems relativistic effects give rise to a substantial lowering of the s-band and a rather high surface stress. For the (001) surfaces, the desire to achieve a higher coordination in the top layer is indeed stronger than the cost of breaking (or stretching) some bonds between the first and second layer (see Fiorentini et al., 1993).

in this section). However, it is now known that the reported agreement was purely coincidental, and the concluded physical and chemical properties were grossly incorrect because the alkali-metal atoms were not sitting on the surface (cf. Fig. 5.21a), but in substitutional sites (cf. Fig. 5.21b). Consequently, the nature of the adsorbate chemical bond, the surface electronic structure, and the origin of the coverage dependence of the work function are in fact qualitatively different to what was assumed before 1992 (Andersen et al., 1992; Aminpirooz et al., 1992; Stampfl et al., 1994b; Berndt et al., 1995). Thus, good agreement between theory and experiment and/or a convincing physical picture are no guarantee that the description and trusted understanding is indeed correct.

The associated electronic properties of these surface atomic arrangements, perhaps not surprisingly, also exhibit behavior deviating from expectations based on early ideas. For example, experimental measurements of the change in work function as a function of alkali-metal coverage can be quite different to the “expected” form of Fig. 5.16 and the density of states induced by alkali-metal adsorbates may not correspond to that expected from the model of Gurney.

5.6.1 Na on Al(001)

For Na on Al(001), the adsorption energy for the on-surface hollow site and the substitutional site as a function of adsorbate coverage is shown in Fig. 5.23. It can be seen that the on-surface hollow site is clearly preferred over the substitutional site at low coverages. Its adsorption energy rapidly decreases with increasing coverage indicating a strong repulsive interaction between the Na atoms. The adsorption energy for Na in the surface substitutional site depends much more weakly on coverage than for the on-surface site, and, in fact, the adsorption energy for the $\Theta = 0.5$ substitutional structure is more favorable than even that of the lower coverage substitutional structures.

These results are interpreted as follows: At low coverages, the on-surface adsorption in a homogeneous adlayer is the stable structure for low as well as high temperature, but for higher coverages, on-surface adsorption becomes metastable. For high temperature adsorption, or warming the substrate, the adatoms then switch to substitutional sites, forming islands with a $c(2 \times 2)$ structure. The phase transition from the on-surface hollow site to substitutional

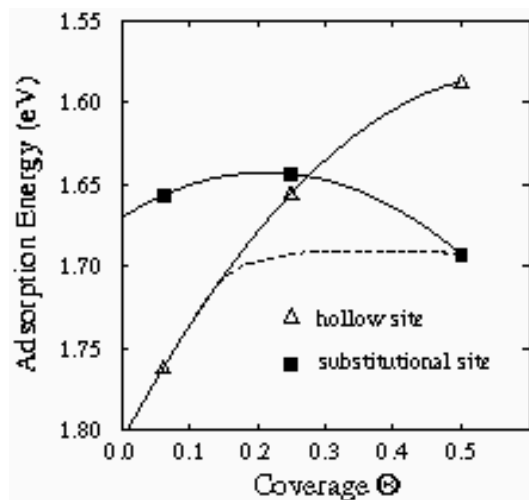


Figure 5.23: Adsorption energy versus coverage for Na on Al(001) in the on-surface hollow site and in the surface substitutional site (from Stampfl and Scheffler, 1995).

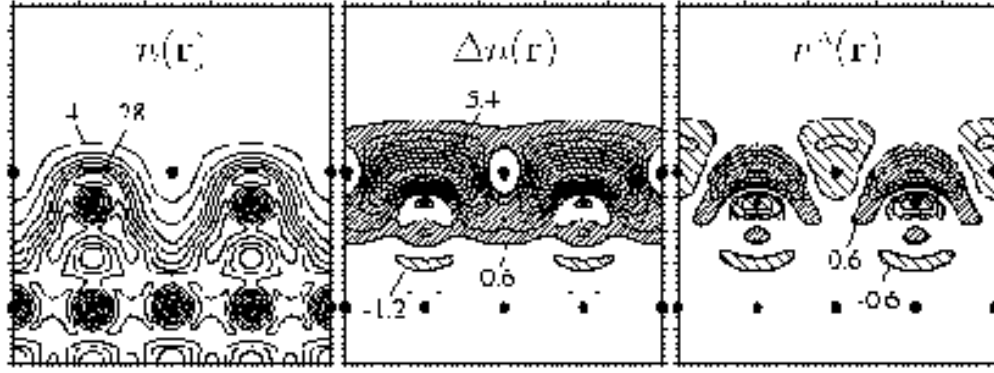


Figure 5.24: Total valence electron density $n(\mathbf{r})$ (left panel), density difference $\Delta n(\mathbf{r})$ (middle panel), and the *difference density* $n^\Delta(\mathbf{r})$ for $f_{3s} = 1$ (cf. Eq. (5.5)) (right panel), of the substitutional geometry of the Na/Al(001) adsorbate system at $\Theta = 0.5$. The units are $10^{-3} \text{ bohr}^{-3}$. The results are from Stampfl et al. (1998).

adsorption is indicated in Fig. 5.23 by the dashed line. This predicted behavior is in good accord with experimental studies, see e.g., Fasel et al. (1996).

The widely differing adsorbate geometries and the strong dependence of them on coverage and temperature, as described above, means that the type of bonding and chemical properties of the adsorption system will vary significantly depending on these factors. In this section we examine the electronic structure and bonding nature of the $c(2 \times 2)$ substitutional structure of Na on Al(001); that of the $c(2 \times 2)$ on-surface hollow structure was briefly touched upon already in Section 5.5.4.

Firstly, it can be noted from Fig. 5.19c for substitutional adsorption that the main band in the experimental results clearly exhibits a $c(2 \times 2)$ periodicity, in contrast to the on-surface hollow structure. This is due to the significantly reconstructed Al(001) surface. It can also be noticed that this band is higher in energy than the surface state band of the clean Al(001) surface. Furthermore, the Na-derived band, as clearly observed for the on-surface phase in Fig. 5.19b in a greater region around $\bar{\Gamma}$ below ϵ_F , is nearly absent in the substitutional phase. However, from Fig. 5.20b which shows the same calculated band structure as in Fig. 5.19c, but where the energy region extends higher into the positive range, it can be seen that a significant Na-derived band (tagged by square symbols) lies well above the Fermi level, i.e., it is unoccupied. Figure 5.20c also shows the calculated surface state bands of the artificial $c(2 \times 2)$ vacancy structure. Here a strong Al-derived band can clearly be seen, its position being higher in energy than that of the clean surface. Similarly to the clean Al(001) surface, the maxima of charge density of the surface states for the vacancy structure lie on top of the uppermost surface Al atoms, having this time the $c(2 \times 2)$ periodicity. On adsorption of Na, as for the on-surface phase, this band shifts down in energy. The character of this Al-derived band is only slightly changed compared to that of the vacancy structure, which explains the well developed $c(2 \times 2)$ character of the band found in Fig. 5.19c.

In this case electron transfer occurs from the Na atoms into the surface state/resonance of the *vacancy structure*. Figure 5.24 (right panel) shows that electron charge has been transferred mainly from the region on top of the Na atoms into the region above the Al atoms, corresponding to the position of the surface states. Compared to the Na-Al bond length of Na in the hollow site, that in the substitutional geometry is approximately 4% (from DFT-LDA) and 11% (from LEED) shorter, indicating a larger ionicity of the bonding.

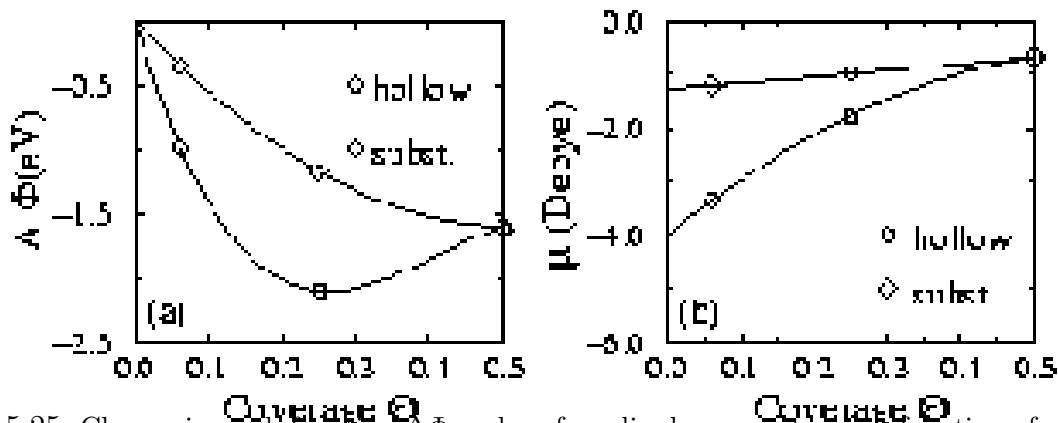


Figure 5.25: Change in work function $\Delta\Phi$ and surface dipole moment μ as a function of coverage for Na in the substitutional (diamonds) and on-surface hollow sites (circles) for Na on Al(001) (from Stampfl and Scheffler, 1995).

The results discussed above, together with Fig. 5.24 (middle panel), which shows the regions where electron density has been increased due to Na adsorption, demonstrates that for the *substitutional* adsorption phase the Na adlayer *cannot* be regarded as a simple metal film on a metallic substrate, and the jellium model is not valid.

Another interesting property which yields insight into the bonding nature are the work function change and surface dipole moment. As discussed in Sections 5.5.1 and 5.5.2, for *on-surface* adsorption the characteristic change in the work function $\Delta\Phi(\Theta)$ with coverage is typically explained in terms of the Gurney picture and the “usual form” can be described reasonably well by assuming a jellium model. The work function change $\Delta\Phi$ and surface dipole moment μ are shown in Figs. 5.25a and 5.25b, respectively, as a function of coverage. For comparison, results for Na in the on-surface hollow structures are also displayed. As is consistent with the traditional picture of alkali-metal adsorption, there is a significant decrease of the surface dipole moment with increasing coverage for the on-surface site and the typical form of $\Delta\Phi(\Theta)$ is observed. The substitutional adsorption, on the other hand, exhibits a much weaker dependence. This reflects the fact that in the substitutional site the Na atoms sit lower in the surface and the repulsive adsorbate-adsorbate interaction is screened better.

As discussed above (cf. Fig. 5.23), under not too low temperature conditions a phase transition to $c(2 \times 2)$ islands occurs at coverage $\Theta \approx 0.15$; thus the local dipole moment will be fixed at the value of the $c(2 \times 2)$ phase and the work function change will vary linearly as $\Delta\Phi = \Theta\mu/\epsilon_0$. At $\Theta=0.5$ it is found that the values of μ (and $\Delta\Phi$) are the same for the on-surface and substitutional adsorption. This is in agreement with experiment, i.e., in all cases (theory and experiment) the value of $\Delta\Phi$ is 1.6 eV (Porteus, 1974; Paul, 1987).

5.6.2 Na on Al(111)

The adsorption of Na on Al(111) was the first alkali metal on close-packed metal system that was discovered to assume substitutional adsorption. Further interesting and unanticipated phenomena were found to occur for higher Na coverages on this surface, in particular, the formation of a “four layer” surface alloy; the complex atomic geometry of which had foiled initial experimental attempts at its determination. This difficulty was related to its relative

complexity, but was also due to conceptual barriers since such a structure was not expected to occur.

In Fig. 5.26 the adsorption energy of Na on Al(111) is displayed for various structures and coverages of Na in on-surface geometries (Fig. 5.26a) and in the substitutional site (Fig. 5.26b). For the latter, the adsorption energy is split into its constituents, namely, the binding energy and the surface vacancy formation energy. For on-surface adsorption, the theory indicates that for low coverages the hollow site is energetically most favorable and strong repulsive adsorbate-adsorbate interactions exist. A condensed (4×4) structure is seen to be energetically more favorable than homogeneous adlayers of Na for coverages larger than approximately $\Theta_{\text{Na}} = 0.1$. In the condensed phase, the coverage is $\Theta_{\text{Na}} = 9/16$ and the structure represents a densely packed hexagonal adlayer with nine Na adatoms per surface unit cell, all occupying different (mostly low symmetry) on-surface sites. Thus, the picture is that for very low coverages, the adsorbates occupy on-surface hollow sites and are uniformly distributed over the surface (homogeneous adlayers) but for coverages greater than about $\Theta_{\text{Na}} = 0.1$, island formation with the condensed structure and a (4×4) periodicity occurs as indicated by the dashed line. In this case it is energetically favorable to build up a metallic-like bonding between the adatoms and to reduce the ionic character of the adatom-substrate bonding.

For the case of substitutional adsorption it can be seen from Fig. 5.26b that the adsorption energy of the substitutional geometry is the most favorable for *all* structures investigated (note the different energy scales of Figs. 5.26a and 5.26b). In particular, substitutional adsorption with a $(\sqrt{3} \times \sqrt{3})R30^\circ$ periodicity has *the* most favorable adsorption energy. It is therefore expected that a condensation into $(\sqrt{3} \times \sqrt{3})R30^\circ$ islands with the Na atoms in substitutional sites occurs, beginning at very low coverages. The atomic structure is displayed in Fig. 5.27. The repulsive character of the binding energy for the $(\sqrt{3} \times \sqrt{3})R30^\circ$ phase can be seen (cf. Fig. 5.26b) to be over-compensated for by the attractive interaction of the surface vacancies.

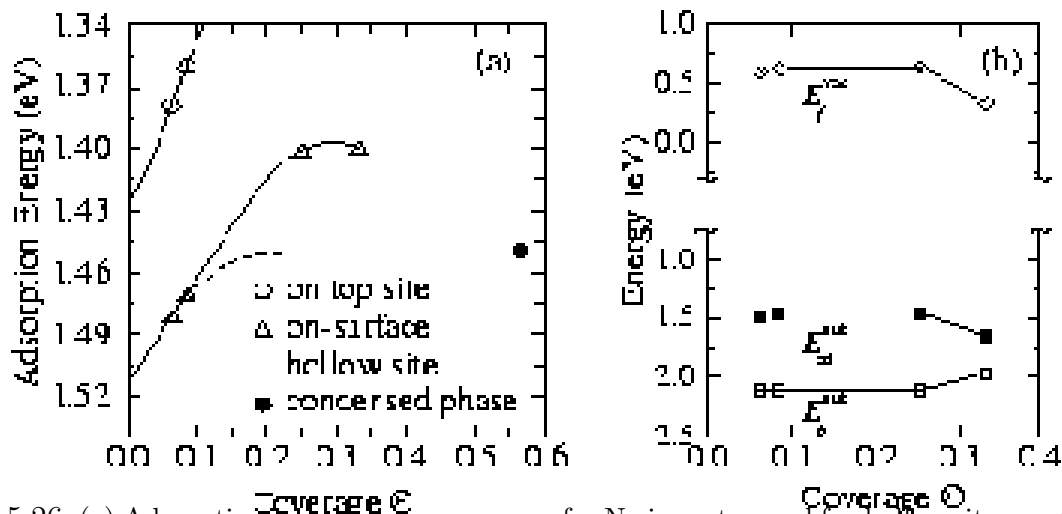


Figure 5.26: (a) Adsorption energy versus coverage for Na in on top and fcc-hollow sites on Al(111). The dashed line marks the phase transition from the homogeneous adlayer into adatom islands with a condensed structure. (b) Adsorption energy $E_{\text{ad}}^{\text{sub}}$ and binding energy E_b^{sub} for substitutional adsorption (cf. Eq. (5.21)), and vacancy formation energy E_f^{vac} (from Neugebauer and Scheffler, 1993).

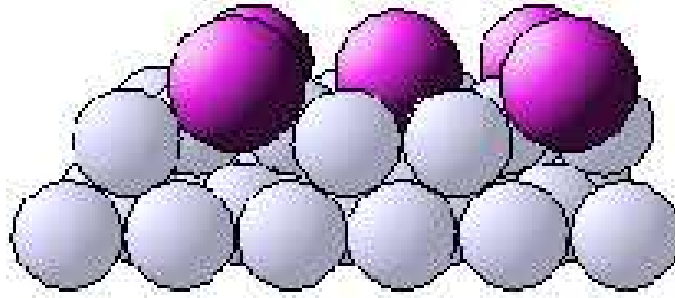


Figure 5.27: Atomic geometry of the $(\sqrt{3} \times \sqrt{3})R30^\circ$ substitutional structure of Na on Al(111). Dark and light gray circles represent Na and Al atoms, respectively.

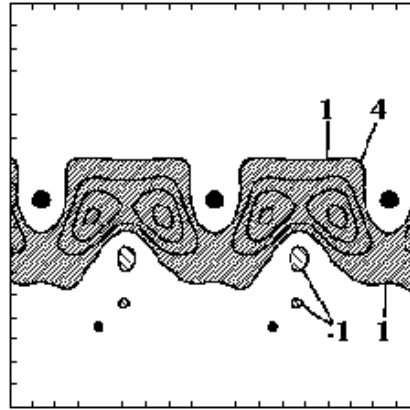


Figure 5.28: Change of the electron density for $(\sqrt{3} \times \sqrt{3})R30^\circ$ -Na on Al(111) with Na in the substitutional site. The reference system is the $(\sqrt{3} \times \sqrt{3})R30^\circ$ surface vacancy structure plus a free standing Na layer. The contours are displayed in a $(\bar{1}21)$ plane. Substrate atoms are represented by small dots and Na atoms by large dots. The units are 10^{-3} bohr $^{-3}$ (from Neugebauer and Scheffler, 1992).

In Fig. 5.28 the difference between the electron density of the $(\sqrt{3} \times \sqrt{3})R30^\circ$ -Na/Al(111) phase and that of the underlying vacancy structure plus a free standing Na layer with also $(\sqrt{3} \times \sqrt{3})R30^\circ$ periodicity is shown. It can be seen that due to Na adsorption, electron density has been displaced from the Na atoms toward the Al atoms of the substrate. As noted above, the reason for the favorable adsorption energy of Na in this structure is due to the particularly low vacancy formation energy; the reason for this has been attributed to the formation of covalent-like, in-plane bonding between the remaining top-layer Al atoms, the honey-comb arrangement of which is similar to that of graphite. The electronic structure of the reconstructed surface is found to be largely responsible for that of the $(\sqrt{3} \times \sqrt{3})R30^\circ$ -Na/Al(111) phase. In particular, new states close to the bottom of the Al valence band are found as well as broad unoccupied bands. In this case, the role of Na is apparently mainly to create the vacancy but not to modify very much the electronic structure of the vacancies (Wenzien et al., 1993).

On further deposition of $1/6$ of a monolayer of Na onto the substitutional $(\sqrt{3} \times \sqrt{3})R30^\circ$ -Na surface, a (2×2) structure forms with two Na atoms per unit cell. As discussed above, the atomic geometry of this phase proved initially difficult to determine. Its correct structure was first proposed on the basis of DFT-LDA calculations (Stampfl and Scheffler, 1994c)

and was subsequently confirmed by a LEED intensity analysis (Burchhardt et al., 1995). From consideration of the atomic structure of the (2×2) phase, it would seem that no mass transport is necessary in its formation, i.e., there is an Al atom missing due to the substitutional adsorption of Na, but there is an additional Al atom embedded between the Na atoms. However, the lower coverage $(\sqrt{3} \times \sqrt{3})R30^\circ$ substitutional structure involves displacement of $1/3$ of a monolayer of Al atoms, which are assumed to diffuse across the surface to be re-bound at steps. The results indicate, therefore, that formation of the (2×2) structure from the $(\sqrt{3} \times \sqrt{3})R30^\circ$ structure involves the reverse process, that is, diffusion of $1/3$ of a monolayer of Al atoms back from the steps which are used in the formation of the (2×2) structure. This process is depicted in Fig. 5.22b.

Interestingly, in a manner similar to that discussed above for the two substitutional structures of Na on Al(001) and Al(111), the *occupied* part of the surface band structure of the (2×2) Na-Al surface alloy can be explained largely in terms of the underlying Al structure. The latter corresponds to the reconstructed Al (2×2) vacancy layer *plus* the Al atom in the hcp-hollow site on this structure. In particular, a significant peak is observed at approximately 2 eV below the Fermi level. Analyzing the wave functions of this state at $\bar{\Gamma}$ shows that it is localized on top of the uppermost hcp-hollow Al atoms. For the surface alloy, in addition, unoccupied features are identified which are associated with the Na atoms, and at $\bar{\Gamma}$, they are centered above the uppermost Na atoms (Stampfl and Scheffler, 1994c).

5.6.3 Co on Cu(001)

In the above sections it was shown that the substitutional adsorption of alkali-metal atoms is driven by the strong dipole moment of adatoms, a rather low formation energy of surface vacancies, and the fact that the adsorbate-adsorbate repulsion is reduced in the substitutional geometry. Thus, substitutional adsorption does not occur for single adatoms, but only when the coverage has reached a critical value where the adatom-adatom interaction becomes significant (cf. Fig. 5.23).

For cobalt adsorbed on Cu(001) the situation is different. Here the adatoms can assume a substitutional geometry at the lowest coverages and with increasing coverage a structural phase transition occurs toward the formation of close-packed islands. The difference compared to alkali-metal adsorption is due to the fact that cobalt, as a transition metal from the middle of the $3d$ series, likes to involve its d -electrons in the chemical binding. This implies that Co likes to assume a highly coordinated site. A single Co adatom on a Cu(001) surface in the on-surface hollow site has four Cu neighbors. However, in the substitutional site it is embedded in the electron density provided by eight Cu neighbors. Thus adsorption in a substitutional site (i.e., in a surface vacancy) is clearly more favorable than adsorption in an on-surface site. In fact, the energy difference between on-surface adsorption and into-surface-vacancy adsorption is larger than the energy to create a surface vacancy. Thus, single Co adatoms tend to kick out Cu atoms from the surface and assume their sites. We note that the Cu atoms taken out of the surface are re-bound at kink sites at steps where they attain the Cu-bulk cohesive energy (cf. Section 5.2.3). In this context it is also relevant that Cu adatoms on Cu(001) have a higher mobility than Co adatoms, which implies that thermal equilibrium with kink sites can be attained easily for Cu adatoms, but is hindered for Co adatoms.

Figure 5.29 shows the adsorption energies for on-surface and substitutional adsorption of

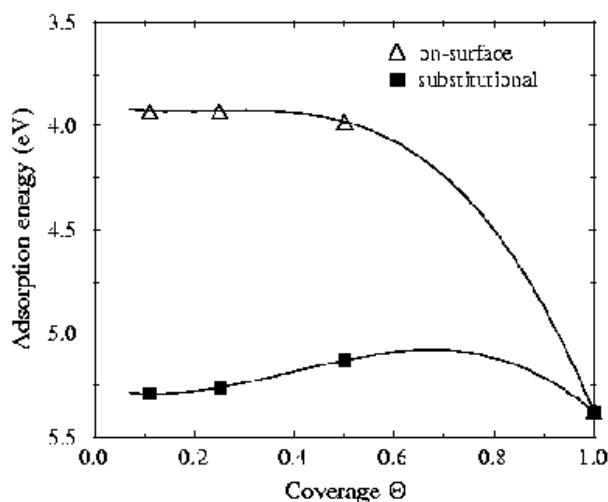


Figure 5.29: Adsorption energy versus coverage for Co on Cu(001) in the on-surface hollow site and in the surface substitutional site (from Pentcheva and Scheffler, 2000).

Co. For low coverages substitutional adsorption is energetically favorable. For higher coverage it is still more energetically favorable for an open adlayer to adsorb substitutionally than on-surface, but the energetically lowest configuration is that of a close-packed Co islands. In other words, Fig. 5.29 tells us that substitutionally adsorbed Co atoms form strong bonds with their eight Cu neighbors. However, the strongest bonds are achieved when Co adatoms form close-packed Co islands. Thus, for higher coverages, and/or higher temperature, when Co adatoms perceive the existence of other Co atoms on the surface, isolated, substitutionally adsorbed Co atoms are predicted to leave their site and close-packed Co islands will be formed. In fact, recent DFT calculations predict that these islands preferentially will have a thickness of 2-3 Co layers and are capped by a Cu layer (Pentcheva and Scheffler, 2000).

5.7 Adsorption of CO at transition metal surfaces

– a model system for a simple molecular adsorbate

The adsorption of a diatomic molecule on a surface represents the next degree of complexity with respect to the adsorption of a single atom and serves as a link to understanding the behavior of more complex molecular adsorbates, as well as to the important area of carbonyl chemistry. As such, CO adsorption has become a paradigm for the study of a simple molecular adsorbate on a surface and has been extensively studied both experimentally and theoretically, see, e.g., Hermann et al. (1987), Hoffmann (1988), Campuzano (1990), and references therein. This interest in CO adsorption also originates from the technological importance of oxidation catalysis (e.g., the car exhaust catalytic converter).

The three outer valence orbitals of a free CO molecule are sketched in Fig. 5.30. With decreasing ionization energies, these are the 5σ orbital (largely C $2s$, C $2p_z$), the doubly degenerate 1π orbital (largely C $2p_x, p_y$, O $2p_x, p_y$) and the 4σ orbital (largely O $2s$, O $2p_z$). The first unoccupied state, shown at the far right in the figure, is the antibonding C $2p_x, p_y$, O $2p_x, p_y$ ($2\pi^*$) orbital. The two most important orbitals are the 5σ and the $2\pi^*$ orbitals which correspond to the HOMO and LUMO, respectively (see Fig. 5.30). The notation here is that “ σ ” indicates orbitals that are rotationally invariant with respect to the inter-nuclear

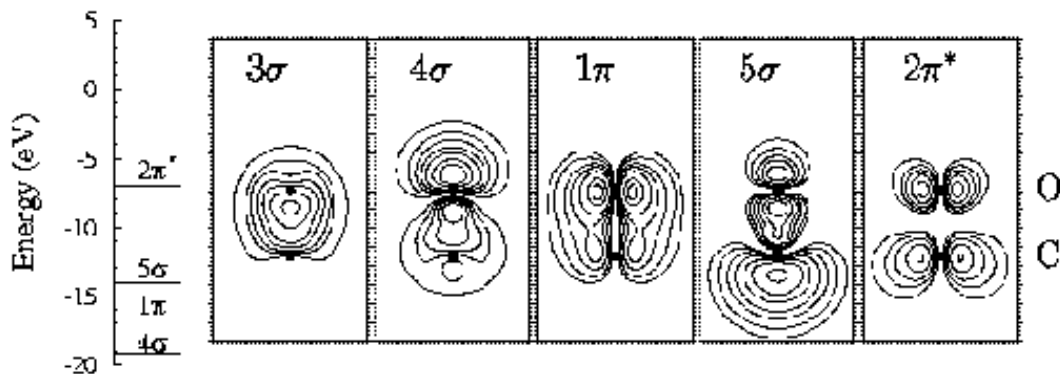


Figure 5.30: Electron density of the valence molecular orbitals of a free CO molecule and their DFT-GGA Kohn-Sham eigenvalues (far left) with respect to the vacuum level. The lower and upper small black dots represent the positions of the C and O atoms, respectively. The first contour lines are at $8 \times 10^{-3} \text{ bohr}^{-3}$, except for the $2\pi^*$ orbital where it is $15 \times 10^{-3} \text{ bohr}^{-3}$, and the highest-valued contour lines are at 0.5, 0.3, 0.2, 0.15, and 0.15 bohr^{-3} for the 3σ , 4σ , 1π , 5σ , and $2\pi^*$ orbitals, respectively.

axis and “ π ” represents orbitals that are lacking this symmetry.

When CO is brought toward a metal surface the CO 5σ is significantly perturbed by the hybridization with the substrate d -electrons. The energy of the 5σ orbital changes most strongly because the bonding to the substrate is governed by the interaction of this orbital. This gives rise to charge transfer from the CO 5σ orbital to the metal, but the metal gives charge back into the antibonding $2\pi^*$ -CO orbital. This is called the donor-acceptor model for CO bonding (Blyholder, 1964, 1975), which is known from the metal carbonyls and is similar to the results for H_2 adsorption (see the discussion of Fig. 5.37 in Section 5.9.2 below). The back donation from the substrate into the $2\pi^*$ -CO orbital weakens the bonding within the CO molecule and strengthens the bond to the substrate. At close distances the ordering of the 1π - and the 5σ -derived levels is reversed compared with the gas phase (see also the discussion of CO on Ni by Hermann and Bagus (1977), and of CO on Cu by Hermann et al. (1987)). In the Blyholder model the lower lying 4σ and 1π MOs (as well as the 3σ and

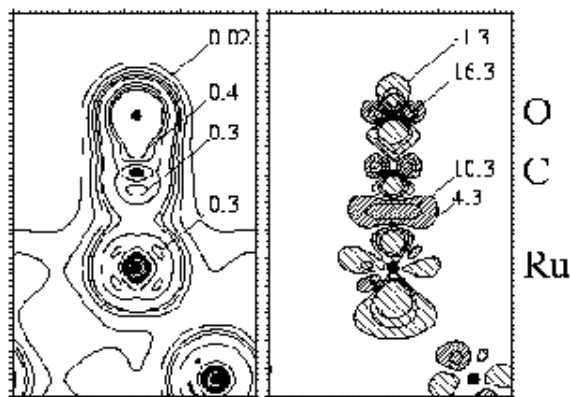


Figure 5.31: Valence electron density (left) and *difference density* $n^\Delta(\mathbf{r})$ (cf. Eq. (5.5)) for the adsorption of CO in the on top site on Ru(0001). Units are bohr^{-3} in the left panel and $10^{-3} \text{ bohr}^{-3}$ in the right panel.

of course the core states) are assumed not to play an important role in the CO-metal bond formation.

In the following we will use Ru(0001) as the substrate for the discussion of CO adsorption but note, that the basic results are valid for other transition-metal substrates as well. In the left panel of Fig. 5.31 the valence electron density of CO in the on-top site on the Ru(0001) surface is shown, and in the right panel of Fig. 5.31 is the difference between the electron density of the CO/Ru(0001) system and the superposition of Ru(0001) and free molecular CO. From the latter, the electron redistribution can be seen to be in good general agreement with the Blyholder donor-acceptor model: Depletion is clearly seen from the σ orbitals of CO and an increase in electron density into the $2\pi^*$ orbitals. Depletion can also be clearly noted from Ru states with d_{z^2} -like character, as well as a significant increase in electron density in the region of the adsorbate-substrate bond, i.e., between the C and Ru atoms. A similar behavior was found for CO on other substrates (see, e.g., Wimmer et al., 1985 and Bagus et al., 1986). It is pointed out that in addition, there is participation to the CO-metal bonding by the Ru atoms in the *second* layer.

The Kohn-Sham eigenvalues of the free CO molecule shift noticeably upon adsorption on the Ru(0001) surface; in particular, a significant downward shift of the 5σ orbital energy due to hybridization with Ru states, and also a small downward shift of the 4σ level is observed. The 1π -level is changed only little, and the $2\pi^*$ -level moves up in energy reflecting the increased occupation. Also, correspondingly, the development of antibonding states occurs. Thus, the behavior follows that of Section 5.3.1; and we realize that the effects (ii) and (iii) are apparently small for the on-top adsorbed CO. In Fig. 5.32 the spatial distribution of some of these CO-derived states are displayed. It can be seen that the 3σ orbital remains unperturbed (compare with Fig. 5.30) by CO adsorption on the substrate since it lies significantly lower in energy and away from the surface. The 4σ orbital interacts with Ru d_{z^2} -like states, as does the strongly interacting 5σ orbital. The 1π orbital on the other hand interacts only weakly with the substrate. The unoccupied $2\pi^*$ -orbital hybridizes with Ru states of d_{xz} and d_{yz} -character. Certain of these adsorbate-substrate bonding states also

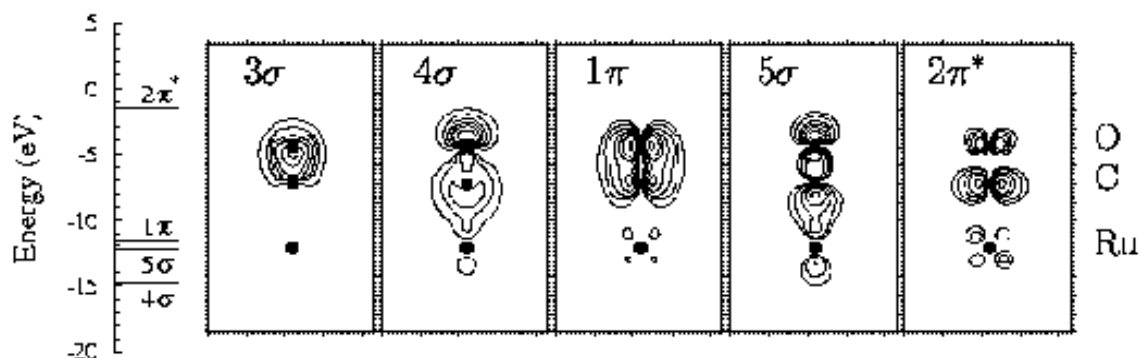


Figure 5.32: Electron density distribution of the CO-derived states for CO adsorbed in the on-top site of Ru(0001) and their DFT-GGA Kohn-Sham eigenvalues (far left) with respect to the vacuum level. The black dots represent the positions of the O, C, and Ru atoms. The first contour lines are at $8 \times 10^{-3} \text{ bohr}^{-3}$, except for the 1π orbital where it is $4 \times 10^{-3} \text{ bohr}^{-3}$. The highest-valued contour lines are at 0.5 for the 3σ and 4σ orbitals and at 0.2, 0.3, and 0.09 bohr^{-3} for the 1π , 5σ , and $2\pi^*$ orbitals, respectively.

have an antibonding partner (not shown), the weight of which resides predominately in the substrate.

We see therefore that the first-principles calculations support in general the Blyholder model, but that the details of the bonding are somewhat more complicated; similar observations have been pointed out and discussed in more detail by Hu et al. (1995) for first-principles studies of CO on Pd(110) and from experiments by Nilsson et al. (1997).

5.8 Co-adsorption [the example CO plus O on Ru(0001)]

A prerequisite to understanding heterogeneous catalytic reactions is knowledge of the behavior of the various reactants (e.g., the adsorption sites and binding energies), as well as their mutual interactions. The co-adsorption system ($m\text{CO}+n\text{O}$)/Ru(0001) represents a well-studied model system, not least due to the drive aimed at obtaining an understanding of the catalytic oxidation of CO by O_2 , but also as a “simple” model system for oxidation catalysis in general. Despite the considerable interest, it is only recently that the detailed atomic structure of some of the phases of ($m\text{CO}+n\text{O}$) on Ru(0001) have been determined, and new ones discovered. Depending on the experimental conditions, co-adsorption of CO and O on Ru(0001) can form the following phases: (2×2) -(1O + 1CO) [Kostov et al., 1992; Narloch et al., 1995], (2×2) -(2O + 1CO) [Narloch et al., 1994], and (2×2) -(1O + 2CO) [Schiffer et al., 1997]. These mixed ($m\text{CO}+n\text{O}$)/Ru(0001) surface structures are depicted in

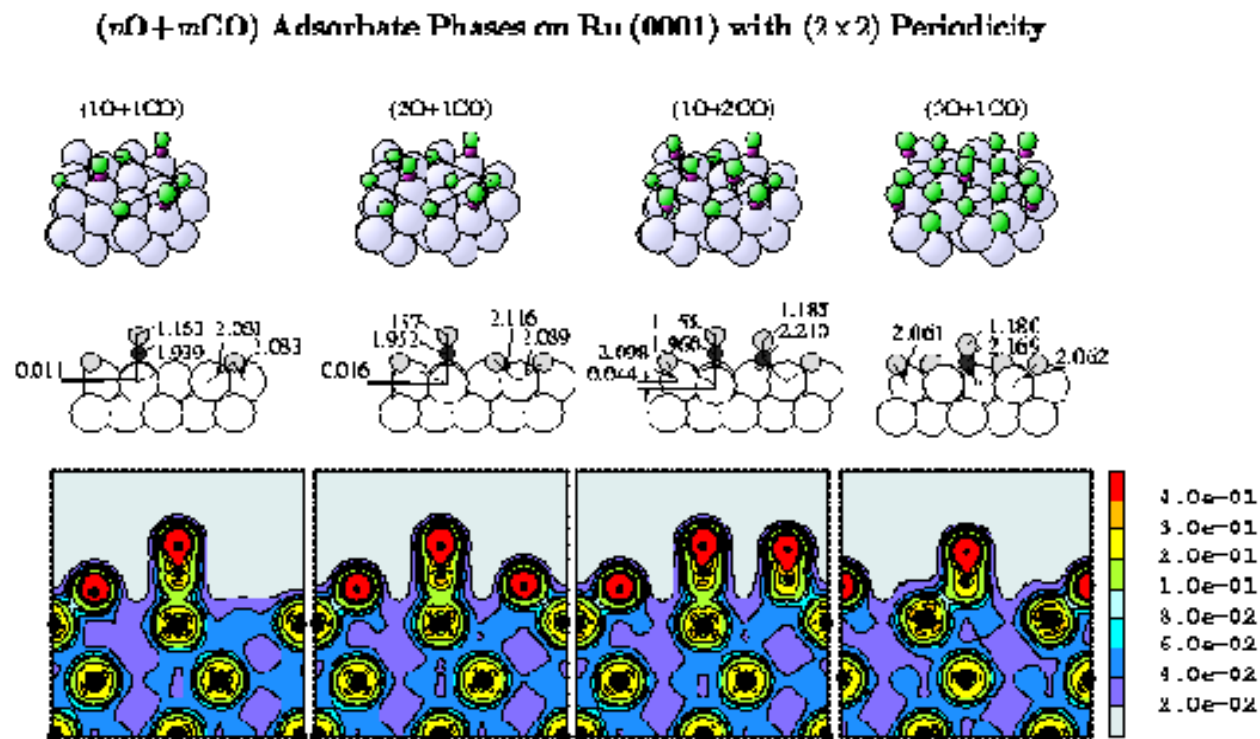


Figure 5.33: Perspective and side views of the various phases of O and CO on Ru(0001). Large and small (green and red) circles represent Ru, O, and C atoms, respectively. The lower panel shows the electron density of the valence states. The contour lines are in bohr $^{-3}$ and distances are in Å (from Stampfl and Scheffler, 1998).

the top panel of Fig. 5.33.

For the first two structures, low-energy electron diffraction (LEED) intensity analyses have been performed: In the first phase, the O atoms occupy hcp sites and the CO molecule adsorbs in the on-top site. In the second phase, a restructuring induced by CO adsorption of the O atoms of the (2×1) (Lindroos et al., 1989) phase occurs: Half of the O atoms, initially occupying the hcp sites, switch to fcc sites and CO adsorbs again in the favored on-top site. For the $(1\text{O} + 2\text{CO})$ structure, there has been no LEED intensity analysis, but infrared absorption spectroscopy (IRAS) and X-ray photoelectron spectroscopy (XPS) experiments (Schiffer et al., 1997) indicate that the O atoms occupy hcp sites and the CO molecules occupy on-top and fcc sites.

To obtain insight into the behavior of these co-adsorption systems, DFT calculations have been carried out. The calculated atomic geometries are displayed in the middle section of Fig. 5.33. Good agreement with the LEED determined geometry was found for the first two of these phases for which comparison is possible (Stampfl and Scheffler, 1998). The calculations show that for the $(2\text{O} + 1\text{CO})$ structure, it is indeed energetically more favorable (by 0.59 eV) for half of the O atoms to occupy the less favorable fcc sites and CO to adsorb in the on-top site rather than maintaining the (2×1) -O arrangement and CO adsorbing in a hollow site. In addition to those phases that have been experimentally identified, the theory predicts the stability of another phase (Stampfl and Scheffler, 1998), namely (2×2) -($3\text{O} + 1\text{CO}$)/Ru(0001), seen in the far right-hand-side of Fig. 5.33. The adsorption energy of CO in this structure is notably weaker than for CO in the on-top site; it is, however, still appreciably exothermic with a value of 0.85 eV. An important consideration concerning whether a structure can in fact form, is the kinetics. The possibility of kinetic hindering due to energy barriers induced by the adsorbed O atoms was investigated by calculating the total energy of CO at various distances above the hcp-hollow adsorption site, i.e., above the vacant O site of the (2×2) - 3O /Ru(0001) structure. Incidentally, this structure has recently been shown to represent a new stable phase of O on Ru(0001) (Kostov et al., 1997; Kim et al., 1998; Gsell et al., 1998). The calculations show that there is an energy barrier to adsorption of ≈ 0.35 eV. This implies that rather high CO pressures would be required in order to realize this structure experimentally. Similar calculations were carried out for the $(1\text{O} + 2\text{CO})$ phase for the CO molecule above the fcc site. It was found in this case there is also an energy barrier, but slightly smaller of about 0.2 eV, thus (at least partially) explaining the low sticking coefficient and the necessary high exposures found experimentally in order to create this phase (Schiffer et al., 1997).

The valence electron density of the various phases are also shown in Fig. 5.33. The oxygen atoms appear as the red (i.e., high electron density), almost spherical features. Both CO and O can be seen to induce a significant redistribution of the electron density of the top-layer Ru atoms. For CO in the hollow sites, it is apparent that the bond strength (per bond) is weaker than that for CO in the on-top site. In the hollow sites, however, CO forms *three* bonds with the metal surface so it is expected that they be longer and weaker. The calculations show nevertheless that the adsorption energy is significantly weaker in the hollow sites than in the on-top site for these structures; this is not the case for the clean surface where the energy difference is only about 0.04 eV. Thus, this significant energy difference is a consequence of the co-adsorbates. These $(m\text{CO}+n\text{O})$ /Ru structures depicted in Fig. 5.33, each possessing the same periodicity but with varying numbers of species and adsorption sites, represent an ideal model co-adsorption series for study by first-principles calculations. From analysis of

the results of such calculations much can be learnt about the various interaction mechanisms at play.

5.9 Chemical reactions at metal surfaces

This section summarizes some basic aspects of the present understanding of the reactivity of surfaces. Here the term “reactivity” usually refers to the surfaces’ ability to break bonds of an approaching molecule and to adsorb the fragments, which is often the rate limiting step in catalytic reactions. For example, in the ammonia synthesis it is the dissociation of N_2 , and for various examples of oxidation catalysis (e.g., the catalytic oxidation of CO) it is the dissociation of O_2 (see Section 5.10 below). Just having referred to “catalysis” a word of warning is appropriate because industrial catalysis involves many more aspects than just dissociation of a certain molecule. Other aspects are “selectivity”, which means that only the desired reaction should take place, and competing reactions yielding unwanted products are suppressed. Also the buffering of intermediate chemical products is important, as is the self-maintenance of the catalyst, the possible role of the catalyst’s support and of promoters. And (often) it is important that no poisonous by-products are released.

5.9.1 The problem with “the” transition state

We will discuss the surface reactivity in terms of molecules approaching the surface considering all relevant atomic coordinates. The total energy as function of the atomic coordinates is called the “potential-energy surface” (PES), cf. Section 5.2.2. It represents the energy surface on which the atoms will move. Whereas the electrons are assumed to be in their ground state of the instantaneous geometry, the wave functions of the nuclei describe the details of the atoms’ dynamics, i.e., the vibrations, rotations, center-of-mass translation, the scattering at the surface, the dissociation, and the surface diffusion of the fragments.

In order to keep the discussion simple we will discuss the situation of a molecular beam which is sent toward the surface, and in which the molecules have a certain center-of-mass kinetic energy, and are in a well defined vibrationally and rotationally excited state or the ground state. The probability of dissociation then is considered to be a measure for the surface reactivity. It contains

- information concerning the surface electronic structure, i.e., on the relevance of so-called frontier orbitals (Wilke et al., 1996, and references therein),
- information about the high-dimensional PES on which the approaching molecule travels toward the surface,
- the statistical average over many trajectories which finally determines with what probability the active sites at the surface are found and the molecule will dissociate, or if it will be reflected into the gas phase.

To discuss the dissociation probability of incoming molecules, it is often assumed that the reaction proceeds along a one-dimensional (or low-dimensional) reaction coordinate and that it will cross a well defined “transition state” (cf. Fig. 5.34). Then the reaction probability is given by an Arrhenius behavior with the energy barrier given by this transition state. While the concept behind Fig. 5.34 has proven useful (at least often) in gas-phase chemistry, it

may be misleading for the description of surface chemical reactions. In particular, we note that the phase space for a molecule-surface reaction has very high dimensionality. For example, even in the simplest surface reaction, i.e., when H_2 molecules are sent toward the surface and if the substrate atoms do not move during the scattering event, the translations, vibrations and rotations of the two H atoms take place in a 6-dimensional configuration space, i.e., a 12-dimensional phase space. As a consequence, the assumption of “the” transition state, as depicted in Fig. 5.34 can be grossly misleading. Instead, many transition states exist, and which of them is taken with what probability depends on the details of the incident H_2 dynamics, i.e., the H_2 translational kinetic energy, and the vibrations and rotations. Consequently, a good treatment of the statistics of the many possible trajectories is mandatory.

As noted in Section 5.2.2 we will restrict the discussion in this chapter to situations where the Born-Oppenheimer approximation is justified. Still, a severe problem remains, namely that knowledge of the PES barely exists. Up until recently only rough, and as we now know, often incorrect semi-empirical models were used, and these earlier studies of the dissociation dynamics were restricted in their dimensionality. For example, in the past the dissociation of H_2 was described in terms of only 2 or 3 coordinates (out of the six important coordinates), and the dependence of the PES on the other coordinates was simply neglected. The only reason for this simplification was that evaluating a PES using good-quality electronic structure theory is elaborate. Since about 1994 the situation has changed, i.e., several groups started to take into account the higher dimensionality (see Gross and Scheffler, 1998, and references therein). Though involved, even treating the six-dimensions of the two hydrogen atoms is not yet complete because in general it could happen that electronic excitations play a role in the scattering event which is outside the Born-Oppenheimer approximation, and furthermore, it is well possible that the dynamics of the substrate atoms will play a role. These concerns may not be very important for the systems studied so far, but for other systems they may well be relevant. With respect to the validity of the Born-Oppenheimer approximation we are not aware of a serious breakdown, although sometimes it has been speculated. For adsorbates at metal substrates, levels are typically broadened, which implies that excited states have a short life time and thus relaxation into the ground state configuration will be

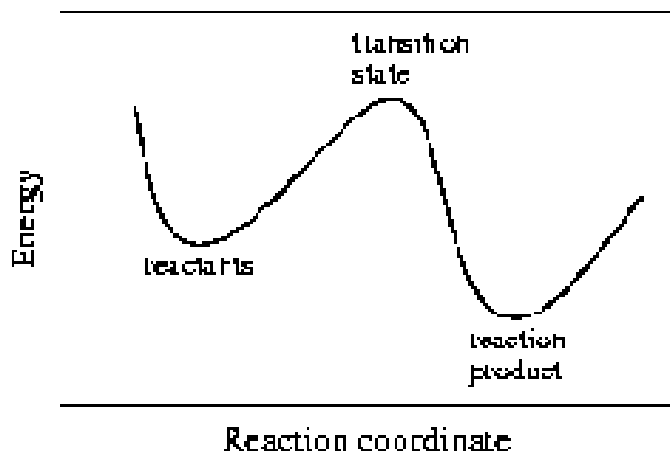


Figure 5.34: Energetics of a chemical reaction in which reactants (their energy is that of the left minimum) reach the reaction product (energy of the right minimum) via a well defined transition state.

(nearly) instantaneous on the time scale of the nuclear motion. Obviously, for insulators and semiconductors the situation is different (see, e.g., the discussion in Gross et al., 1997). Also, the situation would be different if laser excitations are involved (i.e., photo-chemistry), but this is not the topic of this chapter.

5.9.2 Dissociative adsorption and associative desorption of H_2 at transition metals

Dissociative adsorption (or the time-reversed process, which is associative desorption) is a dynamical process, and because of the high dimensionality of the PES, a proper treatment of the dynamics is indeed crucial. Typically the dynamics of atoms is treated classically, i.e., by Newton’s equation of motions, but the underlying PES and the forces acting on the atoms are (or could be and should be) calculated by DFT. This is what is called “*ab initio* molecular dynamics”. It started with the seminal work of Car and Parrinello (1985). The elegance of their approach appears to imply that typically it is not very efficient, and since their original paper several alternative (and numerically more efficient) formulations have been developed (see, e.g., Payne et al., 1992; Kresse and Furthmüller, 1996; Bockstedte et al., 1997; and references therein).

When the moving nuclei are hydrogen atoms, it is often necessary to treat also the nuclei as quantum particles. For such problems a rather involved, high-dimensional “*ab initio* quantum dynamics” method has been implemented (Gross et al., 1995, 1998; Kroes et al., 1997; and references therein). This is probably the most advanced approach and for heavy particles (obviously) it becomes identical to *ab initio* molecular dynamics.

In the following section we describe some general features of the PES and then we show examples which demonstrate the importance of a quantum dynamical treatment of scattering and dissociation of molecules at surfaces. The dissociative adsorption of H_2 appears to be a very simple reaction. However, due to the quantum nature of the hydrogen nuclei, the actual processes are rather complex. Again, as always in this chapter, we will keep the discussion simple, and for more details we refer to papers by Gross and Scheffler (1998), Gross (1998) and Kroes (1999).

5.9.2.1 The potential-energy surface of H_2 at transition-metal surfaces

A good knowledge of the high-dimensional PES of the molecule-surface system is mandatory for a detailed understanding, as the PES rules the scattering and the dissociation. The high-dimensionality implies that the dynamics of the problem will be complex and therefore typically it will be impossible to analyze the PES by simply looking at it. In fact, looking at a PES with dimensionality equal to or higher than six is only possible in terms of cuts along planes in configuration space. Figure 5.35 shows three examples of what is usually called an “elbow plot” because it often looks like an elbow. The planes in configuration space are identified by the insets in the figure. Along these planes the height of the molecule Z and the H–H distance d_{H-H} is varied, and lines of constant potential energy are displayed. Obviously, the cut through the PES shown in Fig. 5.35a looks very different to those in Figs. 5.35b, c.

If the H_2 -surface distance (i.e., Z) is large the contour lines in Fig. 5.35 reflect the energetics of a free H_2 molecule, which has the equilibrium separation of 0.75 Å. We can also read off the nearly harmonic potential underlying the H–H vibration, which implies an H_2 zero-point energy of 0.26 eV, and a vibrational excitation energy of 0.52 eV.

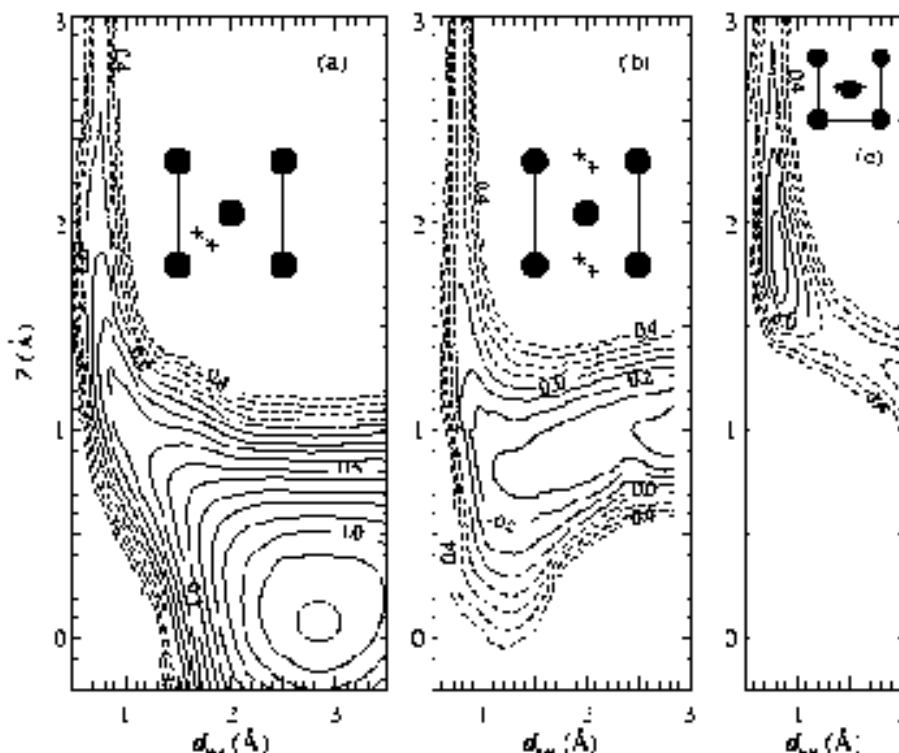


Figure 5.35: Cut through the six-dimensional potential energy surface (PES) of an H_2 molecule above of $\text{Pd}(001)$. We display “elbow plots” where Z is the height of the H_2 center of mass over the surface, and $d_{\text{H-H}}$ is the distance between the two hydrogen atoms. Each cut is defined by the lateral H_2 center-of-mass coordinates in the surface unit cell and the orientation of the molecular axis, i.e., the coordinates $X, Y, \theta_{\text{H}_2}$, and ϕ_{H_2} : The molecule is kept parallel to the surface ($\theta_{\text{H}_2} = 90^\circ$) at an azimuthal orientation, ϕ_{H_2} , and X, Y coordinates shown in the insets. The units of the potential energy are eV and the interval between adjacent contour lines is 0.1 eV. The results are from Wilke and Scheffler (1996).

Although the knowledge of one elbow plot is already much better than just knowing the transition state, as the latter is just one point in the whole configurations space, restricting the world to only one elbow ignores the fact that two H-atoms have six degrees of freedom, not just two. It is obvious from Fig. 5.35 that neglecting the high dimensionality, i.e., assuming that the elbows for different choices of $(X, Y, \theta_{\text{H}_2}, \phi_{\text{H}_2})$ are similar, is by no means justified.

We will now discuss one aspect of the PES which explains the general trend of the reactivity of different transition-metal surfaces. However we already like to add the warning that an appropriate (and reliable) analysis of chemical reactivity has to include a good *statistical treatment* of the *dynamics* of the atoms, which will be discussed in the next section.

Figure 5.35a shows that on $\text{Pd}(001)$ there is at least one pathway toward dissociative adsorption which is not hindered by an energy barrier. In fact, if we inspect the PES for Rh (the left neighbor of Pd in the periodic table) [see Eichler et al., (1999a)] one sees that here the PES offers even more pathways without barriers: For molecules with their axis parallel to the surface almost all dissociation paths are non-activated. On the other hand, for Ag (the right neighbor of Pd) we find that all pathways toward dissociative adsorption are hindered by a significant energy barrier (Eichler et al., 1999a). This result simply reflects the higher chemical activity of the true transition metals compared to the noble metal silver. Figure

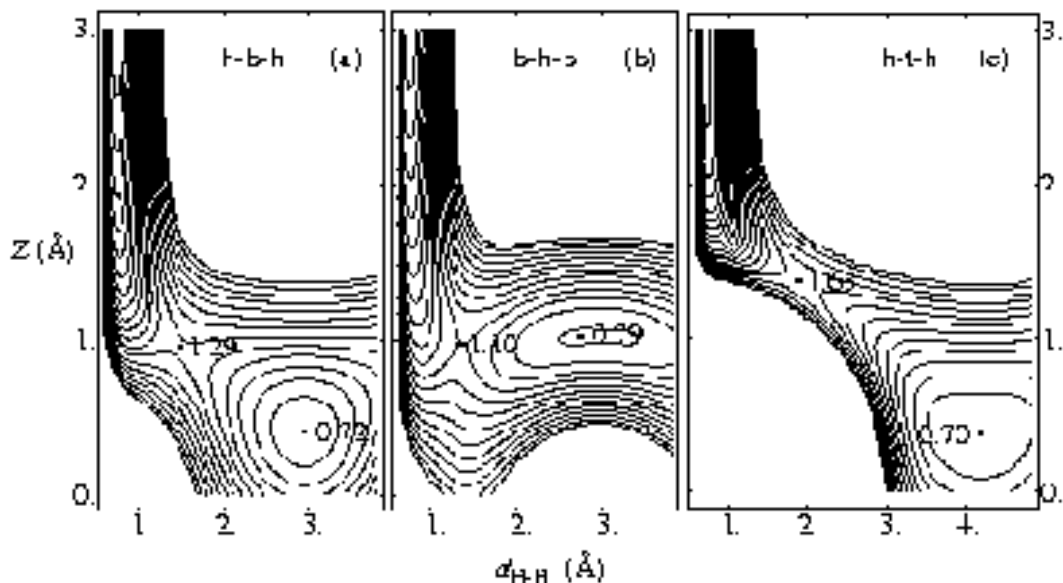


Figure 5.36: Same as Fig. 5.35 but for H_2 at $\text{Ag}(001)$. The results are after Eichler et al. (1999a) and private communication.

5.36 shows the PES of H_2 at $\text{Ag}(001)$. The important aspect in comparing the (a) panels of Figs. 5.35 and 5.36 is not just that there is an energy barrier for the silver substrate, but *where this barrier is located* in configuration space: The lowest barrier (see Fig. 5.36) is found very close to the surface and at a H–H distance which is significantly stretched (by about 100%) compared to the free molecule. We also note in passing that the adsorption state of H on $\text{Ag}(001)$ is only metastable, i.e., at a higher energy than the free H_2 molecule.

Keeping the problems with “the” transition state in mind (we will come back to it in the next section) we now analyze its properties. The fact that the transition state in Fig. 5.36 is found at small Z and significantly stretched $d_{\text{H-H}}$ values implies that the H–H bond is nearly broken when the molecule has reached the top of the barrier. In fact, the detailed analysis of the wave functions of the H_2 –surface system at the geometry of the barrier shows that the differences between different metals should be described in a covalent (or tight-binding) picture. Earlier attempts, which applied a description in terms of Pauli repulsion, and/or frontier orbitals of the unperturbed constituents do not account properly for the character and strength of the interaction: At the barrier we find that the interaction between the molecule and the substrate is already significant and the electronic states ruling the energetics are very different from those of the clean surface. Figure 5.37 summarizes the view developed by Hammer et al. (1994, 1995) in their analysis of H_2 at $\text{Cu}(111)$ and H_2 at $\text{NiAl}(110)$ [see also the earlier study by Hjelmberg et al. (1979) for H_2 at jellium]. Because of obvious reasons, this figure looks similar to that in Section 5.3.1, but now the interacting particle is an H_2 molecule and the geometry is that of the transition state, and not of an adsorbate equilibrium configuration. At the transition state the interaction of the molecule with the surface has already produced a clear splitting into states which are bonding between the molecule and the substrate and which are antibonding. Assuming a substrate from the middle of the transition-metal series (e.g., Ru or Rh) implies that the low energy resonances, which are σ_g and σ_u derived, are filled with electrons. These states are bonding

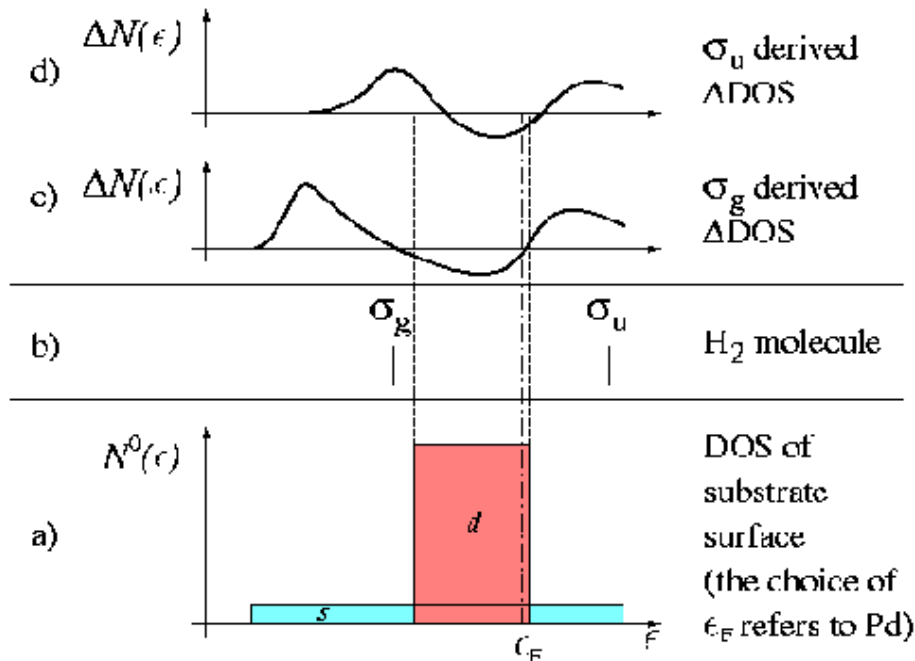


Figure 5.37: Schematic description of the interaction of H_2 at the transition state toward dissociative adsorption at transition-metal surfaces. The bottom panel (a) shows the density of states for a transition metal before adsorption, and panel (b) shows the energy levels of a free H_2 molecule: the bonding state [$\phi_{\sigma_g} = \phi_{1s}(\mathbf{R}_1) + \phi_{1s}(\mathbf{R}_2)$] and the antibonding state [$\phi_{\sigma_u} = \phi_{1s}(\mathbf{R}_1) - \phi_{1s}(\mathbf{R}_2)$]. The σ_g -level is filled with two electrons and the σ_u -level is empty. The interaction between the H_2 σ_g -level and the substrate s - and d -bands gives rise to a broadening and the formation of an antibonding level at about the upper edge of the d -band and a bonding level below the d -band, see panel (c). Panel (d) shows that the interaction between the H_2 σ_u -level with the substrate s - and d -bands gives rise to a broadening and the formation of a bonding level (at about the lower edge of the d -band) and an antibonding level (above the d -band).

with respect to the molecule-substrate interaction and thus their filling implies an attraction of the molecule to the surface. But the filling of the σ_u resonance also implies a weakening of the H–H bond. Thus, when the substrate Fermi-level is in the middle of the d -band, we understand that molecules are strongly attracted to the surface and at the same time the molecular bond is broken.

On the other hand, when the substrate Fermi level is well above the d -band, as for a noble metal, also the states which are antibonding with respect to the molecule-surface interaction get filled (the high energy DOS in panels (c) and (d) of Fig. 5.37). This implies that the net interaction between the molecule and the substrate is repulsive. Thus, an energy barrier is built up which hinders the dissociation.

5.9.2.2 The dynamics of H_2 dissociation at transition-metal surfaces

We have seen that the dissociative adsorption of H_2 at Pd(001) can proceed without an energy barrier. However, this holds only for few pathways; in particular, it is necessary that the molecule reaches the surface with an orientation parallel to the surface in order to be able to dissociate. Molecules arriving with an orientation of their axis perpendicular to the surface will be reflected. In order to understand in more detail what goes on and

to determine the probability of dissociation it is necessary to calculate the dynamics along the high-dimensional PES. This has been done by Gross et al. (Gross et al., 1995, 1998). They treat also the hydrogen nuclei as quantum particles, and a comparison with a classical treatment of the dynamics showed in great detail, which quantum effects are important (mainly zero-point vibrations, and only little tunneling).

Figure 5.38 displays the sticking probability S for two different substrates. The sticking probability is the probability that an incoming H_2 molecule dissociates and that the atoms then adsorb at the surface. One could also say that $(1-S)$ is the probability that an incoming H_2 molecule gets reflected back into the vacuum. The calculated sticking curve exhibits many oscillations. This is not noise, but reflects the quantum nature of the dissociative adsorption and the scattering event: The reflected H_2 beams, which differ by reciprocal lattice vectors of the surface, and the rotationally and vibrationally excited beams are subject to quantum interferences. Thus, the oscillations have a quantum mechanical origin, and when the hydrogen nuclei were treated classically, they were absent. Similar oscillations are well known for other quantum mechanical scattering studies, such as the scattering of electrons (LEED) or that of He. We trust that at some time they will be also observed experimentally for the H_2 scattering at metal surfaces, but clearly such experiments are very demanding. More details on the nature of the quantum interference effects of H_2/Pd scattering can be found in the paper by Gross and Scheffler (1998). When the theoretical results were broadened with the energy resolution of typical experiments, most of the oscillations were averaged out.

One unexpected and surprising result of Fig. 5.38 is that for low kinetic energies ($E_i < 0.05$ eV) the sticking probabilities for the Pd and Rh substrates are very similar (we recall that the PES of Rh offers many pathways with vanishing energy barriers toward dissociation but Pd only a few). Despite their differences in electronic structure (Pd is more noble than Rh) and the clear differences in the PESs, both substrates give an S value as high as 75% for low E_i . In fact, this low energy range corresponds to the typical thermal kinetic energies. While for Rh the sticking probability always remains high, it decreases for Pd to about 25%.

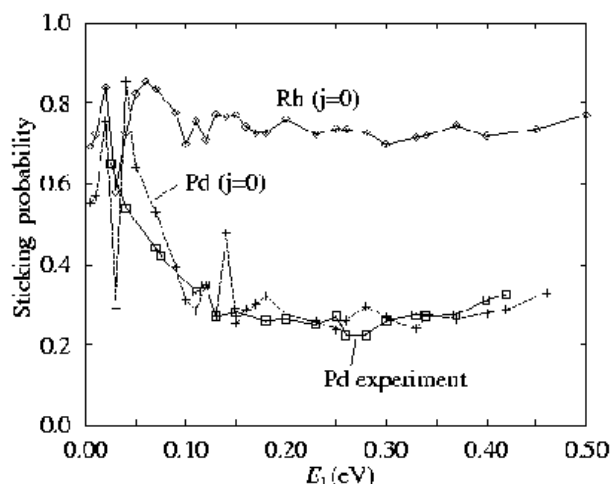


Figure 5.38: Initial sticking probability versus kinetic energy for an H_2 beam under normal incidence on a clean Pd(001) and Rh(001) surface. The H_2 molecules are incident normal to the surface and are in their rotational and vibrational ground state. Theoretical results are from Eichler et al. (1999a), and the experimental data are from Rendulic et al. (1989).

The sticking probability for H_2 at $\text{Pd}(001)$ starts at a high value and then it goes down; this is found in the theory as well as in the experimental data. Earlier, it had been suggested that this behavior is due to the existence of a precursor adsorption, where H_2 is trapped close to the surface from where it can undergo many attempts to dissociate. Whereas this concept is valid for some systems, the theoretical PES does not exhibit such a precursor state and thus, the explanation for this behavior of $S(E_i)$ must have a different origin. The analysis of the H_2 dynamics revealed that the effect is best described by the word “steering”, which means the same as on the road. If one is going slowly, one will make it well along a curvy street. However, when one is going too fast one is pulled out of the curve. Thus, molecules which are approaching slowly will be able to follow a pathway along curvy valleys and find (along the high-dimensional PES) the way toward the point where they can dissociate without an energy barrier. They will dissociate even if their initial orientation is unfavorable (e.g., perpendicular to the surface) because they are steered toward a more favorable transition state geometry. On the other hand, fast molecules will not be able to make it around all the curves. They will bump against an energy barrier and be reflected back into the gas phase.

Thus, the behavior we see for the Pd substrate which increases the sticking to nearly 75% at low energies of the H_2 beam, is truly a dynamical effect. In a static picture the high reactivity of Pd cannot be understood. The efficiency of steering depends on the speed of the incoming molecule and on the shape of the PES. Therefore, to evaluate the sticking probability, which we consider a good measure of the surface reactivity, it is important to consider all degrees of freedom and the dynamics of the nuclei. Obviously, as much as “steering” is important to understand the high reactivity of Pd at low E_i , for other systems, which on the grounds of the electronic structure alone may be expected to exhibit a high reactivity, an “anti-steering” may occur, which drives approaching molecules not toward the best transition state but against an energy barrier.

We add some words on the influence of rotations of the incoming molecule. For rapidly rotating molecules steering is suppressed because the molecules will quickly rotate out of favorable orientations for dissociation (so-called rotational hindering) (Darling and Holloway, 1994; Gross et al., 1996a, b, c). But, there is also a steric effect (Gross et al., 1995): molecules rotating in the so-called helicopter fashion (i.e., parallel to the surface) with $m = j$ dissociate more easily than molecules rotating in the so-called cartwheel fashion (i.e., perpendicular to the surface) with $m = 0$, because the helicoptering molecules have their axis already oriented preferentially parallel to the surface which is the most favorable orientation for dissociation. This orientation effect can be so strong that it even over-compensates the rotational hindering. Furthermore we note that, for example, the hindering effect of the rotational motion may be counterbalanced by the transfer of rotational energy to translational energy (see Eichler et al., 1999b, and Gross and Scheffler, 1996b, for more details).

5.10 The catalytic oxidation of CO

Just as the dissociative adsorption of H_2 discussed above in Section 5.9.2 may be regarded as the model system for studying the dynamics of the dissociative adsorption and associative desorption of small molecules, the CO oxidation reaction may be regarded as the most simple prototype model system of a surface heterogeneous catalytic reaction – a process involving molecular adsorption (chemisorption of CO is non-dissociative under the conditions of cat-

alytic oxidation) and dissociative (atomic) adsorption, surface diffusion, surface reaction, and desorption of products. The oxidation of carbon monoxide has been extensively studied which is largely due to its technological importance (e.g., in car exhaust catalytic converters where the active components are transition metals such as Pt, Pd, and Rh) but is also related to its (relative) “simplicity” (Engel and Ertl, 1979, 1982; Bieláński and Haber, 1991; Peden, 1992, and references therein). Therefore there exists a large data-base concerning its macroscopic behavior and in these terms it is reasonably well understood. On a *microscopic* level, however, an understanding is still lacking. Steps in this direction have recently been made via first-principles calculations (Stampfl and Scheffler, 1997, 1999; Alavi et al., 1998; Eichler and Hafner, 1999). The results of one of these studies is briefly discussed below.

We first like to mention that the investigation of this type of surface process is more complex than that described above for H_2 dissociation; firstly significant substrate relaxations may be induced by CO and O adsorption, and the surface should not be treated as rigid. Secondly, the nature of the problem is different; here a “real” surface chemical reaction takes place where a product is formed that desorbs from the surface. So not only the coordinates of one adparticle need to be considered, but also those of the reacting partner, i.e., the problem has an even higher dimensionality.

Catalytic oxidation of CO at the ruthenium transition metal surface has been reported to exhibit unusual behavior compared to other transition metals when studied at high pressures (Peden, 1992, and references therein). In particular, the reaction rate over Ru for oxidizing conditions (i.e., at CO/O_2 pressure ratios < 1) is the highest of the transition metals considered. In contrast, under ultra-high vacuum conditions (UHV), the rate is by far the lowest. In addition, the kinetic data for the reaction over Ru (e.g., the temperature and pressure dependencies of the rate) deviate compared to the other metals and highest reaction rates occur for high oxygen concentrations at the surface. Interestingly, under these conditions, it was speculated that the reaction mechanism may proceed via an Eley-Rideal interaction (Peden et al., 1986, 1991), that is, a scattering reaction where a particle from the gas-phase reacts with an adsorbed species without adsorbing on the surface first. The usual mechanism by which reactions at surfaces take place is via the Langmuir-Hinshelwood mechanism where both species are adsorbed on the surface prior to reaction.

Under standard UHV conditions using O_2 , the saturation coverage has been reported to be approximately half a monolayer. Recent studies employing NO_2 or very high exposures

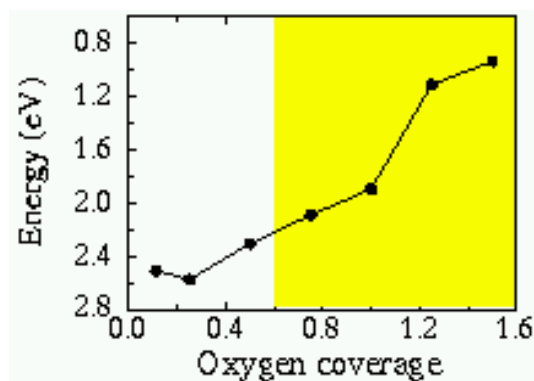


Figure 5.39: Average adsorption energy of O on Ru(0001) for various coverages, with respect to $1/2 \text{ O}_2$. From Stampfl and Scheffler (1997).

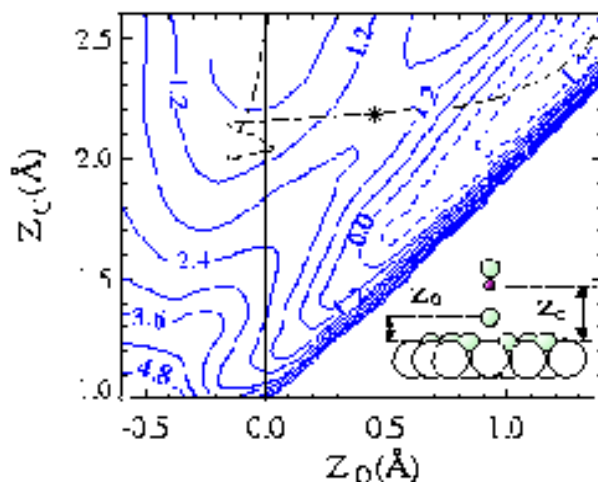


Figure 5.40: Cut through the high-dimensional potential energy surface (PES) as a function of the positions of the C atom, Z_C , and the O adatom, Z_O (see inset). The molecular axis is constrained to be perpendicular to the surface. Positive energies are shown as continuous lines, negative ones as dashed lines. The contour-line spacing is 0.6 eV. The dot-dashed line indicates a possible reaction pathway. From Stampfl and Scheffler (1997).

of O_2 have shown, however, that Ru(0001) can support higher coverages; namely ordered structures (2×2) -3O (Kostov et al., 1997; Kim et al., 1998; Gsell et al., 1998) and (1×1) -O (Stampfl et al., 1996), as had initially been predicted by DFT-GGA calculations (Stampfl and Scheffler, 1996), and that subsurface adsorption occurs after completion of the monolayer structure at elevated temperatures (≈ 600 K) (Stampfl et al., 1996; Mitchell and Weinberg, 1996; Böttcher and Niehus, 1999). Subsurface oxygen can apparently occur as well as the formation of surface oxides⁷, and surfaces with different domains of high oxygen concentration but different stoichiometry are assumed to actuate the high catalytic reactivity of Ru. Thus, the (apparent) oxygen saturation coverage noted above for low (or room) temperature UHV conditions and typical exposure by O_2 is solely due to kinetic hindering for O_2 dissociation.

The adsorption energy of O on Ru(0001) decreases notably with increasing coverage; in particular, for concentrations ≥ 1 ML the bond strength is atypically weak compared to the lower coverage structures. This can be seen from Fig. 5.39. A good catalyst should actuate dissociation of O_2 but at the same time should not bind the dissociated entities too strongly, as then they have a good capability to diffuse and react. Too strongly bound constituents would have little reason to react at all. It is expected therefore that these weaker adsorption energies for $\Theta \geq 1$ will lead to an enhanced reaction rate of CO_2 formation. Indeed, recent experimental studies of CO oxidation over Ru(0001) surfaces loaded with such high oxygen concentrations, have found even higher rates (Böttcher et al., 1997, 1999).

When a complete (1×1) -O structure is present, the calculations show that CO cannot adsorb. However, a scattering reaction of gas-phase CO with adsorbed oxygen (i.e., an Eley-Rideal mechanism) is possible, and the minimum energy barrier was found to be about 1.1 eV with a corresponding bent transition state geometry (Stampfl and Scheffler, 1997). Figure 5.40 shows an appropriate cut through the high-dimensional PES. The minimum

⁷We note that the term “surface oxide” is not well defined, and in particular for Ru, which can exist in many oxidation states, it may be difficult, if not impossible, to distinguish between a 2-3 layer thick “surface oxide” and an on-surface plus sub-surface adsorbate phase.

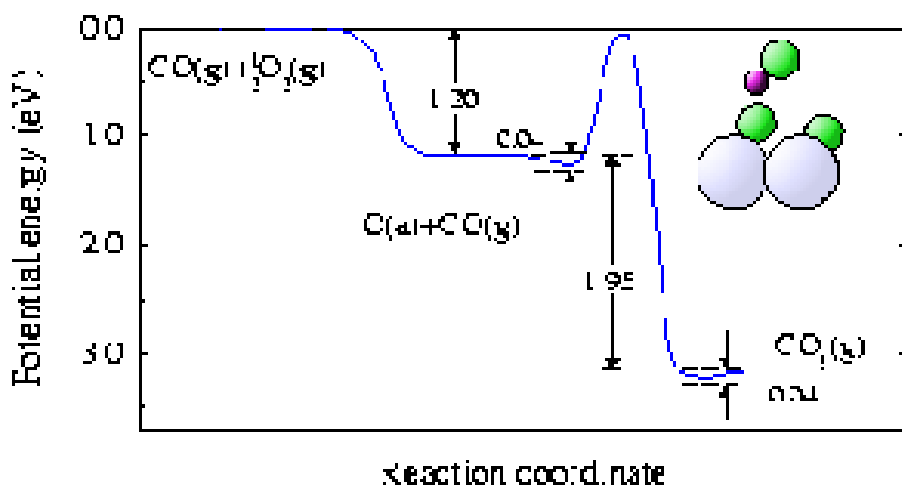


Figure 5.41: Calculated energy diagram for a scattering reaction of gas-phase CO (Eley-Rideal mechanism) with an adsorbed O atom of the 1 ML phase on Ru(0001). Note, 1.20 eV is the energy required to remove one O atom (relative to $1/2 \text{ O}_2$) from the 1 ML structure as calculated in a (2×2) surface unit cell – or, equivalently, the energy gained by the system on adsorbing this atom in the vacant site, i.e., it is not the average adsorption energy at 1 ML as shown in Fig. 5.39. The geometry of the transition state is indicated in the inset. From Stampfl and Scheffler (1997).

barrier corresponds to a tilted CO molecular axis of about 131° as depicted in the inset of Fig. 5.41 which shows the corresponding energy diagram. It can be seen that due to the surface reaction there would be a significant energy gain of about 1.95 eV so that the produced CO_2 molecules would be highly energetic. Assuming this energy barrier would be the rate-limiting step of CO_2 formation via this mechanism, then an estimate of the reaction rate can be made using an Arrhenius-like equation. The prefactor being taken as the number of CO molecules hitting the surface per site per second at a given temperature and pressure. The rate obtained in this way was found to be significantly lower than that measured experimentally (Peden and Goodman, 1986) indicating that this mechanism alone cannot explain the enhanced CO_2 turnover frequency.

To investigate other possible reaction channels, it is conceivable that there may be vacancies in the (1×1) -O adlayer (see Stampfl and Scheffler, 1997), e.g., created by the above mentioned scattering reaction. CO molecules may then adsorb at these vacant sites and react via a Langmuir-Hinshelwood mechanism (see Fig. 5.42). In Section 5.8 it was seen that there is an energy barrier for CO to adsorb in such a vacancy; however, at the high pressures and elevated temperatures employed in catalytic reactor experiments, it is expected that a barrier of such size can be readily overcome.

In view of the weaker CO-metal bond strength compared to that of the O-metal bond strength at this coverage, i.e., 0.85 eV compared to 2.12 eV⁸ (with respect to gas phase $1/2 \text{ O}_2$), it may be expected that the energetically favorable reaction pathway is via movement of CO toward the O atom. Indeed, among the various pathways investigated, this turns out to be the case where the determined energy barrier is about 1.5 eV. Some selected geometries along the reaction path are shown in Fig. 5.43. We refer to Stampfl and Scheffler (1999) for further details.

⁸Here 2.12 eV is the average adsorption energy of O at coverage $\Theta = 0.75$ (cf. Fig. 5.39), i.e., corresponding to the (2×2) -3O structure.

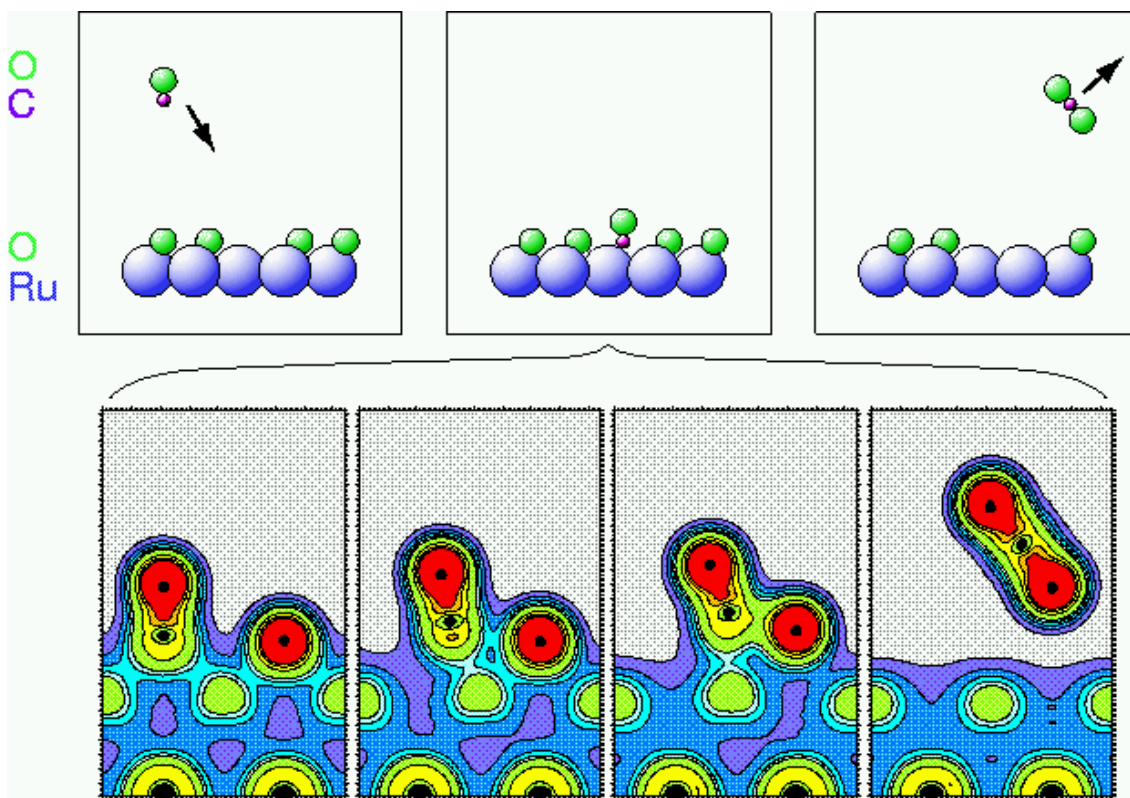


Figure 5.42: Snapshots of the Langmuir-Hinshelwood reaction (top panel) of CO oxidation at Ru(0001). The bottom panels display the electron density distribution along a reaction path close to the transition states. The units are bohr^{-3} , and the colors and contours are the same as in Fig. 5.33.

It can be seen that at the transition state (also shown in the inset of Fig. 5.44), the C-O(a) bond⁹ is almost parallel to the surface. The CO axis is bent away from O(a) yielding a bent CO-O(a) complex with a bond angle of 125° ; similar to that found for the Eley-Rideal mechanism. The C-O(a) bond length is 1.59 \AA (about 29% stretched compared to that in CO_2) and the CO bond length is 1.18 \AA . At the transition state CO and O begin to lift-off the surface as they break their metal bonds in favor of developing a C-O(a) bond. This behavior can also be seen from the corresponding valence electron density distribution shown in Fig. 5.42. The corresponding energy diagram is given in Fig. 5.44. In the work of Alavi et al. (1998) and Eichler and Hafner (1999) bent transition state geometries were also identified for the CO oxidation reaction over the Pt(111) surface for the case of low ($\Theta = 0.25$) oxygen coverages. Alavi et al. (1998) attributed the main contribution to the activation barrier to the weakening of the O-metal bond strength, which supports the general understanding in this respect.

We end this section by noting that despite its high reactivity for CO oxidation, elemental Ru will not be used in automotive catalysts because a volatile Ru oxide exists which is highly poisonous. Nevertheless, trying to understand why Ru is so much more effective than other transition metals may help to design materials with similar properties as Ru. Furthermore, as noted above, there is an interesting and likely conceptionally important aspect of Ru

⁹ O(a) labels the oxygen atom which is adsorbed to the metal substrate

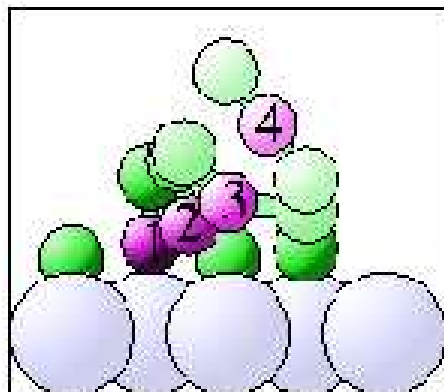


Figure 5.43: Atomic positions along a reaction energy pathway to CO_2 formation. The large, small, and small (labeled) circles represent Ru, O, and C atoms, respectively. The numbers indicate the sequence along the reaction path.

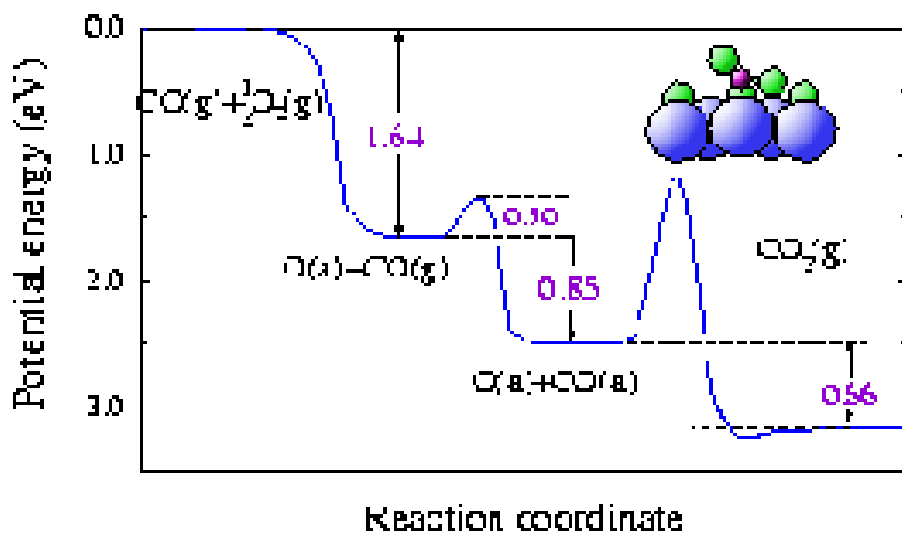


Figure 5.44: Calculated energy diagram for a Langmuir-Hinshelwood reaction mechanism at Ru(0001) for high oxygen coverages on the surface. Note, 1.64 eV is the energy required to remove one O atom (relative to $1/2 \text{O}_2$) from the $(2 \times 2)\text{-3O}$ structure – or, equivalently, the energy gained by the system on adsorbing this atom in an hcp site of the (2×1) structure, yielding the $(2 \times 2)\text{-3O}$ structure. The transition state is indicated in the inset (from Stampfl and Scheffler, 1999).

studies: Ru can exist in many oxidation states and the result (see Fig. 5.39) that its surface region can be loaded with a high concentration of oxygen, poses the question whether it is appropriate to call the reactive surface an adsorbate system, or if it more appropriate to call this a surface oxide (a RuO_2 -like system in the present case). The highly reactive surface of O/Ru(0001) apparently is one with oxygen concentration much higher than $\Theta = 1$ and a coexistence of several domains of different stoichiometry.

5.11 Summary outline of main points

A deeper understanding of chemisorption, surface chemical reactions, and heterogeneous catalysis is currently one of the main aims of surface science (other important topics are, e.g., crystal growth, surface magnetism). In the context of this complex problem, the nature of the chemisorption bond, the energetics of adsorption, and adsorbate geometries and bond-lengths receive considerable attention. While several simple rules have been found to be useful as in the area of molecular chemistry, others should be applied with much caution. Below we summarize some of the findings discussed in this chapter in terms of a brief list:

- 1) Density-functional theory has evolved into an important tool for analyzing surface geometries. For example, the four-layer surface alloy of Na on Al(111) was first predicted and analyzed by DFT calculations (Stampfl and Scheffler, 1994c) and subsequently confirmed by a LEED intensity analysis (Burchhardt et al., 1995); in view of the high number of structural parameters, it was indeed important to start with the DFT analysis. Similarly, the existence of a (1×1) ordered adlayer of O on Ru(0001) and of the (2×2) -3O adlayer was first predicted by DFT calculations (Stampfl and Scheffler, 1996) with detailed specification of the geometry. And more examples exist.
- 2) In addition to providing accurate atomic geometries, DFT calculations also (and in particular) offer the potential of analysis of the underlying mechanisms which determine if and how a certain geometry can be attained and what the nature of the chemical bond is.
- 3) Whereas the geometry is (typically) well described by DFT-LDA and DFT-GGA calculations, the resulting *energies* must be taken with some more caution. Adsorption energies are typically not more accurate than about 0.2 eV per adatom. And we do not expect that new exchange-correlation functionals will improve this to better than 0.1 eV per adatom in the near future (the letter “A”, as in LDA and GGA, will remain part of exchange-correlation functionals employed in actual DFT calculations). However, energy *differences* of chemically similar bonding situations (in particular energies of small distortions and phonons) are described with very well (possibly even meV) accuracy.
- 4) The influence of thermally induced vibrations of the substrate surface and adatoms is often ignored, even today. Still, it is quite clear that some geometries (e.g., the unreconstructed surface of Au(111), or the in-registry adsorption of Xe on fcc(111) surfaces) are stabilized by vibrational energy and entropy. We also mention that surface stress can be noticeably affected by the surface thermal expansion. Thus, sometimes it may be necessary to include the influence of thermal expansion in theoretical studies (see, e.g., Cho and Scheffler, 1997; Xie et al., 1999).

- 5) Unlike a chemical reaction in molecular chemistry, adsorption on a surface involves very unequal partners. For example, the substrate surface gives rise to broadening of adsorbate levels, has an infinite number of electrons, and fixes the electron chemical potential.
- 6) Despite item 5), electronegativity differences between adsorbate and substrate species appear to give a qualitatively correct description of the nature of the chemical bond.
- 7) Item 6) may hold less true for higher coverages when the adsorbate-adsorbate interaction becomes noticeable.
- 8) The correlation between local-coordination and bond-strength, as noted for molecules by Pauling, appears to be (typically) fulfilled for adsorbates. The energy per atom scales roughly proportional to the square root of the coordination. For covalent systems, some geometries may have a more favorable energy than that of this simple proportionality, e.g., when coordination numbers and/or bond-angles conform with the number of available valence electrons.

In this context we also re-emphasize that unexpected behavior of atoms can occur at surfaces (i.e., the discussed substitutional adsorption and alloy formation). At this time knowledge about the energetics of the underlying processes, as, e.g., the formation of surface vacancies and the adsorption of adatoms at step sites, is not sufficiently well developed that a prediction of the adsorbate site (in particular at low coverage) is possible without performing a DFT calculation.

- 9) The validity of a correlation between local coordination and bond-length (in principle a consequence of the local-coordination–bond-strength correlation), appears to be rarely fulfilled for adsorbates. This is due to the fact that geometries are quite constrained, as the atoms of the substrate surface are well bonded to the rest of the substrate, and thus the adsorbate bonds may not succeed to attain their optimum bond angle. Thus, surface bonds may be subject to a “frustrated” hybridization of the adatom orbitals or the substrate-surface orbitals.
- 10) A metal surface attempts to reach charge neutrality on a rather short length scale. In fact, typically a perturbation is even slightly over-screened on the length scale of the nearest-neighbor distance and then the induced electron density is slowly decaying in an oscillatory manner. This highly localized screening is achieved by locally shifting valence electron density of states to higher or lower energies and thus changing the occupancy.
- 11) Reactivity concepts of molecular chemistry, which explore the electron density of the *unperturbed* partners, are only of limited value for dissociation at surfaces. It appears that the lowest energy transition states are (often) so close to the surface where the interaction is already so strong, that “new states” are formed, which differ considerably from the clean surface states and the free adatom orbitals. The filling of these “new states” (determined by the substrate Fermi level) rules (at least partially) the reactivity.
- 12) In addition to item 11) it is important to include the *dynamics* of the approaching molecules: It is not enough to know just the energy of the lowest-energy transition state,

but it is important to know whether or not (or with what probability) the transition state will be found by an approaching molecule. This stresses the importance of the high dimensionality of the potential-energy surface on which an approaching molecule travels and of *the statistics*.

- 13) Some often used concepts still need qualification. For example, it is not clear how a term like that of a “surface oxide” or “surface hydride” describes a situation (or phase) which is different from an “adsorbate”. Clearly, this problem only arises for high-coverage adsorption ($\Theta > 1$).
- 14) We trust that the future will bring more studies which are performed under finite pressure of a well defined atmosphere (getting out of the vacuum) and in which the temperature is changed systematically (warming up and cooling down). This will show which of the previous studies were concerned with a thermal equilibrium geometry and which dealt with a (possibly very special) metastable state.

Acknowledgement

We are grateful for the collaborations with many colleagues and friends, the results of whom have been discussed in this chapter. In particular we mention Jörg Bormet, Axel Gross, and Jörg Neugbauer, but this list could easily be extended. We thank Kristen Fichthorn, Klaus Hermann, and Karsten Reuter for helpful comments on the manuscript.

References

- Adams, D.L., 1996, Appl. Phys. A **62**, 123.
- Alavi, A., P. Hu, T. Deutsch, P.L. Silvestrelli and J. Hutter, 1998, Phys. Rev. Lett. **80**, 3650.
- Aminpirooz, S., A. Schmalz, N. Pangher, J. Haase, M.M. Nielsen, D.R. Batchelor, E. Bøgh and D.L. Adams, 1992, Phys. Rev. B **46**, 15594.
- Andersen, J.N., M. Qvarford, R. Nyholm, J.F. van Acker and E. Lundgren, 1992, Phys. Rev. Lett. **68**, 94.
- Andersen, J.N., D. Hennig, E. Lundgren, M. Methfessel, R. Nyholm and M. Scheffler, 1994, Phys. Rev. B **50**, 17525.
- Antoniewicz, P.R., 1978, Phys. Status Solidi (B) **86**, 645.
- Bader, R.F.W., 1990, Atoms in Molecules. A Quantum Theory, International Series of Monographs on Chemistry, Vol. 22, Oxford University Press, Oxford.
- Bader, R.F.W., 1994, Phys. Rev. B **49**, 13348.
- Bagus, P.S., K. Hermann, W. Müller, and C.J. Nelin, 1986, Phys. Rev. Lett. **57**, 1496.
- Barnes, C.J., 1994, in: The Chemical Physics of Solid Surfaces, Vol. 7, Phase Transitions and Adsorbate Restructuring at Metal Surfaces, eds. D.A. King and D.P. Woodruff. Elsevier, Amsterdam, p. 501.
- Behm, R.J., 1989, in: Physics and Chemistry of Alkali Metal Adsorption, eds. H.P. Bonzel, A.M. Bradshaw and G. Ertl. Elsevier, Amsterdam, p. 111.

- Berndt, W., D. Weick, C. Stampfl, A.M. Bradshaw and M. Scheffler, 1995, *Surf. Sci.* **330**, 182.
- Bielański, A. and J. Haber, 1991, *Oxygen in Catalysis*. Dekker, New York, p. 472.
- Blyholder, G., 1964, *J. Phys. Chem.* **68**, 2772.
- Blyholder, G., 1975, *J. Vac. Sci. Technol.* **11**, 865.
- Bockstedte, M., A. Kley, J. Neugebauer and M. Scheffler, 1997, *Comput. Phys. Commun.* **107**, 187.
- Bormet, J., J. Neugebauer and M. Scheffler, 1994a, *Phys. Rev. B* **49**, 17242.
- Bormet, J., B. Wenzien, J. Neugebauer and M. Scheffler, 1994b, *Comput. Phys. Commun.* **79**, 124.
- Born, M. and R. Oppenheimer, 1927, *Ann. Phys.* **84**, 457.
- Born, M. and K. Huang, 1954, in: *Dynamical Theory of Crystal Lattices*, eds. N.F. Mott and E. C. Bullard. Clarendon, Oxford, p. 420.
- Böttcher, A. and Niehus, 1999, *J. Chem. Phys.* **110**, 3186.
- Böttcher, A., Niehus, S. Schwegmann, H. Over and G. Ertl, 1997, *J. Phys. Chem.* **101**, 11185.
- Böttcher, A., M. Rogozia, H. Niehus, H. Over and G. Ertl, 1999, *J. Chem. Phys.*, accepted.
- Bradshaw, A.M. and M. Scheffler, 1979, *J. Vac. Sci. Technol.* **16**, 447.
- Brivio, G.P. and M.I. Trioni, 1999, *Rev. Mod. Phys.* **71**, 231.
- Bruch, L.W., M.W. Cole and E. Zaremba, 1997, *Physical Adsorption: Forces and Phenomena*, Clarendon, Oxford.
- Burchhardt, J., M.M. Nielsen, D.L. Adams, E. Lundgren, J.N. Andersen, C. Stampfl, M. Scheffler, A. Schmalz, S. Aminpirooz and J. Haase, 1995, *Phys. Rev. Lett.* **74**, 1617.
- Callaway, J., 1964, *J. Math. Phys.* **5**, 783.
- Callaway, J., 1967, *Phys. Rev.* **154**, 515.
- Campuzano, J.C., 1990, in: *The Chemical Physics of Solid Surfaces and Heterogeneous Catalysis*, Vol. 3a: Chemisorption Systems, eds. D.A. King and D.P. Woodruff. Elsevier, Amsterdam, p. 389.
- Car, R. and M. Parrinello, 1985, *Phys. Rev. Lett.* **55**, 2471.
- Cho, J.-H. and M. Scheffler, 1997, *Phys. Rev. Lett.* **78**, 1299.
- Christensen, O.B. and K.W. Jacobsen, 1992, *Phys. Rev. B* **45**, 6893.
- Christensen, S.V., J. Nerlov, K. Nielsen, J. Burchhardt, M.M. Nielsen and D.L. Adams, 1996, *Phys. Rev. Lett.* **76**, 1892.
- Darling, G.R. and S. Holloway, 1994, *J. Chem. Phys.* **101**, 3268.
- Dreizler, R.M. and E.K.U. Gross, 1990, *Density Functional Theory*. Springer, Berlin.
- Echenique, P.M. and J.B. Pendry, 1975, *J. Phys. C* **8**, 2936.
- Eichler, A., J. Hafner, A. Gross and M. Scheffler, 1999a, *Phys. Rev. B* **59**, 13297.
- Eichler, A., J. Hafner, A. Gross and M. Scheffler, 1999b, *Chem. Phys. Lett.* **311**, 1.
- Eichler A. and J. Hafner, 1999, *Phys. Rev. B* **59**, 5960.
- Engel, T. and G. Ertl, 1979, *J. Chem. Phys.* **69**, 1267; *Adv. Catal.* **28**, 1.
- Engel, T. and G. Ertl, 1982, in: *The Chemical Physics of Solid Surfaces and Heterogeneous Catalysis*, Vol. 4, Fundamental Studies of Heterogeneous Catalysis, eds. D.A. King and D.P. Woodruff. Elsevier, Amsterdam, p. 73.
- Fasel, R., P. Aebi, R.G. Agostino, L. Schlapbach and J. Osterwalder, 1996, *Phys. Rev. B* **54**, 5893.
- Feibelman, P.J., 1990, *Phys. Rev. Lett.* **65**, 729.
- Finnis, M.W., R. Kaschner, C. Kruse, J. Furthmüller and M. Scheffler, 1995, *J. Phys.: Con-*

dens. Matter **7**, 2001.

Fiorentini, V., M. Methfessel and M. Scheffler, 1993, Phys. Rev. Lett. **71**, 1051; 1998, Phys. Rev. Lett. **81**, 2184.

Ganduglia-Pirovano, M.V., J. Kudrnovský and M. Scheffler, 1997, Phys. Rev. Lett. **78**, 1807.

Grimley, T.B., 1975, Prog. Surf. Membr. Sci. **9**, 71.

Gross, A., S. Wilke and M. Scheffler, 1995, Phys. Rev. Lett. **75**, 2718.

Gross, A. and M. Scheffler, 1996a, Chem. Phys. Lett. **256**, 417.

Gross, A. and M. Scheffler, 1996b, Prog. Surf. Sci. **53**, 187.

Gross, A., S. Wilke and M. Scheffler, 1996c, Surf. Sci. **357/358**, 614.

Gross, A., M. Bockstedte and M. Scheffler, 1997, Phys. Rev. Lett. **79**, 701.

Gross, A. and M. Scheffler, 1998, Phys. Rev. B **57**, 2493.

Gross, A., 1998, Surf. Sci. Rep. **32**, 291.

Gsell, M., M. Stichler, P. Jacob and D. Menzel, 1998, Israel J. Chem. **38**, 339.

Gurney, R.W., 1935, Phys. Rev. **47**, 479.

Hammer, B., M. Scheffler, K.W. Jacobsen and J.K. Nørskov, 1994, Phys. Rev. Lett. **73**, 1400.

Hammer, B. and M. Scheffler, 1995, Phys. Rev. Lett. **74**, 3487.

Hammer, B. and J.K. Nørskov, 1997, in: Chemisorption and Reactivity on Supported Clusters and Thin Films, eds. R.M. Lambert and G. Pacchioni. Kluwer, Dordrecht, p. 285.

Heine, V. and D. Marks, 1986, Surf. Sci. **115**, 65.

Hennig, D., M.V. Ganduglia-Pirovano and M. Scheffler, 1996, Phys. Rev. B **53**, 10344.

Hermann, K. and P.S. Bagus, 1977, Phys. Rev. B **16**, 4195.

Hermann, K., P.S. Bagus, and C.J. Nelin, 1987, Phys. Rev. B **35**, 9467.

Hjelmberg, H., B.I. Lundqvist and J.K. Nørskov, 1979, Phys. Scr. **20**, 192.

Hoffmann, P., C. von Muschwitz, K. Horn, K. Jacobi, A.M. Bradshaw, K. Kambe and M. Scheffler, 1979, Surf. Sci. **89**, 327.

Hoffmann, R., 1988, Rev. Mod. Phys. **60**, 601.

Horn, K., M. Scheffler and A.M. Bradshaw, 1978, Phys. Rev. Lett. **41**, 822.

Hu, P., D.A. King, M.-H. Lee and M.C. Payne, 1995, Chem. Phys. Lett. **246**, 73.

Jacobi, K., C. von Muschwitz and K. Kambe, 1980, Surf. Sci. **93**, 310.

Janak, J.F., 1978, Phys. Rev. B **18**, 7165.

Jennings, P.J., 1979, Surf. Sci. **88**, L25.

Kambe, K. and M. Scheffler, 1979, Surf. Sci. **89**, 262.

Kim, Y.D., S. Wendt, S. Schwegmann, H. Over and G. Ertl, 1998, Surf. Sci. **418**, 267.

Kleinman, L., 1997, Phys. Rev. B **56**, 16029.

Kohn, W. and K.H. Lau, 1976, Solid State Commun. **18**, 553.

Kostov, K.L., H. Rauscher and D. Menzel, 1992, Surf. Sci. **278**, 62.

Kostov, K.L., M. Gsell, P. Jakob, T. Moritz, W. Widdra and D. Menzel, 1997, Surf. Sci. **394**, L138.

Kresse, G. and J. Furthmüller, 1996, Phys. Rev. B **54**, 11169.

Kroes, G.J., E.J. Baerends and R.C. Mowrey, 1997, Phys. Rev. Lett. **78**, 3583; 1998, Phys. Rev. Lett. **81**, 4781.

Kroes, G.J., 1999, Prog. Surf. Sci. **60**, 1.

Lang, N.D. and W. Kohn, 1971, Phys. Rev. B **3**, 1215.

Lang, N.D., 1971, Phys. Rev. B **4**, 4234.

Lang, N.D., 1973, Solid State Phys. **28**, 225.

- Lang, N.D. and A.R. Williams, 1977, Phys. Rev. B **16**, 2408.
- Lang, N.D. and A.R. Williams, 1978, Phys. Rev. B **18**, 616.
- Langmuir, I., 1932, J. Am. Chem. Soc. **54**, 2798.
- Liebsch, A., 1978, Phys. Rev. B **17**, 1653.
- Lindroos, M., H. Pfnür, G. Held and D. Menzel, 1989, Surf. Sci. **222**, 451.
- McRae, E.G., 1971, Surf. Sci. **25**, 491.
- Methfessel, M., D. Hennig and M. Scheffler, 1992a, Phys. Rev. B **46**, 4816.
- Methfessel, M., D. Hennig and M. Scheffler, 1992b, Appl. Phys. A **55**, 442.
- Methfessel, M., D. Hennig and M. Scheffler, 1995, Surf. Rev. Lett. **2**, 197.
- Miller, A.R., 1946, Proc. Cambridge Philos. Soc. **42**, 492.
- Mitchell, W.J. and W.H. Weinberg, 1996, J. Chem. Phys. **104**, 9127.
- Muscat, J.P. and D.M. Newns, 1978, Prog. Surf. Sci. **9**, 1.
- Muscat, J.P. and D.M. Newns, 1979, Phys. Rev. B **19**, 1270.
- Narloch, B., G. Held and D. Menzel, 1994, Surf. Sci. **317**, 131.
- Narloch, B., G. Held and D. Menzel, 1995, Surf. Sci. **340**, 159.
- Naumovets, A.G., 1994, in: The Chemical Physics of Solid Surfaces, Vol. 7, Phase Transitions and Adsorbate Restructuring at Metal Surfaces, eds. D.A. King and D.P. Woodruff. Elsevier, Amsterdam, p. 163.
- Neugebauer, J. and M. Scheffler, 1992, Phys. Rev. B **46**, 16067.
- Neugebauer, J. and M. Scheffler, 1993, Phys. Rev. Lett. **71**, 577.
- Nilsson, A., N. Wassdahl, M. Weinelt, O. Karis, T. Weill, P. Bennich, J. Hasselström, A. Föhlisch, J. Stöhr and M. Samant, 1997, Appl. Phys. A **65**, 147.
- Nørskov, J.K., 1990, Rep. Prog. Phys. **53**, 1253.
- Nouvertné, F., U. May, M. Bammig, A. Rampe, U. Korte, G. Güntherodt, R. Pentcheva and M. Scheffler, 1999, Phys. Rev. B **60**, 14382.
- Oppo, S., V. Fiorentini and M. Scheffler, 1993, Phys. Rev. Lett. **71**, 2437.
- Over, H., H. Bludau, M. Gierer, and G. Ertl, 1995, Surf. Rev. Lett. **2**, 409.
- Palmberg, P.W., 1971, Surf. Sci. **25**, 598.
- Paul, J., 1987, J. Vac. Sci. Technol. A **5**, 664.
- Pauling, L., 1960, The Nature of the Chemical Bond and the Structure of Molecules and Crystals: An Introduction to Modern Structural Chemistry. Cornell University Press.
- Payne, M.C., M.P. Teter, D.C. Allan, T.A. Arias and J.D. Joannopoulos, 1992, Rev. Mod. Phys. **64**, 1045.
- Payne, M.C., I.J. Robertson, D. Thomson and V. Heine, 1996, Philos. Mag. B **73**, 191.
- Peden, C.H.F., D.W. Goodman, M.D. Weisel and F.M. Hoffmann, 1991, Surf. Sci. **253**, 44.
- Peden, C.H.F. and D.W. Goodman, 1986, J. Phys. Chem. **90**, 1360.
- Peden, C.H.F., 1992, in: Surface Science of Catalysis: In Situ Probes and Reaction Kinetics, eds. D.J. Dwyer and F.M. Hoffmann. Am. Chem. Soc., Washington DC.
- Pedersen, M.O., I.A. Bonicke, E. Laegsgaard, I. Stensgaard, A. Ruban, J.K. Nørskov and F. Besenbacher, 1997, Surf. Sci. **387**, 86.
- Pentcheva, R. and M. Scheffler, 2000, Phys. Rev. B, in print.
- Perdew, J.P. and M. Levy, 1997, Phys. Rev. B **56**, 16021.
- Petersen, M., P. Ruggerone and M. Scheffler, 1996, Phys. Rev. Lett. **76**, 995; 2000, Phys. Rev. B, submitted.
- Pleth Nielsen, L., F. Besenbacher, I. Stensgaard, E. Lægsgaard, C. Engdahl, P. Stoltze, K.W. Jacobsen and J.K. Nørskov, 1993, Phys. Rev. Lett. **71**, 754.

- Porteus, J.O., 1974, *Surf. Sci.* **41**, 515.
- Rader O., W. Gudat, C. Carbone, E. Vescovo, S. Blügel, R. Kläsger, W. Eberhardt, M. Wuttig, J. Redinger and F.J. Himpsel, 1997, *Phys. Rev. B* **55**, 5404.
- Rendulic, K.D., G. Anger and A. Winkler, 1989, *Surf. Sci.* **208**, 404.
- Robertson, I.J., D.I. Thomson, V. Heine and M.C. Payne, 1994, *J. Phys. Condens. Matter* **6**, 9963.
- Scheffler, M., K. Kambe and F. Forstmann, 1978, *Solid State Commun.* **25**, 93.
- Scheffler, M., K. Horn, A.M. Bradshaw and K. Kambe, 1979, *Surf. Sci.* **80**, 69.
- Scheffler, M. and A.M. Bradshaw, 1983, in: *The Chemical Physics of Solid Surfaces and Heterogeneous Catalysis*, Vol. 2: Adsorption at Solid Surfaces, eds. D.A. King and D.P. Woodruff. Elsevier, Amsterdam, p. 165.
- Scheffler, M., Ch. Droste, A. Fleszar, F. Máca, G. Wachutka and G. Barzel, 1991, *Physica B* **172**, 143.
- Schiffer, A., P. Jakob and D. Menzel, 1997, *Surf. Sci.* **389**, 116.
- Schmalz, A., S. Aminpirooz, L. Becker, J. Haase, J. Neugebauer, M. Scheffler, D.R. Batchelor, D.L. Adams and E. Bøgh, 1991, *Phys. Rev. Lett.* **67**, 2163.
- Seyller T., M. Caragiu, R.D. Diehl, P. Kaukasoina and M. Lindroos, 1998, *Chem. Phys. Lett.* **291**, 567.
- Skriver, H., 1985, *Phys. Rev. B* **31**, 1909.
- Somorjai, G.A. and M.A. Van Hove, 1989, *Prog. Surf. Sci.* **30**, 201.
- Spanjaard, D. and M.C. Desjonquères, 1990, in: *Interaction of Atoms and Molecules with Surfaces*, eds. V. Bortolani, N.H. March and N.P. Tosi. Plenum, New York, London, p. 255.
- SRL, 1995, *Surf. Rev. Lett.* **2**, 315. A special issue of *Surface Review and Letters* devoted to alkali-metal adsorption, containing review articles by several groups.
- Stampfl, C., M. Scheffler, H. Over, J. Burchhardt, M. Nielsen, D.L. Adams and W. Moritz, 1992, *Phys. Rev. Lett.* **69**, 1532.
- Stampfl, C., M. Scheffler, H. Over, J. Burchhardt, M. Nielsen, D.L. Adams and W. Moritz, 1994a, *Phys. Rev. B* **49**, 4959.
- Stampfl, C., J. Neugebauer and M. Scheffler, 1994b, *Surf. Sci.* **307/309**, 8.
- Stampfl, C. and M. Scheffler, 1994c, *Surf. Sci.* **319**, L23.
- Stampfl, C. and M. Scheffler, 1995, *Surf. Rev. Lett.* **2**, 317.
- Stampfl, C. and M. Scheffler, 1996, *Phys. Rev. B* **54**, 2868.
- Stampfl, C., 1996, *Surf. Rev. Lett.* **3**, 1567.
- Stampfl, C., S. Schwegmann, H. Over, M. Scheffler and G. Ertl, 1996, *Phys. Rev. Lett.* **77**, 3371.
- Stampfl, C. and M. Scheffler, 1997, *Phys. Rev. Lett.* **78**, 1500; *J. Vac. Sci. Technol. A* **15**, 1635; *Surf. Sci.* **377-379**, 808.
- Stampfl, C., K. Kambe, R. Fasel, P. Aebi and M. Scheffler, 1998, *Phys. Rev. B* **57**, 15251.
- Stampfl, C. and M. Scheffler, 1998, *Israel J. Chem.* **38**, 409.
- Stampfl, C. and M. Scheffler, 1999, *Surf. Sci.* **433-435**, 119.
- Taylor, J.B. and I. Langmuir, 1933, *Phys. Rev.* **44**, 423.
- Topping, J., 1927, *Proc. Roy. Soc. London Ser. A* **114**, 67.
- Wang, X.-G., W. Weiss, Sh.K. Shaikhutdinov, M. Ritter, M. Petersen, F. Wagner, R. Schlögl and M. Scheffler, 1998, *Phys. Rev. Lett.* **81**, 1038.
- Wilke, S. and M. Scheffler, 1996, *Phys. Rev. B* **53**, 4926.
- Wilke, S., M.H. Cohen and M. Scheffler, 1996, *Phys. Rev. Lett.* **77**, 1560.

- Wenzien, B., J. Bormet, J. Neugebauer and M. Scheffler, 1993, Surf. Sci. **287/288**, 559.
- Wenzien, B., J. Bormet and M. Scheffler, 1995, Comput. Phys. Commun. **88**, 230.
- Wimmer, E., C.L. Fu and A.J. Freeman, 1985, Phys. Rev. Lett. **55**, 2618.
- Xie, J., S. de Gironcoli, S. Baroni and M. Scheffler, 1999, Phys. Rev. B **59**, 970.
- Yang, L., G. Vielsack and M. Scheffler, 1994, unpublished.
- Yu, B.D. and M. Scheffler, 1997, Phys. Rev. B **56**, R15569.